INFORMATION TO USERS

This manuscript has been reproduced from the microfilm master. UMI films the text directly from the original or copy submitted. Thus, some thesis and dissertation copies are in typewriter face, while others may be from any type of computer printer.

The quality of this reproduction is dependent upon the quality of the copy submitted. Broken or indistinct print, colored or poor quality illustrations and photographs, print bleedthrough, substandard margins, and improper alignment can adversely affect reproduction.

In the unlikely event that the author did not send UMI a complete manuscript and there are missing pages, these will be noted. Also, if unauthorized copyright material had to be removed, a note will indicate the deletion.

Oversize materials (e.g., maps, drawings, charts) are reproduced by sectioning the original, beginning at the upper left-hand corner and continuing from left to right in equal sections with small overlaps.

Photographs included in the original manuscript have been reproduced xerographically in this copy. Higher quality 6" x 9" black and white photographic prints are available for any photographs or illustrations appearing in this copy for an additional charge. Contact UMI directly to order.

ProQuest Information and Learning
300 North Zeeb Road, Ann Arbor, MI 48106-1346 USA
800-521-0600

UMI®

NON-EQUILIBRIUM GLIDING ARC AND CORONA DISCHARGES FOR ABATEMENT OF VOLATILE ORGANIC COMPOUNDS

BY

NIKOLAY YUREVICH KALASHNIKOV
M.S., University of Florida, Gainesville, FL, USA, 1995
M.S., Moscow State Technical University n.a. Bauman, Moscow, Russia, 1994

THESIS

Submitted as partial fulfillment of the requirements
for the degree of Doctor of Philosophy in Mechanical Engineering
in the Graduate College of the
University of Illinois at Chicago, 2002

Chicago, Illinois

UMI Number: 3058109

UMI®

UMI Microform 3058109

Copyright 2002 by ProQuest Information and Learning Company.
All rights reserved. This microform edition is protected against
unauthorized copying under Title 17, United States Code.

ProQuest Information and Learning Company
300 North Zeeb Road
P.O. Box 1346
Ann Arbor, MI 48106-1346

THE UNIVERSITY OF ILLINOIS AT CHICAGO
Graduate College
CERTIFICATE OF APPROVAL

June 26, 2002

I hereby recommend that the thesis prepared under my supervision by

NIKOLAY YUREVICH KALASHNIKOV

entitled NON-EQUILIBRIUM GLIDING ARC AND CORONA DISCHARGES FOR ABATEMENT OF VOLATILE ORGANIC COMPOUNDS

be accepted in partial fulfillment of the requirements for the degree of

DOCTOR OF PHILOSOPHY

Adviser (Chairperson of Defense Committee)

I concur with this recommendation

Department Head/Chair

Recommendation concurred in:

Members of Thesis or Dissertation Defense Committee

UIC University of Illinois at Chicago

ACKNOWLEDGEMENTS

I would like to acknowledge my deepest appreciation to my thesis defense committee members for their guidance and supervision: Professor Alexander Fridman, Professor Lawrence Kennedy, Professor Kenneth Brezinsky, Research Professor Alexei Saveliev and Doctor Alexander Gutsol. I am also very grateful to Professors Selcuk Guceri and Yury Gogotsi, and Dr. Eugeny Dyakov for giving me a great opportunity to study at the University of Illinois at Chicago.

I address special thanks to my friends and collaborators: Dr. Andrey Romanets, Gyuzel Fatykhova, Inga Kuznetsova, Bogdan Krautsov, Mikhail Kossitsyn, Kamilla Iskanderova, Alexander Chirokov, Mario Sobacchi, Jacques Bingue, Alek El-Khoury, Wilson M. Merchan, Joseph Libera, Dr. Vladislav Domnich and Dr. Pavel Chamara.

I am very grateful to my wife Lilia Kalashnikova for her patience and support all the years of my study.

N.Y.K

TABLE OF CONTENTS

LIST OF TABLES

LIST OF FIGURES

FIGURE PAGE

LIST OF FIGURES (Continued)

FIGURE PAGE

LIST OF FIGURES (Continued)

FIGURE PAGE

LIST OF ABBREVIATIONS AND NOMENCLATURE

DBD	Dielectric Barrier Discharge
DMS	Dimethyl Sulfide
DRE	Destruction and Removal Efficiency
EPA	Environmental Protection Agency
FID	Flame Ionization Detector
GCMS	Gas Chromatograph Mass Spectrometer
GPCR	Gas-Phase Corona Reactor
HV	High Voltage
NCASI	National Council on Air and Stream Improvement
PEC	Projected Energy Cost
SEI	Specific Energy Input
VOC	Volatile Organic Compounds
E	Electric field
eV	Electron-Volt
e-beam	Electron Beam
l	Length of the arc
N	Number of particles
P	Power
r	Coordinate, radius of the arc
To	Temperature in the center of the arc
Tr	Temperature at the radius r of the arc

SUMMARY

The application of plasma chemistry for removal of Volatile Organic Compounds (VOC) in the forest products industry is studied in this work. An extensive research was done to understand the physical and chemical processes with VOC in pulsed corona and gliding arc discharges at conditions typical for the exhaust streams in paper mills and strandboard press vents.

A linear stability analysis of the low-current gliding arc discharge in the transitional regime was performed to explain the observed experimental effects in VOC removal. It was shown that the gliding arc remains stable during the evolution and gradually transforms into a more non-equilibrium one. The low-current arc discharge can propagate with the effect of "overshooting" at which the gliding arc extinguishes long after its maximum power has been achieved. Analytical and numerical solutions explain the general behavior of the low-current gliding arc and are in a good agreement with our experiment.

A semi-empirical approach of coupling physical parameters of a pulsed corona discharge with its chemistry is proposed. A fraction of high-energy electrons produced by the discharge was found using reaction mechanism of NOx formation in pure dry air. An assembled plasma-chemical elementary-reaction mechanism for methanol and dimethyl sulfide showed the validity of this approach. A Projected Energy Cost (PEC) was proposed to generalize the obtained experimental data. The optimum PEC for VOC removal exists at 2% of absolute humidity. The worst removal rate was observed at 130°C. The results were used for the process improvement in the mobile pulsed-corona pilot plant that is currently under construction. A concept of the plant is discussed.

1. INTRODUCTION

1.1. Current Technologies for VOC Abatement

The forest product industry is coming under increasing pressure from the U.S. Environmental Protection Agency as well as state and local agencies to control emissions from pulp mills and wood products plants. Incineration (and other high temperature processes) is widely used environmental-control technologies for concentrated volatile organic compound (VOC) emissions; however they may not be appropriate for the dilute VOC process emissions commonly found in the forest products industry. Although direct incineration of dilute VOC streams is technically feasible, it will typically be much more expensive than low-temperature technologies that avoid heating the entire process stream with supplemental fuels, especially in the case of high-volume streams. Potential low-temperature purification technologies include low-temperature catalysis, biofiltration or biotreatment, and low-temperature, non-equilibrium plasmas. Low-temperature catalytic purification processes have disadvantage of catalyst that are subject to plugging and poisoning. Thus, these systems tend to have higher maintenance and replacement costs than the plasma technologies. Biofiltration requires high surface areas and long residence times for VOC capture and destruction. This results in substantially larger process volumes than those that can be handled by plasma technologies. Biofiltration may also require more careful process control in order to maintain bioactivity for VOC control. Biological treatment is a substance-sensitive. In this thesis the biofiltration will not be considered for comparison.

Low-temperature, non-equilibrium plasmas (also called "non-thermal" plasmas) are an emerging technology for abating diluting VOC emissions. These plasmas may be produced by a variety of electrical discharges or electron beams. The comparison of non-thermal plasma technologies with incineration techniques is given in Table I.

The basic feature of plasma technologies is that they produce plasma in which the majority of the electric energy (more than 99%) goes into production of energetic electrons, instead of heating the entire gas stream. These energetic electrons produce excited species, free radicals and ions) as well as additional electrons through the electron impact ionization, excitation and ionization of the background molecules. These excited species, in turn, oxidize, reduce, or decompose the pollutant molecules. This is in contrast to the mechanism involved in thermal processes (such as plasma torches or furnaces, Regenerative Thermal Oxidation (RTO) and several chemical techniques) which require heating the entire gas stream in order to destroy pollutants. In additional, the low-temperature plasma technology is highly selective and has relatively low maintenance requirements. Its high selectivity results in relatively low energy costs for emissions control while low maintenance keeps annual operating expenses low. Furthermore, these plasma discharges are very uniform and homogeneous (except gliding arcs) which results in high process productivity.

Specific niches of incineration and plasma technologies are clearly seen in Table I. As mentioned above, RTO is more effective at high concentrations of VOC. Plasma is normally used al lower concentrations of VOC and in the cases where combustion is not effective, such as removal of NO_x or sulfur-containing compounds. Scrubbing of exhaust gases with water might be required for both techniques, but some plasma reactors can be designed as a single unit with a scrubber to reduce the equipment cost. Moreover, it was shown in this thesis, that higher than

1000 ppm concentrations of VOC can be successfully treated in pulsed corona reactors. In the foreseen future, due to new environmental regulations plasma may take a substantial share of the gas abatement market.

TABLE I. COMPARISON OF RTO AND NON-THERMAL PLASMA TECHNOLOGIES

Gas treatment method	Regenerative Thermal Oxidation (RTO)	Non-equilibrium Plasma Technologies
Applications	Gas Streams with high concentration of VOC (> 1000 ppm)	Gas Streams with low concentration of VOC (< 1000 ppm); removal of NO_x and SO_2
Method Selectivity or Electrical Efficiency	Not selective, heating of the entire flow up to high temperatures (> 1000 °C)	Up to 99% of electrical energy could go to production of active species, almost no heating of gas
Safety	Potential problems of major accidents in case of lack of treated air flow, or control power outage. High temperatures.	Safe, but employs high voltage equipment
Equipment and Maintenance Cost	High	Medium
Need for Additional Gas/Liquid Supply	Needs considerable amounts of natural gas to support combustion	Might need some scrubbing water
Potential Problems with Byproducts	Sulfur-containing compounds must be treated additionally	Dangerous by-products may be present in the stream; process is sensitive to the kind of VOC; complex compounds require longer residence time

1.2. Overview of Plasma Technologies for Abatement of VOC

Low-temperature, non-equilibrium plasma processes have been shown to be effective in treating a wide range of emissions including aliphatic hydrocarbons, chlorofluorocarbons, methyl cyanide, phosgene, formaldehyde, as well as sulfur and organophosphorus compounds. Although the products of these plasma processes are virtually undistinguishable from incineration products (CO_2, H_2O, SO_2, etc.), chemical reactions occurring in these technologies are substantially different than in incineration ([11], [62]).

Large electric fields in discharge reactors create conditions for electric breakdowns during which many electron-ion pairs are formed. Primary electrons are accelerated by the electric field and produce secondary ionization, and so forth. Created excited species, atoms, radicals, molecular and atomic ions, electrons and radicals are capable of interacting with VOCs to a certain degree. Some processes are more effective than the others. The most important are those leading to formation of *OH* radicals. Typically, the major mechanisms controlling the chemistry of VOCs fall in five major categories.

1.3. Radical-Induced VOC Destruction

Hydroxyl radicals are formed through a three-step mechanism initiated by energetic electrons, which ionize any specie (M):

$$e + M \rightarrow M^+ + e + e$$

and followed by the fast charge transfer

$$M^+ + H_2O \rightarrow M + H_2O^+$$

The positive water ions react rapidly with neutral water molecules to form the following radicals:

$$H_2O^+ + H_2O \rightarrow H_3O^+ + OH^{\bullet}$$

This mechanism is especially important in high voltage discharges, such as pulsed corona and dielectric-barrier discharges, and electron-beam systems.

Excited and ground state atomic oxygen ($O(^1D)$ and $O(^3P)$) species are also important radicals for producing hydroxyl radicals

$$O(^1D) + H_2O \rightarrow {}^{\bullet}OH + {}^{\bullet}OH$$

These atomic oxygen species also can produce ozone O_3, which is particularly active in liquid-phase oxidation.

1.4. Direct Electron-Induced VOC Destruction

This mechanism usually only occurs in strongly electronegative gases, when the electron affinity of a gas specie is comparable to its dissociation energy. For example:

$$e + CHCl_3 \rightarrow {}^{\bullet}CHCl_2 + Cl^-$$

or

$$e + CCl_4 \rightarrow {}^{\bullet}CCl_3 + Cl^-$$

Usually a negatively charged particle is lost in fast ion-ion recombinations. Higher electric fields favor such type of mechanism.

1.5. Direct Ion–Induced VOC Destruction

The direct ion-induced decomposition of VOCs is similar to the hydroxyl-formation mechanism discussed earlier. When either the VOC species or their intermediate products produced by another destruction mechanism have a low ionization potential, the charge exchange process can promote further decomposition reactions.

Direct electron impact ionization of nitrogen molecules occurs in collision with an additional nitrogen molecule:

$$N_2 + e \rightarrow N_2^+ + e + e$$

If the ionization potential of a hydrocarbon radical (produced in an earlier VOC-destruction reaction) is very low, the charge exchange process can provide dissociation of organic molecules as well. Methanol decomposition by the positive nitrogen ion is a good example of this direct ion-induced mechanism by the reactive charge exchange process:

$$N_2^+ + CH_3OH \rightarrow CH_3^+ + {}^{\bullet}OH + N_2$$

For all three abovementioned mechanisms of VOC destruction, energy consumption for the gas purification process is directly related to ionization energy. The higher the electric field, the higher the average electron energy, and the greater than the fraction of the total discharge power that will go into ionization, increasing the efficiency of the VOC-destruction process. This fact is one of the key points for applying cold discharge technology to environmental control processes.

1.6. Water Droplet- and Cluster-Enhanced VOC Destruction

The effect of humidity on plasma-chemical efficiency was studied by several authors. While several reports have noted that the humidity has little or no effect, the other reports say that the effect of humidity is detrimental for the removal efficiency. In this thesis the independent investigation of the role of water was carried out.

Ions produced in an atmospheric-pressure discharge are natural nuclei and would stimulate water condensation or cluster formation. The effect of droplets is also dual. Liquid phase catches positive ions and ozone molecules. Captured species induce formation of OH radicals in droplets. The radicals very efficiently destroy VOC molecules when they encounter the droplet.

The experimental data presented in this thesis showed some interesting patterns of dependence of VOC destruction and removal efficiency on water concentration. It has to be noted, however, that even though the diverse role of water for VOC treatment is recognized, quantitative models of all these effects are yet to be developed.

1.7. Ultraviolet VOC Destruction

Ultraviolet (UV) radiation in plasma can also be effective in selective dissociation of VOC (Rusanov and Fridman 1984). Although this effect is not a primary decomposition mechanism in non-equilibrium plasmas, plays a very important role as an ancillary VOC-destruction process. Typically, UV radiation emitted by the plasma discharge breaks molecular bonds.

While multiple VOC-destruction mechanisms take place in plasma processes, the primary mechanism involves the dehydrogenation of an organic site by a hydroxyl radical (*OH*) followed by attachment of oxygen as described in the following sequence of reactions.

$$R\text{-}H\text{-}H_2CH + OH^{\cdot} \rightarrow R\text{-}H\text{-}H_2C^{\cdot} + H_2O$$

$$R\text{-}H\text{-}H_2C^{\cdot} + O_2 \rightarrow R\text{-}H\text{-}H_2C - O\text{-}O^{\cdot}$$

The organoperoxide radical formed in the second reaction then reacts with another organic specie to form an organoperoxide while dehydrogenating the second organic molecule.

$$R\text{-}H\text{-}H_2C - O\text{-}O^{\cdot} - R\text{-}H\text{-}H_2CH \rightarrow R\text{-}H\text{-}H_2C - O\text{-}OH + R\text{-}H\text{-}H_2C^{\cdot}.$$

The organoperoxide is unstable and decomposes to a new specie of one less carbon atom than the original compound and either formaldehyde or formaldehyde radical, which is rapidly oxidized by oxygen to carbon dioxide and water.

$$R\text{-}H\text{-}H_2C - O\text{-}OH \rightarrow R^{(n-1)}\text{-}H + (H_2CO \text{ or } HCO^{\cdot})$$

$$H_2CO \text{ or } HCO^{\cdot} + O_2 \rightarrow CO_2 + H_2O$$

Aromatic and unsaturated organics follow a slightly different decomposition mechanism but are both eventually decompose to carbon dioxide and water. In general, the unsaturated compounds are easier to decompose. The chain of plasma-chemical reactions shown above can be also initiated by atomic hydrogen or nitrogen, but these branches are significantly less probable.

It is seen that presence of considerable amount of water in the treated air is essential for effective destruction of VOC. The electron energy is the primary factor in efficiency of all major plasma-chemical mechanisms of VOC destruction. From this point of view the quality of plasma

produced by electrical discharges or electron beams is different. Table II summarizes the features of major plasma technologies for VOC abatement applications.

TABLE II. COMPARISON OF NON-THERMAL PLASMA TECHNOLOGIES ([1])

Plasma Technology	Average Electron Energy	Capital Cost, $/W	Unit Capacity, kW	Energy Consumption, kWh/m^3	Known Applications	Technical Limitations
Electron Beam Technology	5-6 eV	2.0	1,000	10 - 70	Removal of SO_2, NOx in thermal power plants	Initial energy of electrons in the beam is limited by 1.5 MeV due to x-ray production
Gas-Phase Corona Reactor (GPCR)	2-3 eV	2.1	20	6 - 70	Electrostatic Precipitators	The voltage cannot be as high as in pulsed corona due to spark formation; packed bed limits flow rates.
Pulsed Corona Discharge	3-5 eV	1.0	10	20 - 150	Removal of polyatomic hydrocarbons in aluminum plant	Voltage is limited by the electrical network coupling and capacitance and inductance of the plasma reactor
Dielectric-Barrier Discharge (DBD)	2-3 eV	0.2	0.1	20 - 200	Removal of SO_2, NOx, industrial ozone generators	The voltage cannot be as high as in pulsed corona due to spark formation; low unit capacity
Gliding Arc	1-1.5 eV	0.1	120	20 - 250	Laboratory study on removal of methanol, o-xylene	Discharge is non-uniform, high temperatures of the gas, possible NOx generation.

Electron beams produce plasma of the best quality with average electron energy of 5-6 eV. Pulsed corona discharges stand very close (3-5 eV). But corona discharges have advantage of lower capital cost. Generally, both technologies have already found applications for gas treatment form NO_x and SO_2 emissions in coal power plants. Capability of treating large gas streams make e-beams and pulsed corona discharges the primary candidates considered for VOC abatement.

1.8. Goals of the Forest Project

The goal of this project is to test four candidate VOC control technologies based on non-thermal plasma, and demonstrate the best technology on a mill. They are: 1) dielectric packed bed corona discharge (GCPR); 2) electron beam discharge; 3) non-thermal gliding arc discharge; and 4) heterogeneous pulsed corona discharge. The development of the last two technologies (gliding arc and pulsed corona discharge) will be discussed in this thesis.

The target streams for this study are the vent streams from brownstock washers and oriented strandboard presses and dryers. Very little data exists on contaminants of interests in the forest products industry and test conditions were far from typical industrial streams.

Press vents are especially attractive for application of non-thermal plasma due to it intermittent nature. Most of the time press vents operate with very little concentration VOC. However, a spike of VOC is emitted when the press is open. This spike can create problems for thermal control technologies. They are wasting the energy during a great fraction of the operation cycle. Non-thermal plasmas, on the other hand, are essentially "instant on". This opens the opportunity for operating non-thermal plasma device "off" or "idle" until just before the spike arrives and then turn on (or increase) the power for the duration of the spike. Significant energy savings are expected from this type of "pulsed" operation.

The laboratory experiments will determine which of the four plasma technologies would be most suitable for treating specific VOC emissions of concern to the wood products industry. Simulated VOC emissions (typical of current operations) will be prepared in the laboratory by blending a combination of gases and liquids to obtain realistic gas compositions, humidity, and temperatures as shown in Table III. Concentrations during spikes are described as the worst-case scenario. The feed gas compositions will be confirmed chromatographically.

TABLE III. TYPICAL STREAM COMPOSITIONS CONSIDERED IN THE PROJECT

	HVLC Brownstock Washer Went Emissions	**Oriented Strandboard Press Vent Emissions**	**Oriented Strandboard Dryer Vent Emissions**
Gas Composition:			
Acetaldehyde	-	-	7 ppm
Dimethyl Sulfide	2 ppm	-	-
Methanol	83 ppm	25 ppm	8 ppm
Acetone	3 ppm	1 ppm	28 ppm
Terpenes	209 ppm	4 ppm	16 ppm
1,2,4-Trichlorobenzene	-	-	2 ppm
Acrolein	-	-	2 ppm
Humidity	100% RH @ 110°F	70% RH @ 100°F	90% RH @ 200°F
Process Conditions:			
Temperature	110°F	100°F	200°F

The demonstration of the selected technologies will be conducted at mills selected by Georgia-Pacific Corporation. These demonstrations will allow us to validate performance over typical mill operating conditions, determine equipment performance over an extended (2-4 months) period, and determine maintenance requirements, which will govern the true cost of ownership.

1.9. Development of the Trailer-Mounted Pilot Plant

The ultimate goal of this project is testing the prospective pulsed corona technology at actual on-site operating conditions of the process plants in paper industry. A Louisiana paper mill plant of Georgia-Pacific Corporation in Port Hudson was selected for the testing, scheduled for Fall 2002. The testing on streams from the Brownstock Washer Vents will be the introductory phase of the pilot testing. In case of successful operation in Port Hudson, the technology should be demonstrated on exhaust streams from the Oriented Strandboard Press Vents and from the Oriented Strandboard Dryer Vents. The major compounds being treated in all three cases are essentially the same. However, their concentrations, temperatures and absolute humidity of the exhaust gases might differ.

Recognizing the need to evaluate nonthermal plasma technology for application in the forest products industry, National Council for Air and Stream Improvement (NCASI) reviewed the technology options.

Table IV shows the input data on VOC used in the report [1] issued by NCASI in 1999. The expected gas composition of in the paper mill considered in the report appeared to be significantly below the real concentration of noxious species in the vent stream ("the worst-case scenario").

TABLE IV. COMPARISON OF DATA ON BROWNSTOCK WASHER VENT EMISSIONS

Composition	NCASI	"The worst case scenario"
Dimethyl Disulfide	2 ppm	20 ppm
Dimethyl sulfide	-	1727 ppm
Methanol	83 ppm	2330 ppm
Acetone	3 ppm	-
Terpenes	209 ppm	62 ppm
H_2S	-	Up to 100 ppm
Conditions		
Temperature	103 F	150 F
Relative Humidity	100 %	100 %

The following differences of "the worst case scenario" must be underlined because they constitute additional challenges for the successful pilot plant operation.

Concentrations of methanol and dimethyl sulfide exceed the expected value about 20 times. Such concentrations of VOC are very challenging for the corona unit to be designed. Typically, corona is most feasible for concentration of VOC in the range of 100 ppm.

Methanol, presented in such amounts, must be removed in the earliest stage. Otherwise, it will degrade the performance of the corona by consuming a major fraction of the active radicals produced by corona.

The stream contains dangerous amounts of H_2S. It is about 100 times larger than the threshold limit imposed by regulations. Additional technical measures would be required to maintain the safety of the pilot plant operation.

Presence of large amount of water in the stream makes it difficult to predict performance of the pilot plant at high absolute humidity and at elevated temperatures. Water molecules change the property of the discharge and also might take effect on chemistry.

The evident lack of experimental data for the given substances and on performance of the pulsed corona at high absolute humidity, high concentration of VOC, and at elevated temperatures, motivated the research presented in this thesis.

Actual demand of capacity of the process gas treatment equipment in the paper mills exceeds 100,000 standard cubic feet per minute. It is expected that such treatment facility will be built from basic units of much smaller capacity (about 1:100). From the purpose of technology demonstration, it is sufficient to test in field just this unit for the time comparable with actual lifetime of the equipment or with maintenance cycle. It was proposed to test the pilot plant for at least 3 weeks in the regime of continuous operation. Table V summarizes the chosen design parameters of the pulsed corona pilot plant. Research and development of the pilot plant was done in collaboration of several organizations.

University of Illinois at Chicago (later Drexel University) leaded the effort. The author of this thesis supervised the design of the pilot plant hardware and did the engineering work on integration of the pilot into the trailer, proposed the program of on-site testing. Research on physics and chemistry of pulsed corona discharge was done in collaboration with Mario Sobacchi and Dr. Andrey Romanets, and under the supervision of Professor Alexei Saveliev. The

feasibility study and theory development of the gliding arc discharge was completed in collaboration with Mario Sobacchi and Inga Kuznetsova.

TABLE V. OPERATIONAL PARAMETERS OF THE PULSED CORONA PILOT PLANT

Gas flow rate	Up to 600 m^3/hour
Consumed Electric Power	Up to 10 kW
Consumption of water for the scrubber and corona units	Up to 0.7 m^3/hour
Consumption of compressed air for the spray	40 m^3/hour
Pressure of air inside the pilot plant	6 negative inches of water (vacuum).

ECOS Ltd (Kurchatov Institute of Atomic Energy, Russia) developed a prototype corona cell that was used to build a pilot plant. They built the pilot plant hardware.

Georgia-Pacific Corporation paper mill plant in Port Hudson was chosen as a place for the testing.

Argonne National Laboratory provided the expertise on project management and interfacing with local engineering teams.

Pacific Northwest National Laboratory developed a packed-bed corona pilot installation for testing according to phases II and III of the project.

Joint efforts of the team succeeded in conceptual 3D design of the mobile pilot plant (Figure 1) and in development of logic of its operation.

The pilot plant will be mounted on a 48-foot long single-drop flatbed trailer to minimize the overall height. A standard 10-foot long mobile office will serve as a control room and an analytical laboratory.

As seen in Figure 1, the pilot plant seems very tall and narrow. Its center of gravity is high. Unfortunately, the vertical dimension is the least customizable. It is set for the given mass transfer rate in the scrubber and in corona, and is less than the height of bridges on the highways. To avoid flipping of the trailer in the sharp turns, it must be much heavier than the plant. For the selected trailer this condition holds.

The width of the installation should not exceed the width of the trailer and should allow some space around the plant for service work. Narrow cargo helps stabilize the trailer at high speeds on highways and at side winds.

The installation is centered with respect to the longitudinal axis of the trailer. For this, the preliminary design of the pilot plant was modified to move very heavy transformers from the side to the front of the trailer.

1.9.1. Description of the Design of the Mobile Pulsed Corona Plasma Pilot Plant

According to the concept of operation, the pilot plant incorporates three different cleaning technologies, represented by individual modules: a) scrubber; b) pulsed corona module; c) activated carbon bed/mist separator module. All three modules are assembled as a single unit with a common enclosure. Auxiliary equipment, including a waste water pump, air blower and high voltage transformers, will be mounted outside the enclosure directly on the flatbed.

Scrubber

The air with VOC is supplied for treatment to an incineration facility by a major vent pipeline. To avoid potential hazards due to leakage, the air in the pipe is always under slight negative pressure (vacuum) of 6 in of water. The pilot plant works on the same principle. The flow through the modules is sustained by a powerful auxiliary blower capable of producing up to more than 10 negative inches of pressure with the required flow rate. It is located downstream of the pilot plant on the exhaust pipe. A 6-in diameter flexible hose will connect the pilot and the vent. If the blower should fail or the hose should leak, the air will be sucked back into the major pipe, so no dangerous release of VOC would occur.

The air might contain a large amount of methanol (up to 2000 ppm) along with other more dangerous VOCs. Fortunately, methanol is highly soluble in water and could be removed by scrubbing. The water is sprayed on the scrubber packed bed, which is about 6 feet high and is filled with porous media enhancing mass transfer between the liquid and gas phases.

Downstream of the scrubber, the water will be virtually free from methanol. The air will contain 100% of relative humidity. As will be seen in the research part of this thesis, the operation of corona in humidified air is more efficient, than with dry air.

Pulsed corona module

The design of the corona module is very similar to scrubber. Instead of a packed bed, there are 12 standard corona "blocks" (4 stacks x 3 blocks). The design of a corona block is shown in Figure 2.

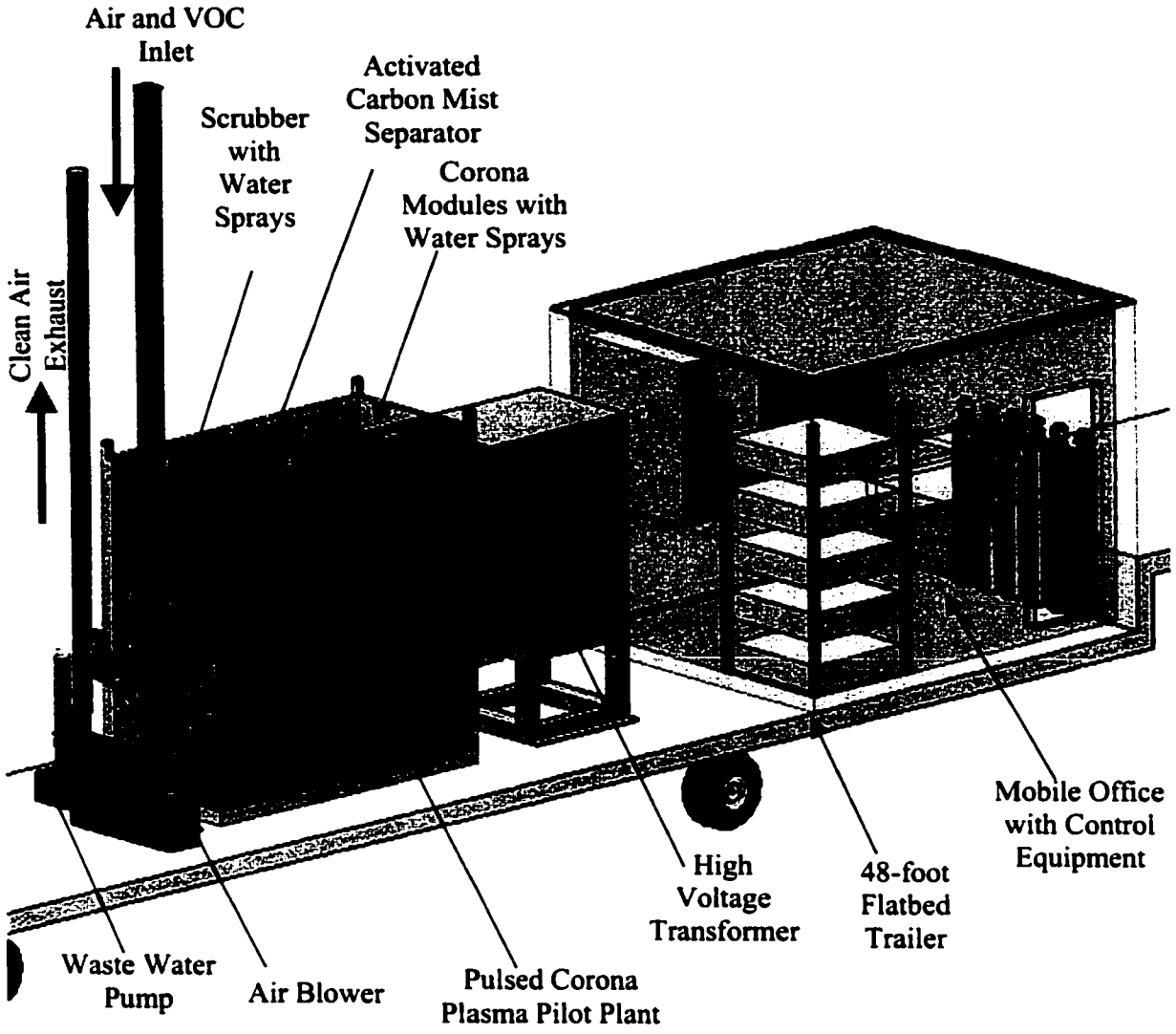

Figure 1. A 3D-view of the trailer-mounted pulsed corona pilot plant.

The block consists of intermitting layers of negative and ground electrodes. Such configuration creates a quasi-uniform volumetric discharge with minimum dead volume. The sprayed water plays a multiple role. It could dissolve some additional amounts of non-soluble

compounds such as dimethyl sulfide or terpenes (primarily alpha-pinene) in accordance with Henry's law.

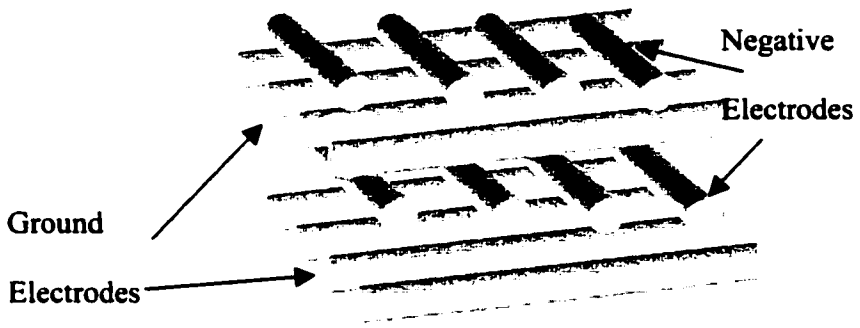

Figure 2. Design of a corona block.

But water also dissolves dangerous byproducts of VOC destruction. This fact is very useful for applications. Instead of converting VOCs completely into final products such as CO_2 and H_2O, one can spend much less energy on creation of solvable byproducts with OH groups. Solubility of such molecules is higher due to polarity of OH groups. Therefore, higher removal rates could be achieved in scrubbing of non-soluble in water compounds. Once in the solution, the organic material could be treated by more efficient methods such as biofiltration.

Droplets of water capture significant amount of ozone. Whereas ozone does not react with molecules of VOC in the gas phase, in the water it immediately creates additional OH radicals that hunt for primary VOC, dissolved in water according to Henry's law, or for byproducts. This also increases the overall efficiency. The effect of enhancement should be pronounced in strong alkaline solutions (pH > 9), because the solubility of ozone exponentially increases with pH.

Mist Separator

It is desirable to collect and recycle all the water sprayed over the corona. The droplets with sizes smaller than 0.1 mm will be drugged away by air. Therefore, the sprays in scrubber and corona modules should produce droplets larger than 0.1 mm. However, too large droplets should be also avoided because they reduce the surface for mass transfer. In the current pilot plant the sprays produce droplets with diameters in the range between 0.1 and 1 mm.

A stack of trays with activated carbon in the mist separator will effectively retain the droplets. After the corona module, the stream will contain very small amount of VOCs. Those quantities are very difficult and expensive to treat. But the carbon will retain the rest of VOC and byproducts on its surface and accumulate them for some additional time. It is known that the surface also promotes reactions of ozone with organics. The reaction rate of ozone on the surface of activated carbon will be high, and less than 1 ppm of VOC will be expected to leave the pilot plant after the mist separator.

Control Equipment

The advantage of pulsed corona is in the possibility to adjust its power by changing the pulse repetition rate (PRR). As will be described later in this thesis, the production rate of free radicals in corona is proportional to the corona power. It was found by the modeling of corona chemistry that VOC react with free radicals according to the first-order reaction. Therefore, there is an almost linear dependence of VOC destruction rate on corona power.

The control network of the corona pilot plant consists of several instruments. The Total Hydrocarbon Analyzer (THC, TEI Inc) is a robust industrial instrument capable of instant monitoring of the hydrocarbon concentration in the gas stream. The sample of air is burnt in the hydrogen flame in the Flame Ionization Detector (FID) that produces the electrical signal

proportional to hydrocarbon concentration. The signal is logged into the Data Acquisition System (DAQ) based on a PC-type computer. DAQ adjusts the output power of the corona control module via the pulse repetition rate. The Gas Chromatograph / Mass Spectrometer (GCMS, Varian Inc.) takes periodic sampling of the exhaust gas. GCMS work cycle is from 1 to 15 minutes. Therefore, instant control over the exhaust is impossible. Fortunately, the VOC concentration in the major vent pipe changes very slow with cycle of about 30-60 minutes. So, the presented instrumentation will be sufficient for the pilot operation to demonstrate the technology and maintain safe operation.

1.10. Scientific Problems and Research Objectives in Development of the Wet Pulsed Corona Technology

In previous paragraphs we discussed the hardware for demonstration of the pilot pulsed corona technology. The logic and optimization of its testing and foregoing operation demanded specific data on physics and chemistry of the discharge at conditions of the "worst case scenario". The summarized peculiarities of this scenario are:

1. Concentrations of major components are out of the guaranteed operational range of corona.
2. Poisoning of discharge with methanol.
3. Large amount of water in the stream.
4. Possible variation of stream temperature (operation of corona with or without sprays).
5. Existence of the liquid-gas interface in the discharge.

Some items in the list above would constitute a real technical problem. The information on others would bring new knowledge on plasma chemistry and physics of non-equilibrium atmospheric-pressure discharges. Let us state the relevant objectives of the research. The

testing and further application of the pulsed corona technology to treat VOC emissions in the forest products industry.

Here we underline the tasks to fulfill this objective.

1. Investigate the possibility of operating corona reactors at high (>1000 ppm) concentrations of VOC, particularly with large content of methanol, DMS and acetone.
2. Study the effects of absolute humidity and temperature on the removal efficiency of VOC.
3. Develop a model of corona chemistry using a sample substance (methanol).
4. Using the model categorize the nature of observed effects (physical, chemical).
5. Predict removal of the other VOC (provided the detailed chemical mechanism for these compounds is known).
6. Develop recommendations for the operational regimes during testing of the pulsed corona pilot plant.
7. Develop relevant figures of merit and compare pulsed corona technology with gliding arc.

Following these objectives, a theoretical and experimental work on corona discharges and gliding arc will be presented in the next chapters.

2. NON-EQUILIBRIUM LOW-CURRENT GLIDING ARC DISCHARGE

2.1. Introduction

The gliding arc is a high-pressure gas discharge with high electron temperature and density and has been proposed for chemical gas processing [2]. The arc (Figure 3) starts in a narrow gap between two or more diverging electrodes in a gas flow when the electric field in this gap reaches approximately 3 kV/mm in air [4]. Then the arc current increases very rapidly, and the voltage on the arc drops. If the gas flow is strong enough, it forces the arc to move along the diverging electrodes and to elongate. The growing arc demands more power to sustain itself. At the moment when its resistance becomes equal to the total external resistance, the discharge consumes one-half of the power delivered by the source. This is the maximum power that can be transferred to the arc from the constant-voltage power supply. Next, the length continues increasing, but the supplied power will be insufficient to balance the energy lost in heat transfer to the surrounding gas. The arc cools down and finally extinguishes. The next cycle starts immediately after the voltage reaches the breakdown value, usually just after the fading of the previous arc. (If the voltage is high enough, and the gap is very narrow, a new arc starts even before extinguishing of the old one [8]). A typical repetition rate of the arc is in the range from 10 Hz to 100 Hz and changes with the gas flow rate: the higher is the flow rate, the higher is the frequency.

Unlike regular high-current thermal arcs where both gas and electron temperatures (T and T_e) could be as high as 10000K, the low-current (from 0.1 to 1 A) gliding arcs are believed to operate in non-equilibrium regimes ($T < T_e$), and have low gas temperatures.

The arc voltage could be as high as several kilovolts. Typical vibrational and translational temperatures of the gas in a low-temperature gliding arc were measured to be respectively about 2000 – 3000K and 800 – 2100 K [3]. Similar features are also intrinsic for microwave discharges. It shows that low-current gliding arcs could be definitely useful for plasma chemistry.

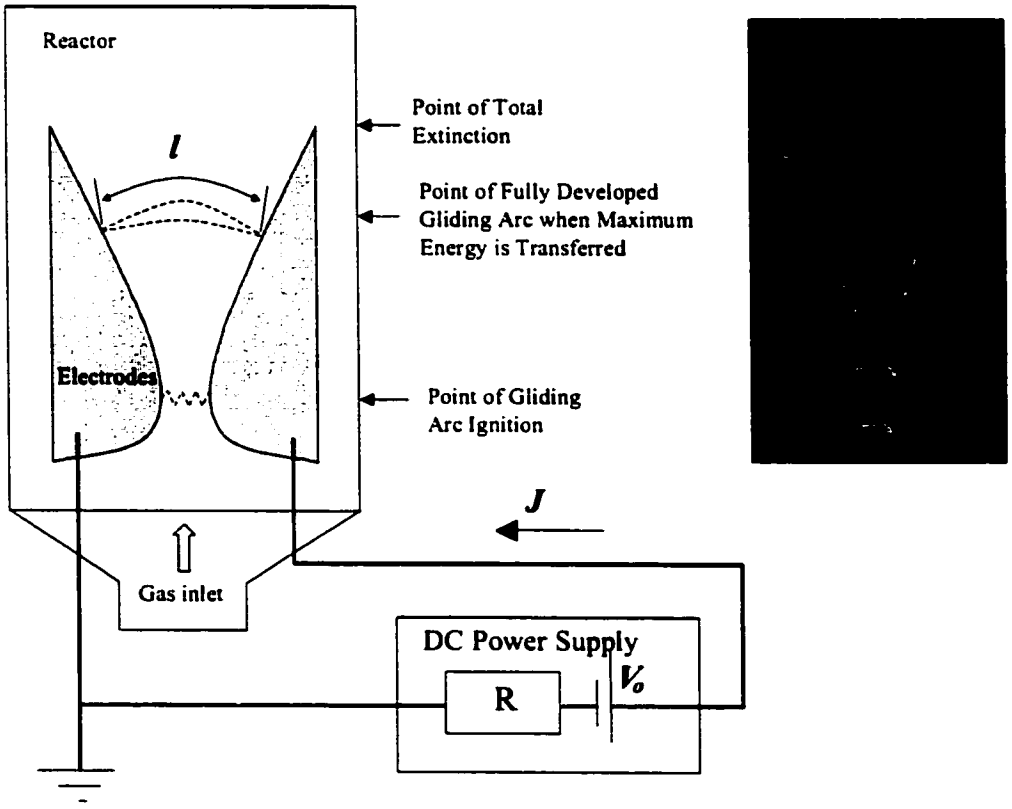

Figure 3. Electrical Schematic of the DC Gliding Arc.

The physics of the gliding arc evolution is not well understood, especially the development of non-equilibrium conditions and stability at diminishing currents. Older models [9] did not account for variation of plasma conductivity and temperature during the gliding arc progress.This approach did not explain some recently discovered non-equilibrium effects in the low-current gliding arcs. An interesting and important experimentally observed [10] feature of such arcs is an effect here after called "overshooting". It refers to unexpected continuation of the gliding arc cycle after the maximum power was achieved (Figure 4).

Mario Sobacchi [13] investigated the possibility of removal of specific chemical compounds with a low-current gliding arc discharge. A typical value of energy consumption for this discharge was 1 $kW \cdot hr/m^3$, when the targeted value was 0.02 $kW \cdot hr/m^3$. It was noted that non-uniformity of the discharge imposes certain difficulties to treat the gas efficiently. Experiments were performed using three different external resistance values, i.e. 25, 50, and 100 kW. The output voltage of the power supply was 10 kV, when the air flow rate ranged from 20 to 80 SLM.

Methanol (100 to 1000 ppm) was used as a substance to demonstrate viability of the gliding arc technology. In some runs, water was sprayed along the flow direction. It was found that at 20 SLM of air and independently of VOC concentration, all methanol was removed from the stream at power consumption of 0.2 $kW \cdot hr/m^3$. No organic byproducts were detected by Gas Chromatography in the exhaust stream. The results were interpreted as encouraging, showing the possibility for further reduction of power consumption. Unfortunately, NO_x was detected in the exhaust at level of 3000 ppm, much exceeding all reasonable limits. It could be expected, however, that for more non-equilibrium arcs with lower currents or higher flow rates of air, the temperature of the arc channel will be lower, and reasonable levels of NO_x will be achieved.

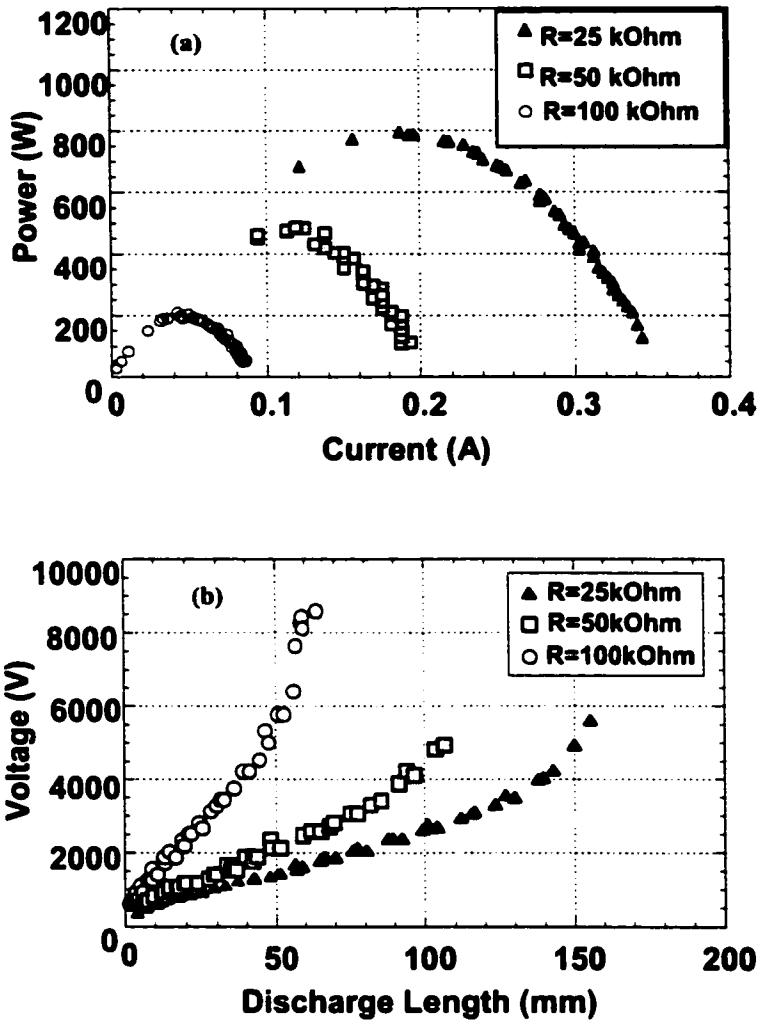

Figure 4. (a) Current – Total Power Experimental Dependence from [9]. The arc evolutes from the state of maximum current and minimum power to the critical point (I_{cr}, P_{max}; negative slope) where it should extinguish in accordance to previous models [6]. But these experimental results demonstrate existence of the arc even after the critical current was reached (positive slope); (b) Discharge Length - Voltage of the Gliding Arc in (a).

In this thesis a new model explaining the evolution of the low-current gliding arcs is presented. Below the factors giving rise to "overshooting" will be discussed in terms of stability of major parameters of the gliding arc. Analytical and numerical solutions explain the general behavior of the low-current gliding arc and are in a good agreement with experiment.

2.2. Phenomenology

There are few parameters to consider in the analysis of the gliding arc. In this section the phenomenology of the discharge and a possible range of major parameters will be discussed.

The characteristic time τ_i of arc formation can be found from the kinetic equation for the electron concentration

$$\frac{dn_e}{dt} = k_i n_e n_o = n_e/\tau_i \qquad (1)$$

where k_i is the ionization constant, and n_e and n_o are electron and gas concentrations. The estimates for clean air and electric current of the arc $J = 1$ A give the value $\tau_i \approx 1$ μs [5]. Within this time, low-resistance plasma is formed and the voltage between the electrodes falls. Usually the time of the arc formation is less than 0.1% of the total gliding arc cycle time.

The arc moves with the gas flow. At small flow rates the velocities of the arc and of the gas are nearly equal. It was shown for relatively small power (200 W) that there was no difference between the absolute velocities of the gas (10 m/s) and that of the gliding arc [6]. At higher power levels (~ 2 kW and above) and flow rates as high as 830 to 2200 cm^3/s (according to our assessments based on data from [7], this flow rates correspond to the range of velocities from 11.5 to 31 m/s), the difference in velocities increases from 1 to 10 m/s. Authors of Ref.[8] showed how the relative velocity of the gliding arc changes with the discharge parameters.

Propagation of the gliding arc can be studied for two types of reactors: 1) Diverging-flow reactor (velocity of the gas decreases when the length of the arc increases, heat losses per unit length of the arc decrease along its path) [8]; 2) Uniform-velocity reactor (gas velocity is the same at every point of the reactor, heat losses per unit length are approximately constant) [9]. For both reactors there were developed qualitative and quantitative theories of arc propagation [8, 12]. Electric parameters of the gliding arc were considered analytically [8, 9] and numerically [8]. Properties of the particular gliding arc can depend on the arrangement and presence of different elements in the electric circuit. Typically, gliding arc discharges have been studied with an external resistance R and a constant-voltage power supply (Figure 3). It is unsurprising, however, that the results obtained on each type of the reactor could not be easily compared with those obtained on a different reactor. Here after a setup with a uniform-velocity reactor (Figure 3) will be considered.

A simple model of the gliding arc was developed from Ohm's law [9]. Power W per unit length (specific power) and energy losses per unit length (specific losses) were assumed constant. The analysis with these assumptions showed that the current of the arc drops to one half of the initial value during the cycle. Obviously, a substantial change of the current should change the arc temperature. So in the current analysis we shall take into consideration the dependence of the arc temperature on current and the dependence of plasma properties on temperature and electric field.

For any kind of gliding arc Ohm's law can be written in the form

$$V_0 = RJ + \frac{Wl}{J} \tag{2}$$

where R is the external serial resistance (Figure 3).

Solve (2) for current:

$$J = \frac{V_o \pm \sqrt{V_o^2 - 4WlR}}{2R} \tag{3}$$

The "+" solution corresponds to a quasi-steady state of the gliding arc column. In case of $W = const$ the "-" implies a negative differential resistance of the circuit

$$\rho = \frac{dV}{dJ} = 2R - \frac{V_0}{J} < 0 \tag{4}$$

and leads to an unstable regime.

As one can see from Eq.(3), the total power of the arc $P = W\,l$ cannot exceed maximum power

$$P_{\max} = \frac{V_0^2}{4R} \tag{5}$$

because if $P > P_{max}$, the expression under the square root becomes negative and no real solution exists.

At constant specific power, P changes only when the length of the arc column l increases. A critical (maximum) value of length

$$l_{cr} = l_0 = \frac{V_0^2}{4WR} \tag{6}$$

cannot be exceeded. Any additional increment of the length would cause the arc instability. That is why in the case of a thermal arc, a fast transition to non-equilibrium (FENETRE) state may take place [5]. The arc would instantaneously and sharply extend. As a final result of transition, the gas in plasma would rapidly cool to temperatures about 1000 - 2000K. Simultaneously, electric field E should increase together with the electron temperature T_e, and the discharge might be sustained for an additional period of time. This post-transition period could constitute a small portion of the total gliding arc cycle time [10]. But in applications, most of the useful plasma chemistry would take place only in this minor interval because only here would T be low enough.

This effect called "explosion of length" was studied in [9]. According to the theory presented there, during such a transition the length l could be as large as 3 l_{cr}. Authors of [3] observed this phenomenon. Other researches [10] could not confirm the "explosion" effect and made a conclusion that the transition between equilibrium and non-equilibrium regimes is smooth. The lack of reproducibility could be probably explained by the influence of some additional parameters of the experimental setup that were not taken into account.

Recent experiments [10], where the total power and plasma voltages were measured as functions of electric current and plasma length (Figure 4), demonstrated some stability of the arc in the "overshooting" regime. When the power of the arc reached maximum possible value, the arc did not extinguish as fast as it was expected. Instead, the power began smoothly decrease and the plasma channel was still visible for considerable time. To explain this phenomenon we take into account that the arc current drops during the cycle, and a substantial change in the current should alter the arc temperature and specific power. A new model of the gliding arc incorporating these features will be described in Section 2.3.

It will be seen later that the theory with $W = const$ underestimated the range of stability of low-current arcs. But it can be used for assessments in cases with a limited set of given parameters such as R, V_0 and I.

The stability analysis of energy balance equation and Ohm's law is carried out in Section 2.4. The energy balance equation and Ohm's law will be solved analytically and numerically in Section 2.5. In section 2.6 we shall discuss the results obtained using our model.

2.3. Transient regime of the gliding arc discharge

It is possible to distinguish the transient regime in the low-current gliding arc evolution. The gas temperature T decreases and departs from electron temperature T_e. The temperature-

sensitive mechanism of thermal ionization yields to the field-sensitive mechanism of direct electron impact ionization. Therefore, one should consider the presence of both mechanisms for modeling. The form of the governing balance equations would remain the same, but now the electrical conductivity must be dependent on the electric field as well. In the following analysis, we introduce a simple form of the field-dependent approximation, which still permits a linear stability analysis.

Consider the arc as a symmetric cylindrical column. The electric field E is aligned with the longitudinal axis and is assumed to be uniform within every cross-section of the arc. All other plasma parameters depend only on the arc radius r_o (Figure 5).

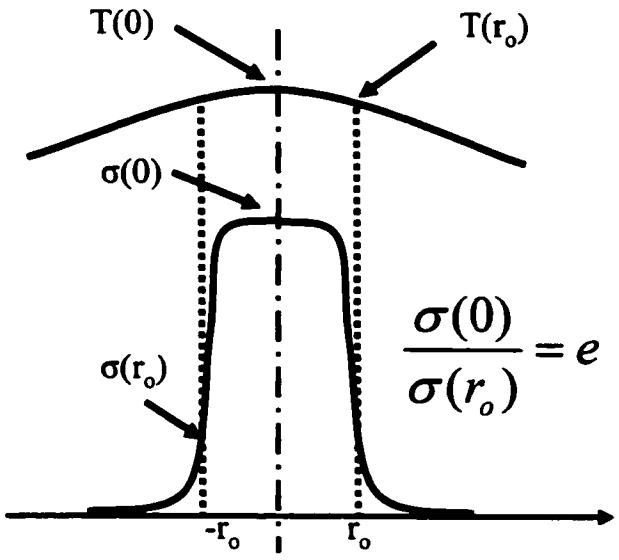

Figure 5. Variables used to describe the arc channel. The radius of the arc is defined by the ratio of conductivities equal to "e" (after Raizer [4]).

A heat transfer balance equation of a quasi-steady arc is derived in accordance with the Elenbaas – Heller model [4]:

$$\frac{1}{r}\frac{d}{dr}\left(r\lambda\frac{dT}{dr}\right)+\sigma(T,E)E^2=0, \tag{7}$$

where $\sigma(T, E)$ and $\lambda(T)$ are the electric and heat conductivity at temperature T and electric field E.

The second equation is Ohm's law in the form:

$$V_0 = JR + El. \tag{8}$$

The first term on the right-hand side of Eq.(8) is the voltage on the resistor R when the current $J = \int \sigma(T,E)E\,dS \approx \sigma(T,E)ES$ flows through the network. Here S is the transversal cross-sectional area of the arc. The second term is the voltage on the plasma column. The electrical conductivity of plasma is taken as a following function of temperature and electric field [4]:

$$\sigma(T,E)=\sigma_0\exp\left(-\frac{I}{2kT_e(T,E)}\right), \tag{9}$$

where σ_0 is a constant for the given gas, k is Boltzmann constant, I is the ionization potential of the gas molecules.

The major difficulty here is to determine the dependence of T_e on T and E. For thermal plasmas $T_e = T$ and the electric conductivity depends solely on the gas temperature. For cold plasmas T_e depends on E only. The intermediate case under consideration, which is the most promising one for many applications, has not been studied in detail. For our semi-quantitative model it is reasonable to extend the equilibrium approach to more non-equilibrium cases by taking electron temperature T_e in a simple form [10]:

$$T_e = T\left(1+\frac{E^2}{E_i^2}\right), \tag{10}$$

where E_i is a reference value of the electric field characterizing transition from thermal to direct electron impact ionization [11]. This value is about 1 kV/cm for air at standard conditions [4]. In the present work the case for which $E < E_i$ is considered. The formula (10) shows that if the arc is almost thermal, its electric conductivity mainly depends on the temperature. The effect of electric field is more significant or even prevailing in transitional and non-equilibrium regimes.

A temperature dependence of thermal conductivity can be expressed as in [4]

$$\lambda(T,E) = \lambda_o \exp\left(-\frac{D}{2kT}\right), \tag{11}$$

where λ_o is a constant, and D is the energy of dissociation.

The logarithmic sensitivities of the electrical and thermal conductivity to gas temperature can be found from Eq.(9) and Eq.(11):

$$\sigma_T = \frac{\partial \ln \sigma(T,E)}{\partial \ln T} = \frac{I}{2kT}, \tag{12}$$

$$\lambda_T = \frac{\partial \ln \lambda(T,E)}{\partial \ln T} = \frac{D}{2kT}, \tag{13}$$

as well as the logarithmic sensitivity of electric conductivity to electric field:

$$\sigma_E = \frac{\partial \ln \sigma(T,E)}{\partial \ln E} = \frac{I E^2}{kT E_i^2}. \tag{14}$$

We shall use Eqs. (12), (13) and (14) for stability analysis in the next section.

The radius of discharge r_o is defined as the distance from the center of the arc to the point at which the electric conductivity drops "e" times (Figure 3 and Ref. [4]):

$$\frac{\sigma(0)}{\sigma(r_0)} = e. \tag{15}$$

The area $S = \pi r_0^2$ is expected to increase with the electric field when the discharge becomes more non-equilibrium. Let us introduce the temperature drop across the arc $\Delta T = T(r_0) - T(0)$. If the temperature behaves as a smooth function of r, it could be expanded in a Taylor series in the vicinity of $r = 0$: $T(r) \approx T(0) + 1/2(\partial^2 T/\partial r^2)_{r=0} r^2$. After rearrangement:

$$\frac{\Delta T}{T} \approx C(T) r_0^2 \quad . \tag{16}$$

Here $C(T)$ is a smooth, slowly changing function of T.

At the same time, from Eq.(9) and Eq.(15):

$$\frac{\Delta T}{T} \approx \frac{2kT}{I}\left(1+\frac{E^2}{E_i^2}\right). \tag{17}$$

Combining Eqs.(16) and (17):

$$S = S_0\left(1+\frac{E^2}{E_i^2}\right), \tag{18}$$

where S_0 is a field-independent coefficient. So, as we expected, the area S increases with the electric field.

Integration of Eq. (7) (see [10]) with $\Delta T/T$ taken as in Eq.(17) results in the following thermal balance equation:

$$\sigma(T,E)E^2 = \frac{16\pi\lambda(T)kT^2}{IS}\left(1+\frac{E^2}{E_i^2}\right), \tag{19}$$

This formula establishes the relationship among the thermal conductivity, electrical conductivity and the electric filed. Equations (18) and (19) of the new model will be used in the next sections for the stability analysis and simulation.

2.4. Stability analysis

According to Ohm's law, the sum of voltage El on the arc and the voltage on the serial resistance R must not exceed the constant external voltage V_0 in Eq.(8). The development of non-equilibrium conditions in the growing gliding arc eventually results in the discharge instability followed by the arc termination. When unstable, the arc cannot exist and propagate for a considerable time. The matter of interest here is to understand whether the arc is still stable in "overshooting", or just decays.

A stability analysis will be done for the thermal balance Eq.(19) taken in a time-dependent form:

$$\rho C_P \frac{dT}{dt} = \sigma(T,E)E^2 - \frac{16\pi k \lambda T^2}{I S_0}, \tag{20}$$

where ρ is a density of the gas and c_p is its specific heat. Substituting electric current $J = \sigma(T,E)ES$ into Eq.(8)

$$V_0 = \sigma(T,E) E S R + E l \ . \tag{21}$$

Let us consider the temperature and electric field fluctuations in the forms

$$\Delta T(t) = \Delta T_0 \exp(\Omega t) \ , \tag{22}$$

$$\Delta E(t) = \Delta E_0 \exp(\Omega t) \ , \tag{23}$$

where ΔT_0 and ΔE_0 are the initial temperature and field perturbations, and Ω is the instability decrement. For a stable regime ($\Omega < 0$) the fluctuations will exponentially decay with time. Conversely, positive Ω will characterize instabilities, i.e. the fluctuations growing in time.

After substituting Eq.(22) and Eq.(23) into Eq.(9) and Eq.(11), and then linearizing the result, we obtained the relative fluctuations of electric conductivity σ and thermal conductivity λ in terms of sensitivities Eqs.(12) – (14):

$$\frac{\Delta\sigma(t)}{\sigma} = \sigma_T \frac{\Delta T(t)}{T} + \sigma_E \frac{\Delta E(t)}{E}\ , \tag{24}$$

$$\frac{\Delta\lambda(t)}{\lambda} = \lambda_T \frac{\Delta T}{T}\ . \tag{25}$$

Now, apply expressions for $\Delta T(t)$ and $\Delta E(t)$ together with Eq.(24) and Eq.(25) on Eqs.(20) and (21). Linearization and elimination of $exp(\Omega t)$ yields

$$\Omega \frac{\Delta T_o}{T} = \omega\left[(\sigma_T - 2 - \lambda_T)\frac{\Delta T_o}{T} + (2+\sigma_E)\frac{\Delta E_o}{E}\right], \tag{26}$$

where $\omega = \sigma E^2 / (\rho\, c_p\, T)$.

Linearization of Eq.(21) gives the relationship between ΔE and ΔT:

$$\frac{\Delta E}{E} = -\frac{\sigma_T}{\sigma_E + 1 + l/l_o}\frac{\Delta T}{T}\ , \tag{27}$$

where $l_o = \sigma\, S\, R$ is the same as l_o in Eq.(6), and it is the length of the arc column when plasma voltage becomes equal to one-half of the external voltage V_o (the point of maximal arc power).

From Eqs.(26) and (27):

$$\Omega = -\omega\left(\sigma_T \frac{1 - l/l_o}{\sigma_E + 1 + l/l_o} + 2 + \lambda_T\right). \tag{28}$$

This important result shows that the arc can be stable beyond the point of maximum power. Indeed, Ω is always negative at $l < l_o$ and becomes positive, i.e. the system looses stability, at some critical length $l_{cr} > l_o$:

$$l_{cr} = l_o \frac{\sigma_T + (2+\lambda_T)(\sigma_E + 1)}{\sigma_T - (2+\lambda_T)}\ . \tag{29}$$

Previously, a stability analysis was carried out in [3], but the decrease of energy losses during the gliding arc evolution was not taken into consideration. There the instability developed immediately after $l = l_o$, and l_{cr} was equal to l_o. In the experiments [5], the instability normally occurred at l significantly larger than l_o. Apparently, the new model is closer to reality for low

currents. Formula (29) does predict the "overshooting" effect as seen in Figure 4a: the total power of the arc reaches the maximum and then declines, and the arc is still stable.

If the system is stable at $l = l_0$, it would be natural to suppose the solution of Eqs. (19) and (21) exists in the vicinity this point. The expression under the square root in Eq. (3) stays positive because the temperature decreases, and so does W. Then the real solution should exist for $l > l_0$. At the same time, as we have mentioned above, the length cannot be indefinitely large because the voltage El of plasma is restricted by the constant external voltage V_0, and E grows together with l. From Eqs. (19) and (21):

$$\frac{dE}{dl} = \frac{E(\sigma_T - 2 - \lambda_T)}{\sigma S R\left[(\sigma_E + 1 + l/l_0)(2 + \lambda_T) + \sigma_T(1 - l/l_0)\right]}. \qquad (30)$$

Rewrite decrement Ω using Eqs. (28) and (30) in the form

$$\Omega = -\frac{\omega E(\sigma_T - 2 - \lambda_T)}{\sigma S R(dE/dl)(\sigma_E l_0 + l_0 + 1)}. \qquad (31)$$

Because the numerical value of $(\sigma_T - 2 - \lambda_T)$ is positive for our set of parameters, the arc would be stable and dE/dl would be positive, as expected. When l approaches l_{cr}, dE/dl blows up. So, the instability develops at the moment when E is close to its maximum possible value and the length could not be any larger.

This simple linear stability analysis revealed and underlined two important results: 1) The gliding arc remains stable during "overshooting" and 2) The instability appears only in the moment when the voltage drop on the serial resistance can no longer compensate the rise of the voltage on the gliding arc. These are the key points of understanding the experimental results [10] (Figure 4).

2.5. Numerical solution

To justify the applicability of our approach, in this section we examine how closely and in what range of parameters our model matches with the experiment.

Generally, the systems of non-linear equations such as Eqs. (18), (19) and (21) cannot be solved directly. A numerical solution will be discussed later. An approximate dependence can be obtained by taking a natural logarithm from both sides of Eq. (19). After rearrangement

$$\frac{I + D(1 + E^2 / E_i^2)}{2kT(1 + E^2 / E_i^2)} = \ln\left(\frac{16\pi k \lambda_0 T^2}{\sigma_o I S_o E^2}\right). \tag{32}$$

Numerically $D << I$ and $1 < (1 + E^2 / E_i^2) < 2$. Here the second term in the nominator on the left-hand side can be neglected. Due to the nature of the logarithm, the function on the right-hand side changes much slower than T. It can be treated as a constant value because in the model the temperature and electric field is not expected to change very much.

Finally,

$$T \approx \frac{A}{1 + E^2 / E_i^2}, \tag{33}$$

where A is a constant. This formula obtained from the balance Eq. (19) is very general, and extremely simple. It seems very useful and broadly applicable. The formula agrees with the experimental fact that when the current and temperature decrease, the electric field increases [10].

In the numerical solution, the ranges of E, T and S were found solving Eqs. (18), (19) and (21) simultaneously. The parameters were set in the following manner. The length l was varied from some minimum values (electrode gap) to the critical values l_{cr}, where solution did not exist. The cross-sectional area S was chosen as in experiments as well as external resistance R.

Constants σ_o, λ_o, I and D were found by fitting the experimental data [4]. The results of numerical solution of Eqs. (18), (19) and (21) are presented in Figure 6 – Figure 9. In Figure 6, the arc starts from large currents and small power (negative slope). Then it reaches maximum power P_{max} at currents J_o. According to the earlier model of the gliding arc [6], it should become unstable and instantly extinguish. Conversely, our calculations with variable specific power of the arc give solutions even after this point for $J < J_o$ up to P^* (positive slope). This is in a good agreement with experimental results [10] (Figure 4a).

The explanation of this "overshooting" effect could be illustrated using Figure 8 and Figure 9, showing calculated electric field strength and gas temperature for different lengths of the arc. Ohm's law restricts the total power of the arc by P_{max}. If the temperature remains constant, there will be no more power to support the arc after l_o ($l_o = l_{cr}$ at constant power losses). Actually, when the arc approaches the critical point, the temperature decreases (Figure 9) as does the power losses per unit length (W), helping to maintain $P_{max} = lW$.

Through the relationship Eq.(10) the model incorporates the change in ionization mechanism in the vicinity of the critical point. According to Eq. (33), the decreasing temperature gives rise to stronger electric fields (Figure 8). When the field approaches E_i this model incorporating a very simple dependence of T_e on T Eq.(10) is no longer applicable. For the real gliding arc (Figure 4a) the electric field may be even stronger, so the arc is sustained farther. Also, the model is not suitable for strong non-equilibrium and for very low currents (case R = 100 kOhm, $J \leq$ 0.1A, in the experiment $E >$ 1 kV/cm, it was assumed that $E_i \sim$ 1 kV/cm), where "overshooting" is very pronounced in experiment, but only partially seen in calculations.

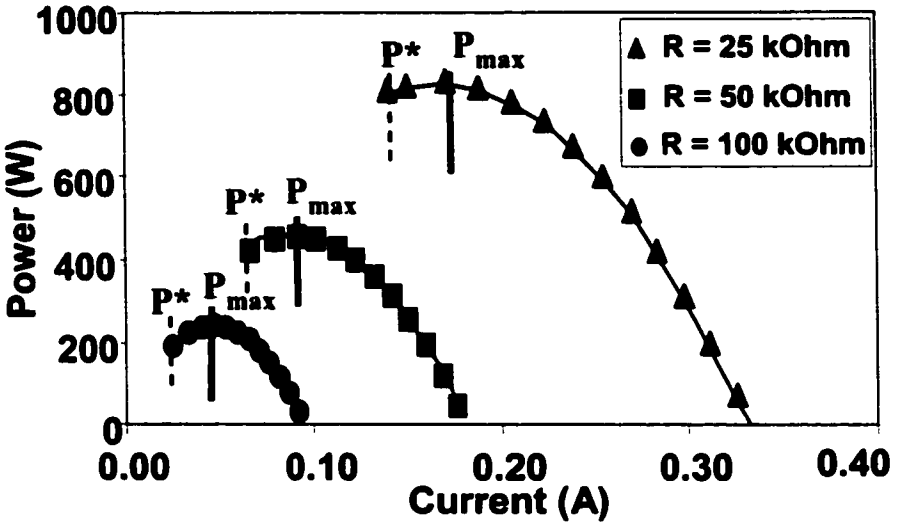

Figure 6. Calculated power-current dependence of the gliding arc. The results are in a very good agreement with experimental results [10] (Figure 4). A stable solution exists beyond the point of maximum power Pmax. No physical solution exists for $P < P^*$. The model is not applicable for small currents ($J < 0.1$ A, R = 100 kOhm).

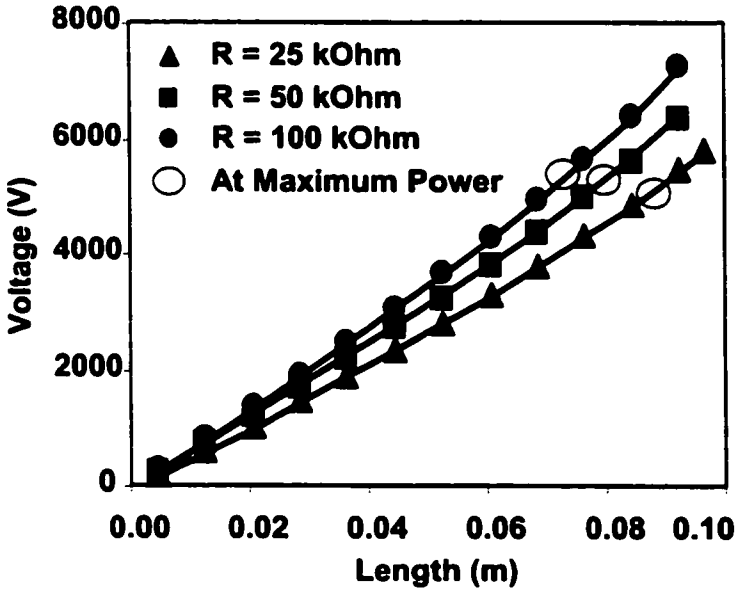

Figure 7. Calculated arc voltage for different lengths of the arc. Circles denote the points of maximum power P_{max} and $l = l_o$.

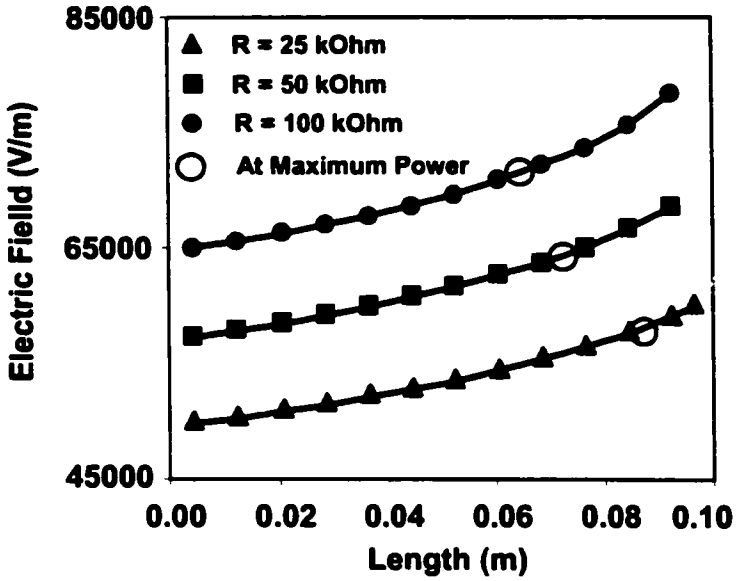

Figure 8. Calculated electric field for different lengths of the arc. Circles denote the points of maximum power Pmax and $l = l_0$. The slope of the curves (dE/dl) increases with length.

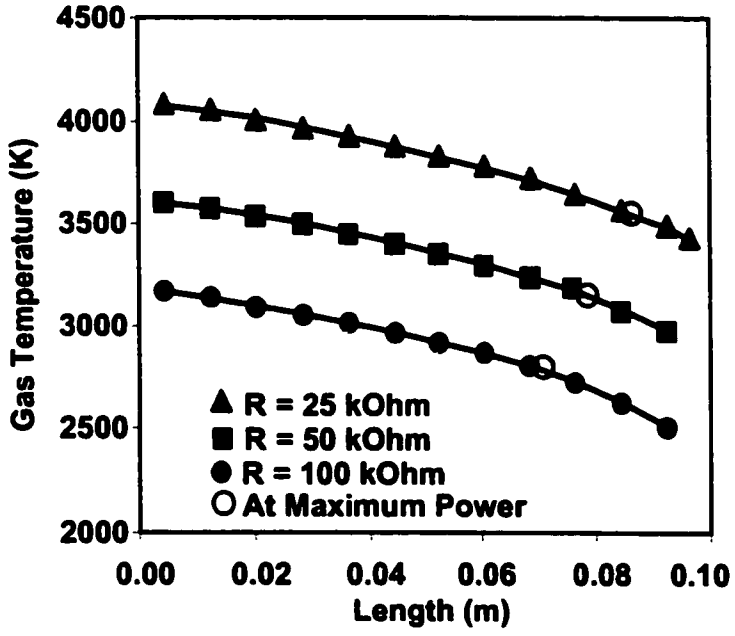

Figure 9. Calculated temperature for different lengths of the arc. Circles denote the points of maximum power Pmax and $l = l_0$. The arc becomes more non-equilibrium as l increases.

Our analysis started from a few basic assumptions about the nature of the discharge and its properties. Also, only a few bulk parameters could be known or found from the experiment. Nevertheless, being a simple phenomenological theory, the model and its numerical solution exhibit a behavior similar to the experiments (Figure 4).

2.6. Conclusions and recommendations for future work

The linear analysis showed the possibility of the low-current gliding arc to remain stable even after the maximum total power P_{max} was reached ("overshooting" effect). This result is in a good agreement with the experiment. The "overshooting" phenomenon was explained through the incorporation of temperature and field sensitive properties (electric and thermal conductivities) into the model. The arc would gradually degrade toward the non-equilibrium. Driven by the falling current, the gas temperature of the arc, the electric conductivity and specific power W also decrease. As a result, the total power could smoothly fall after reaching P_{max} and the expression under the square root in the Eq. (3) (Ohm's law) would stay positive.

Since Ohm's law limits the sum of voltages on the arc and on the serial resistance, the development of non-equilibrium conditions accompanied by the growth of electric field eventually results in discharge instability, and the arc extinguishes. The stability analysis showed that the instability appears at the moment when the voltage drop on the serial resistance can no longer compensate the growth of the voltage on the gliding arc.

Comparison between the experimental results and numerical solutions shows that our model is applicable for the transition regime of gliding arc when the effects of both thermal ionization and direct electron impact ionization must be considered.

3. NON-EQUILIBRIUM PULSED CORONA DISCHARGE

3.1. Introduction

Corona is a self-sustained electrical gas discharge that occurs only when the electric field is sharply non-uniform. The field near one or both the electrodes must be stronger than in the rest of the gap. This situation typically arises when the characteristic size r of the electrode to which the high voltage is applied, is much smaller than the inter-electrode distance d. If we consider a wire-into-cylinder configuration, the electric field in the space between the coaxial cylinders of radii r (internal cylinder) and R is given as a function of the radial coordinate x as:

$$E = \frac{V}{[x \ln(R/r)]} \tag{34}$$

where V is the voltage between the cylinders.

There is always some ionization in atmosphere due to high-energy particles coming from space. Existing electrons are accelerated by the electric field. They can ionize more molecules of the gas. New electrons are accelerated in the field, and so forth. Corona discharge occurs only when the value of the maximum electric field exceeds the breakdown field. For coaxial cylinders, the critical electric field of corona ignition in air is expressed by an empirical formula suggested by Peek (1929):

$$E_c = 31\delta\left(1 + \frac{0.308}{\sqrt{\delta r}}\right) \quad \text{[kV/cm]} \tag{35}$$

where δ is the ratio of air density to the density in standard pressure and temperature. It is clear that a constraint is imposed on the maximum field, which occurs on the surface of the sharp electrode, that is the high field or "corona carrying" electrode.

The formulae given above describe fairly well the physics of the corona with DC or slowly changing fields, such as in Gas Phase Corona Reactors (GPCR). For these applications, to be sustained at non-equilibrium state, the discharge can acquire only small power. Higher power would cause sparking and eventually lead to thermal arc formation.

Natural power limitations of DC corona technology gave rise to development of the pulsed corona technology. In a pulsed corona discharge, voltage is applied to the sharp electrode as a series of fast rising pulses. Incoming pulses generate a number of microdischarges (streamers); the faster the pulse, the more streamers are produced per unit length, increasing the power input per unit gas volume. Some parameters of streamers are given in Table VI.

The width of the applied pulse must be minimized in order to avoid formation of spark discharge or thermalization of the streamers. For most geometries, then, the pulse rise time must be on the order of few nanoseconds and the duration of the pulse on the order of 100 ns. Pulsed corona is more suitable for the goals of the Forest Project, because all range of concentrations of VOC can be treated with the same discharge by simply changing the pulse repetition rate.

To obtain experimental data, used in this work, a negative pulsed corona has been applied. The electron energy, in fact, depends on both the intensity of the electric field (i.e. on the voltage) and the mean free path. For a fast rising pulse, the mean electric field is very high (since the peak voltage is high), allowing the electrons to gain enough energy for the discharge to take place; however, since the duration of each pulse is much smaller than the interval between pulses, the mean required power is low (e.g., it is in the order of few Watts for the setups used for these

experiments) even though the actual power of each single pulse is very high (about 1 MW). The negative polarity is predetermined by the existing equipment.

Table VI. Typical Parameters of Microdischarges (Streamers).

Lifetime	1-20 ns
Current Density	0.1 – 1 kA/cm^2
Transported Charge	100-1000 pCoulomb
Diameter	100-200 μm
Electron Energy	1-20 eV
Electron Density	10^{14}-10^{15} cm^3
Electric Field	E/n = 1-2 (E/n)$_{Paschen}$
Gas Temperature	300 K

Usual DC corona is a uniform discharge. In contrary, the pulsed corona is highly non-uniform. All the discharge power is localized in streamers. To describe the physics of the discharge, one must consider a phenomenon of a streamer as a whole. Electromagnetic model of physics in streamers must be coupled with chemistry of excited species, and with internal particles (electrons, photons) transport. This coupling is very difficult because of enormous amount of computational work. Simplified models were developed, but they are still not adequate for the purposes of trustworthy chemistry prediction. Many parameters are known with great degree of uncertainty, such as electron cross-sections. In this thesis, a simpler way was found to represent the discharge physics and to decouple physical and chemical phenomena.

3.2. Review of Literature

The topic of air pollution control by electrical discharges was subjected to intensive research for decades. In this field, the plasma-chemical processes in the most challenging area of study. Developments in research technique (both software and hardware) for the last 15 years significantly enhanced our knowledge on elementary processes in plasma. The research was stipulated by constantly increasing interest to plasma processing in industry and by new stringent environmental regulations demanding new pollution control techniques.

The pulsed corona discharge is a relatively new technique. In pollution control applications, it competes with electron beam plasma technique. Current applications of both processes include the removal of major polluting constituents of NO, NO_2 and SO_2 encountered in the flue gas streams and vehicle exhausts. The acute problem of removal of VOC from the gas streams has emerged recently due to new environmental regulations.

As mentioned, a science of discharges has a very long history. Electron beam (e-beam) technique has been investigated widely [14]. Due to its uniformity, the plasma generated by e-beams helps study processes in radiation chemistry (Beta-particles are electrons). The methods of modeling (primary Monte-Carlo) of e-beams are also very well developed. The flux of electrons yields the highest ionization rate per 100 eV from any of the plasma discharges. The disadvantage of such systems is their high capital cost and complexity.

In its turn, pulsed corona equipment is cheaper, but the discharge is not uniform. As mentioned previously, it consists of small microdischarges (streamers). The modeling is very complex and requires substantial computer resources. That is why the computational research on streamers has become more common only within the last ten years.

The DC corona is widely described in the literature. There is much less literature on pulsed corona. It is mostly on SO_2 and NO_x removal from streams in power plants. Very little information is available on VOC chemistry in impulse discharges such as pulsed corona or DBD.

A very extensive recent review [14] of air pollution control techniques by electrical discharges summarized the experimental facts about some trends in behavior of pulsed corona and dielectric barrier discharges. The paper demonstrates that this area is mostly descriptive. There is no agreement or no information on such major issues as 1) best polarity of corona (positive or negative); 2) dependence of discharge performance on temperature and humidity; 3) figures of merit (researchers use several ones, but it is difficult to bring the results of different authors to the common ground); and, finally, 4) the upper limits of concentration for which the pulsed corona technology is still applicable. This reflects the experimental fact that at higher concentration of pollutants the efficiency of discharge increases, but more power is required. Studying the recent literature, a developer or user of environmental plasma equipment would find very little guidance through this multitude of experimental facts.

It seems that the plasma-chemical mechanism of NO_x and SO_2 formation or removal is the best development is this area. Various independent experiments refined this mechanism, but some questions still remain. Evidently, this is a good starting point for the further research and development of corona technology. That is why the research presented in this thesis is concentrated on the chemistry of the pulsed corona discharge.

To study the chemistry of DMS, methanol, acetone and terpenes in a pulsed corona discharge, one would use the NO_x mechanism as the foundation or a staring point, and add some reactions relevant to particular compounds. However, there are some hurdles to overcome:

1. The mechanism for every VOC starts from the point when the concentration of radicals formed in the discharge is known. Obtaining this initial concentration requires solution of the streamer problem or finding some approximate theoretical of experimental approaches. A great attention is paid in this thesis to simplify this problem.
2. Majority of chemical mechanism data is available for dry air. When reactions with water and *OH* radicals are added, as in the case of forest industry, some additional verification of mechanism might be required. Also, it is expedient to determine the sensitivity of major reaction channels to minimize computational work.
3. The mechanisms for VOC are taken from atmospheric chemistry. Their applicability for corona was not clear.

Therefore, the primary goal for the further literature research would be obtaining additional information on primary mechanisms (for example, from radiation chemistry), on radicals chemistry, and on chemistry of complex compounds, its theoretical and experimental evaluation.

The properties of the pulsed corona discharge were studied experimentally by numerous authors, for example [49-55]. In [50] the pulsed streamer corona discharge in water was studied with the aid of optical methods. It was found that production of *OH* radicals depends non-linearly on the electric field.

Different aspects of chemistry of inorganic gases, such as NO_x, SO_2, CO and CO_2 were studied experimentally in the works [49, 52-55]. The detailed coverage of theoretical and experimental results on the pulsed corona is given in work [58]. The data used in the present research were taken from the works on radiation chemistry [19, 21, 22, 23]. The detailed kinetic model of chemistry in the corona discharge is represented in work [59].

The issues of formation and decomposition of ozone are illuminated in monograph [48]. The detailed kinetic description of oxidation of SO_2 and formaldehyde CH_2O (major byproduct), and also the kinetics of active particles in the discharge, are taken from [43] and [46].

Several aspects of the low-temperature oxidation of sulfur-containing organic matter, particularly DMS, are described in [15, 16, 25-29, 31, 32, 34-37]. The need of using so significant quantity of sources is related to the fact that at the present moment kinetics of the oxidation of the sulfur-containing organic matter is not completely understood. The matched mechanism of oxidation of DMS under the standard conditions is given in work [17]. Interaction of ozone with VOC in the liquid phase is examined in [17, 26, 40-42, 25, 47].

In the following chapters, the chemistry of elementary processes will be considered. The approach in determination of free radical concentration as an input to VOC chemistry mechanism will be outlined.

3.3. Gas Discharge Chemistry

The chemical processes in discharges start when electrons achieve some threshold energy sufficient to excite or ionize molecules in the gas. In strong electric fields, between collisions with neutral species electrons are capable of gaining the energy that is sufficient for multiple ionization events. The ionized species neutralize and may form free radicals. Very active radicals react with VOC to produce intermediate species. The processes with electrons occur very rapidly, while recombination is much slower. The lifetime of radicals is the longest process if compared with the timeframe of ionization and ions neutralization. Therefore, using the characteristic time as a parameter, all three stages of discharge chemistry can be distinguished (Table VII).

TABLE VII. STAGES IN DISCHARGE CHEMISTRY

Process	Example
1. Electron – neutral collisions in corona streamers	
Dissociation	$N_2 + e \rightarrow N + N + e$
Electronic molecular excitation	$N_2 + e \rightarrow N_2^* + e$
Formation of molecular ions	$N_2 + e \rightarrow N_2^+ + e + e$
Simultaneous ionization and dissociation	$N_2 + e \rightarrow N + N^+ + 2e$
2. Neutralization and quenching	
Quenching of the excited state	$N_2^* + N_2 \rightarrow N_2 + N_2$
Formation of a molecule from individual atoms with participation of the third particle absorbing the excess momentum	$N + N + N_2 \rightarrow N_2 + N_2$
Charge transfer	$N_2^+ + H_2O \rightarrow N_2 + H_2O^+$
With low-energy electrons	$O_2^+ + e \rightarrow O_2$ $O_2 + e \rightarrow O_2^-$
Ion-Ion recombination	$H_3O^+ + NO_2^- \rightarrow H_2O + NO + OH$
3. Chemical reactions with the radicals	
Among radicals	$OH + OH \rightarrow H_2O + O$
Among radicals and VOC	$CH_3OH + OH \rightarrow CH_2OH + H_2O$

Here "*" denotes the electronic excited state.

The non-uniform nature of the corona discharge and existence of its streamer microstructure results in substantial challenge in modeling of the discharge. Typically, the researches model streamers to find electron temperature and to obtain the concentration of chemically active species (*O*, *OH*, *N*, N_2^*, etc). This approach requires exact knowledge of electron transport cross-sections and leads to huge amount of computational work. To reduce the computational time, a set of approximations is used. This gives quite satisfactorily qualitative results, but the quantitative results may significantly deviate from the experiment. Streamers usually have a tree-like structure. Accounting for this phenomenon would need more complex

modeling and much more computational time. Such modeling is very cumbersome for current scientific and engineering applications.

A different approach is used for modeling of the electron beam plasma. As reported in [62], a beam of electrons (typically with a very narrow electron energy distribution) has the highest possible yield of radicals per unit of energy consumed in the discharge. The mechanisms and theory of interaction of electron beams (and other types radiation) with different substances is of primary interest in radiation chemistry. The yield of active species or radicals is usually described in terms of G-factors (Gross-factors), or the number of species of a particular kind produced per 100 eV of energy absorbed in the media of interest. Using G–factors, one can estimate the concentration of radicals produced under the irradiation of the given gas with a beam of electrons of known energy. It will be shown below how to utilize the concept of G-factors for accurate prediction of removal efficiency of VOC in pulsed corona discharges as well.

3.4. Approach in Investigation of Physics and Chemistry of the Pulsed Corona Discharge

Even though a huge amount of experimental data was available on destruction of VOC in different discharges, it was virtually impossible to predict chemistry at conditions different from those described in papers. Systematic studies of dependence of VOC destruction on temperature and humidity were not carried out for the compounds of interest. The novelty of the current research is in the approach of treatment of chemistry of high-energy electrons. A common approach with G-factors used in radiation chemistry was accommodated for the pulsed corona discharge. Methanol has been chosen as a sample substance for validation because its detailed mechanism is well known.

The presented study of chemistry and physics in corona discharge was divided on several logical steps:

1. Theoretical investigation of the discharge using the assembled chemical mechanism for species of air and for a simple VOC. Investigation of applicability of the chosen discharge model.
2. Using the results of theoretical investigation, definition of the matrix of experiments.
3. Selection of the proper quality factors or figures of merit.
4. Modification of the theory using the experimental results.

3.4.1. Description of Bulk Discharge Parameters

In the following analysis the discharge was considered in the cylindrical geometry such as "wire-in-tube". However, the presented approach can be modified for different geometry.

Let us examine some bulk parameters of the experimental installation, used in the computer model, and some relationships between them. Let L be the length of the corona reactor with the inside radius a, and the volume V_R. Then

$$V_R = \pi a^2 L. \tag{36}$$

For our system L = 1200 mm, a = 11 mm, V_R = 45.6 cm^3.

Let us Q_0 for the gas flow rate in *SLM*. With temperature correction

$$Q = Q_0 \times \frac{T}{T_0} \times \frac{10^3}{60} \left(cm^3/\sec\right), \tag{37}$$

where T is the temperature of gas, T_0 = 293 K.

The residence time of the gas in the reactor

$$t_{residence} = \frac{V_R}{Q} = \frac{\pi a^2 L T_0}{Q_0 T}. \tag{38}$$

Specific energy input will be

$$SEI = \frac{W}{Q_0}. \tag{39}$$

where W is the electrical power. The specific power per unit volume is

$$W_0 = \frac{W}{V_R}. \tag{40}$$

It can be seen that the residence time decreases at higher temperatures. A change in the concentration with the temperature was also considered in the model with the aid of standard procedures form the CHEMKIN library. The power of discharge varies with the temperature. The values of power used for numerical modeling are based on those measured in the experiment.

It is possible to assume that the energy of the pulse does not depend on the Pulse Repetition Rate (PRR). The pulse energy is the function of 1) electric potential between the electrodes; 2) temperature of the gas in the reactor; 3) concentration of the components in the gas mixture.

A good assumption on the linearity of the discharge power with PRR was confirmed in actual experimental measurements. The next formula concludes the bulk model of the discharge.

$$W = \varepsilon_{imp} \times \Omega \,. \tag{41}$$

The coupling of bulk parameters of the discharge with its electron chemistry was managed through using concept of G-factors taken from the radiation chemistry.

3.4.2. Elementary Chemistry

Development of chemical mechanism would proceed in two phases. Phase 1 will include preliminary investigation of applicability of a G-factor-based concept to description of pulsed corona discharges at simplified conditions (dry air, no VOC). At Phase 2, VOC and humidity will be added to the gas stream, increasing the complexity of the model.

Current investigation, as mentioned above, uses G-factors to couple the bulk parameters and chemistry of the discharge. G-factors will be defined as a quantity of particles of the type "A" of those appearing in the medium during the absorption by it of 100 eV of energy of radiation. G–factors depend substantially on the density of the media. The concept of "dosimeter" as a standard for measuring the dose of the absorbed radiation is used. The following relationship takes place:

$$G(P)_M = G(P')_D \times \frac{[P]_M}{[P']_D} \times \frac{\rho_D}{\rho_M} \times \frac{D_D}{D_M} \qquad (42)$$

where $G(P)_M$ and $G(P')_D$ are the chemical radiation yields of products P and P' formed in the sample and dosimeter, respectively; $[P]$ and $[P']$ are the chemical yields of the two products in units of mole per unit volume (e.g., mol * m^{-3}, or mol * L^{-1}) when the sample and dosimeter are exposed in the same radiation field; ρ_M and ρ_D are the densities of the sample and dosimeter; and D_D/D_M is the ratio of absorbed dose per unit mass in the sample and in the dosimeter. The ratio D_D/D_M is found for different types of radiation and different types of dosimeters.

Since the data of radiation chemistry were acquired in essence for the pure gases (exception is nitrogen-oxygen mixtures), by the dosimeter we will imply the appropriate pure gas, for example, water vapor, and we will calculate G – factor for the mixture of gases, used in the experiments. In our case this mixture is $N_2/O_2/H_2O$ /VOC.

The ratio of the radiation dose absorbed by pure substance to the dose absorbed by the mixture can be evaluated as

$$\frac{D_1}{D_{mix}} = \omega_1 \times \frac{(Z/A)_1}{(Z/A)_{mix}} = \varepsilon_1 \tag{43}$$

This is the electron fraction of component 1 in the mixture, where ω_1 is the mass fraction of component 1 in the mixture. Through $(Z/A)_1$ is marked the ratio of a total quantity of electrons in the molecule of component 1 to its molecular weight

$$\left(\frac{Z}{A}\right)_i = \frac{\sum_{k=1}^{N_i} Z_k}{\sum_{k=1}^{N_i} A_k}, \tag{44}$$

$$\left(\frac{Z}{A}\right)_{mix} = \sum_i \omega_i \left(\frac{Z}{A}\right)_i. \tag{45}$$

The given formulae reflect the concept, according to which the portion of energy, absorbed by the given component, is proportional to its mass fraction, and the absorption of radiant energy occurs in essence due to interaction with the electron shells of atoms. As a whole the expression

$$\varepsilon_1 = \omega_1 \times \frac{(Z/A)_1}{(Z/A)_{mix}} \tag{46}$$

is called the electronic fraction of this component in the mixture.

If product P can be formed under the radiation effect both from the component A and from the component B in the mixture, then cumulative G–factor can be evaluated as

$$G(P) = G(P)_A \varepsilon_A + G(P)_B \varepsilon_B, \tag{47}$$

where $G(P)_A$ and $G(P)_B$ are the radiation-chemical yields of P from A and B and ε_A and ε_B the electron fractions of A and B, respectively.

Some authors [19] suppose the electrons with the relatively low energy (such as corona electrons) could effectively interact only with the electrons of the outer shells of the atoms. Only they should be accounted for in calculation of (Z/A) because the energy of incident particles is not enough to liberate electrons from the inner shells of atoms. Therefore, the contribution of internal electrons is practically negligible. They do not absorb the incoming radiation.

If all the energy of the electric field would go to high-energy electrons and all these electrons would have the energy above a certain threshold value, one could use data for β-rays from radiation chemistry to calculate the quantity of radicals. However, not all the energy of the electric field goes to high energy electrons. The distribution of electrons is far from narrow with a major fraction of low energy electrons. The electron distribution function must be calculated using Boltzmann equation.

In this thesis it is proposed to find the fraction of energy that goes to high energy electrons by measurements of concentration of long-living chemical species. This approach requires having a very well known detailed chemical mechanism with minimum intermediate steps to minimize inevitable errors.

In our simple kinetic model the temperature is accounted for through the introduction of parameter α, which represents a fraction of the discharge power consumed in formation of active species (Figure 10). It must be the same for all the processes at given temperature. This fact was verified experimentally. At each pulse in corona there forms a specific quantity of primary active particles O, O^*, N, N^*, H, OH:

$$\Delta N_i = g_i^{mix} \cdot \frac{\alpha \varepsilon_{imp}}{100(eV)}, \tag{48}$$

where g_i^{mix} is the G–factor of i–th particle, calculated for this mixture composition, ε_{imp} is the energy of pulse, equal to the ratio of power W to the Pulse Repetition Rate Ω:

$$\varepsilon_{imp} = \frac{W}{\Omega}. \tag{49}$$

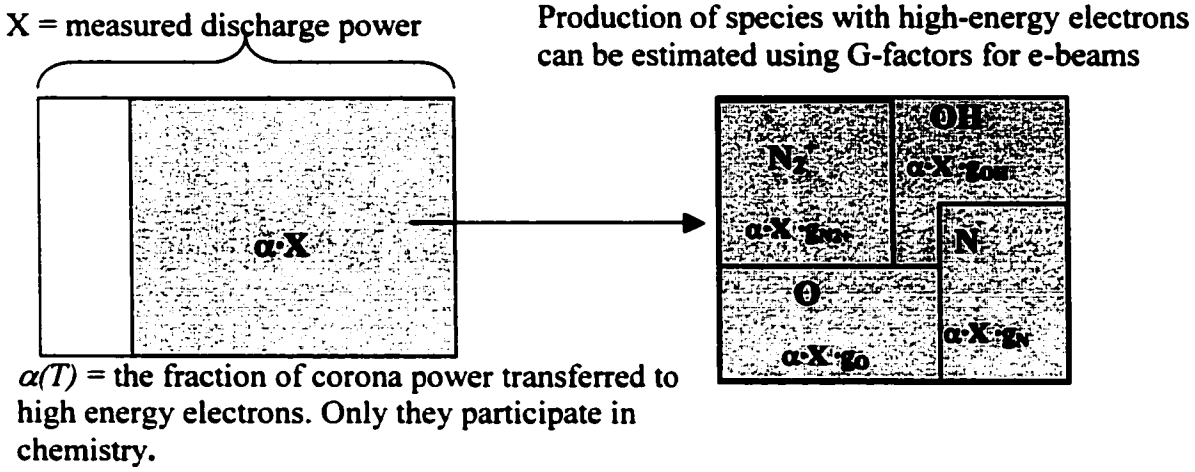

Figure 10. Concept of α parameter.

The increment in concentration of the particles of the i–th kind after pulse

$$\Delta C_i = \frac{\Delta N_i}{V_{reactor}}. \tag{50}$$

When the pulse ends, a certain number of neutral particles are considered to be present in the discharge. The model describes the chemistry of these particles in humid air with respect to VOC. The algorithmic realization of model is based on integration of the Cauchy problem with the initial conditions determined by the species concentrations at the moment after the pulse on the time interval equal to the gap between the adjacent pulses.

In Phase 1 of chemistry investigation, a mechanism of NO_x formation was chosen for determination of $\alpha(T)$ (see Table VIII).

TABLE VIII. REACTION MECHANISM OF NO_X FORMATION TO DETERMINE $\alpha(T)$

Processes with Oxygen	
$O_2 + e \rightarrow O_2^* + e$ (G = 2.0)	$O_2 + e \rightarrow O_2^{**} + 2e$ (G = 2.07 [22])
$O_2 + e \rightarrow O + O^- + 2e$ (G = 1.23. In this case the fraction $O_2 + e \rightarrow O^- + O^* + 2e$ of each of the channels comprises approximately 50 %.)	
$O_2^* \rightarrow O + O^*$	$O^- + O_2 \rightarrow O_2^- + O$
$O_2^- + 2O_2 \rightarrow O_4^- + O_2$	$O_4^- + O_2^- \rightarrow 2O_2 + 2O$
$O + O_2 + M \rightarrow O_3 + M$	$O^* + O_2 + M \rightarrow O_3 + M$
Total G ($O + O^*$) = 2G(O_2^-)+4G(O^-) + 2G(O_2^*) = 13.06. The fraction of excited atoms O^* is about 40 %.	
Processes with Nitrogen	
$N_2 + e \rightarrow N_2^- + e + e$ (G = 2.0)	$N_2 + e \rightarrow N_2^* + e$
$N_2 + e \rightarrow N + N^* + e$ (G = 2.36)	$N_2 + e \rightarrow N^* + N^{**} + e$
$N_2 + e \rightarrow N$ (N^*) + N^+ (G = 0.7)	$N^+ + 2N_2 \rightarrow N_3^+ + N_2$
$N_2^+ + 2N_2 \rightarrow N_4^+ + N_2$	$N_3^+ + e \rightarrow N + N_2^*$
$N_4^+ + e \rightarrow 2N + N_2$	$N + N + M \rightarrow N_2 + M$
Processes with Oxygen and Nitrogen	
$N^- + O_2 \rightarrow NO^- + O^*$	$NO + NO + O_2 \rightarrow NO_2 + NO_2$
$N^- + O_2 \rightarrow O_2^- + N$	$NO_2 + O_2 \rightarrow NO + O_3$
$N_2^- + O_2 \rightarrow O_2^- + N_2$	$O + NO_2 + M \rightarrow NO_3 + M$
$N_4^- + O_2 \rightarrow O_2^- + 2N_2$	$O + NO_2 \rightarrow NO + O_2$
$O^* + N_2 \rightarrow O + N_2$	$O + NO_3 \rightarrow O_2 + NO_2$
$N^* + O_2 \rightarrow NO + O$	$NO + NO_3 \rightarrow NO_2 + NO_2$
$O + N_2 \rightarrow NO + N$	$NO_2 + NO_3 \rightarrow NO + NO_2 + O_2$
$N + O_2 \rightarrow NO + O$	$NO_2 + NO_3 + M \rightarrow N_2O_5 + M$
$N^* + NO \rightarrow N_2 + O$	$N_2O_5 \rightarrow NO_2 + NO_3$
$N^* + NO_2 \rightarrow N_2O + O$	$N + O_3 \rightarrow NO + O_2$
$N^* + N_2O \rightarrow NO + N_2$	$NO + O_3 \rightarrow NO_2 + O_2$
$N^* + NO_2 \rightarrow NO + NO$	$NO_2 + O_3 \rightarrow NO_3 + O_2$
$N + NO \rightarrow N_2 + O$	$O^* + N_2O \rightarrow NO + NO$
$N + NO_2 \rightarrow N_2O + O$	$O + NO + N_2 \rightarrow NO_2 + N_2$
$N + NO_2 \rightarrow NO + NO$	$O + NO + O_2 \rightarrow NO_2 + O_2$

The yield of nitrogen oxides depends on the quantity of excited nitrogen atoms generated in the discharge. Thus, the $\alpha(T)$ dependence could be reconstructed from the experimental temperature-concentration data from corona operation in dry air using a successive iterations method. Determination of alpha for the particular experimental setup will be given in the "Experimental Results" section of this chapter.

The next phase of chemistry investigation (Phase 2) assumes more realistic situation when VOC and humidity are both present in the stream. In addition to oxygen and nitrogen primary reaction channels, in the presence of water there will be additional reactions associated with OH radical formation from H_2O molecules and interaction of OH radicals with other active species (see Table IX). The relevant values of G−factor in the pure water vapor are 3.2 (OH), 0.6 (H), 0.65 (O) and 0.06 (H_2) [19, 22].

For purposes of the analysis of experimental data and simulation of the process of VOC decomposition in the pulsed corona discharge, one should know the detailed mechanisms of oxidation processes of the VOC. This process is initiated and takes place with the participation of the active particles made by the corona. The primary distinctive features of such processes are the conditions at which they occur, i.e. pressure and temperature. In our case the pressure is equal atmospheric, and temperature varies in the range from 20°C to 230°C. Under such conditions we will consider the processes of the low temperature oxidation, which are principally in a number of moments different from the well known processes of combustion, i.e. oxidation at a high temperature.

One of the important differences in the cold oxidation from the combustion is that at low temperatures the action of active particles (radicals) leads to formation of metastable molecules and radicals, which practically do not exist at high temperatures. Thus, for instance, at low

temperature interaction of formaldehyde CH_2O with the radical OH can occur according to the reaction:

$$CH_2O + OH \rightarrow H + HCOOH \ ,$$

which does not occur in the processes of combustion.

TABLE IX. REACTIONS WITH *OH* RADICALS AND WATER MOLECULES

$H_2O + e \rightarrow H_2O^+ + e + e$	$H_2O + e \rightarrow OH^+ + H + e + e$
$H_2O + e \rightarrow H^+ + OH + e + e$	$H_2O + e \rightarrow H_2^+ + O + e + e$
$H_2O + e \rightarrow H_2 + O^+ + e + e$	$H_2O^+ + H_2O \rightarrow H_3O^+ + OH$
$OH^+ + H_2O \rightarrow H_3O^+ + O$	$H^+ + 2H_2O \rightarrow H_3O^+ + H_2O$
$O^+ + H_2O \rightarrow H_2O^+ + O$	$H + H + H_2O \rightarrow H_2 + H_2O$
$H_3O^+(H_2O)_n + H_2O + M \rightarrow H_3O^+(H_2O)_{n+1} + M$	$N_2^+ + H_2O \rightarrow N_2 + H_2O^+$
$O^{\bullet} + H_2O \rightarrow OH + OH$	$O^{\bullet} + H_2O \rightarrow O + H_2O$
$O^{\bullet} + O_2 \rightarrow O + O_2$	$O^{\bullet} + N_2 \rightarrow O + N_2$
$O^{\bullet} + O_2 + M \rightarrow O_3 + M$	$O^{\bullet} + O_3 \rightarrow O_2 + O_2$
$O^{\bullet} + O_3 \rightarrow O_2 + O + O$	$OH + OH \rightarrow H_2O + O$
$OH + OH + M \rightarrow H_2O_2 + M$	$OH + H_2O_2 \rightarrow H_2O + HO_2$
$OH + HO_2 \rightarrow H_2O + O_2$	$O + OH \rightarrow H + O_2$
$OH + O_3 \rightarrow HO_2 + O_2$	$HO_2 + O \rightarrow OH + O_2$
$O\ (O^{\bullet}) + H_2O_2 \rightarrow HO_2 + OH$	$OH + O_3 \rightarrow HO_2 + O_2$
$CH_3O + O_2 \rightarrow CH_2O + HO_2$	$HCO + HO_2 \rightarrow CO_2 + OH + H$
$CH_2OH + HO_2 \rightarrow CH_2O + H_2O_2$	$HO_2 + HO_2 + M \rightarrow H_2O_2 + O_2 + M$
$HO_2 + O_3 \rightarrow OH + O_2 + O_2$	$HO_2 + O \rightarrow OH + O_2$
$H + OH + M \rightarrow H_2O + M$	$H + OH \rightarrow O + H_2$
$OH + H_2 \rightarrow H_2O + H$	$H + O_3 \rightarrow OH + O_2$
$H + H_2O_2 \rightarrow H_2O + OH$	$H + HO_2 \rightarrow OH + OH$
$H + HO_2 \rightarrow H_2 + O_2$	$H + HO_2 \rightarrow H_2O + O$
$H + O_2 + M \rightarrow HO_2 + M$	$O^{\bullet} + H_2O \rightarrow H_2 + O_2$
$NO + OH + M \rightarrow HNO_2 + M$	$OH + HNO_2 \rightarrow NO_2 + H_2O$
$OH + HNO \rightarrow H_2O + NO$	$OH + NO_2 + N_2 \rightarrow HNO_3 + N_2$
$OH + NO_2 + O_2 \rightarrow HNO_3 + O_2$	$OH + NO_2 + H_2O \rightarrow HNO_3 + H_2O$
$OH + HNO_3 \rightarrow NO_3 + H_2O$	$OH + N_2O \rightarrow HNO + NO$
$OH + N \rightarrow NO + H$	$NO + HO_2 \rightarrow NO_2 + OH$
$N_2O_5 + H_2O \rightarrow HNO_3 + HNO_3$	

Furthermore, the temperature dependence of the reaction rate constants at high temperature regions cannot be directly extrapolated in the region of low temperatures (even for the non-threshold reactions with the participation of radicals).

Chemistry of cold oxidation is studied comparatively worse than chemistry of combustion. However, in recent years an essential progress was made in this area, stipulated, first of all, by the interest of researchers to the processes of atmospheric chemistry involving different organic and inorganic compounds and leading to the greenhouse effect, destruction of ozone layer, photochemical smog, acidic rains and so forth. The data of atmospheric chemistry can be used for simulation of VOC decomposition in non-thermal discharges. However, one must consider several limitations of this approach.

In numerical and experimental studies of chemical processes in atmosphere, the concentration of active particles (radicals) is usually assumed constant and equal to some average values. Those values depend on the rate of atmospheric processes (mainly photolysis) and on ambient temperature. It is frequently assumed that chemistry of VOC oxidation, to a certain extent, can be isolated from chemistry of active particles in the atmosphere. When modeling VOC oxidation in the discharge, the formation of radicals under the electron irradiation can be also examined separately. However, some reactions of radical losses with each other must be accounted for along with the reactions of radicals with VOC. That is why the reaction of OH radicals with each other

$$OH + OH \rightarrow H_2O + O$$

$k = 3 * 10^{13}$ mol/ cm^3 sec, must be included in the mechanisms of VOC oxidation in the discharge.

There is a practice in atmospheric chemistry not to consider some active particles because of their short life. In contrary, in the discharge, due to large specific energy inputs the role of these particles is significant. Ozone formation, for example, starts from the excited state of atomic oxygen. The reaction mechanisms used in atmospheric chemistry account for this state only indirectly through the concentration of secondary active species (ozone and *OH*). In the discharge it is possible to have direct interaction of atomic oxygen with VOC molecules.

Mechanism of oxidation of some volatile compounds in the discharges was studied by several authors. Kushner [43, 44] investigated the mechanisms of oxidation of formaldehyde CH_2O and SO_2 in the discharges. The rate constants of the corresponding reactions were in a good agreement with the data from atmospheric chemistry. At the same time, detailed mechanisms of oxidation of more complex substances, such as dimethyl sulfide, α-pinene and acetone, are presently unknown. Here the usage of atmospheric chemistry mechanisms may be justified. The average VOC concentration in the atmosphere is three-order smaller than in our system.

The data collected by the group of atmospheric chemistry from University of Leeds (UK) [56, 57] and the group of Saltelli [17] were used for modeling (Figure 11). The following mechanism of the low temperature oxidation of methanol included the data from atmospheric chemistry and on the reactions of radicals HCO, $HCOOH$, CH_2OH, CH_3O with O, OH and O_2 (Table X). The full mechanism is given in the Appendix.

TABLE X. LOW-TEMPERATURE OXIDATION MECHANISM OF METHANOL

$CH_3OH + OH \rightarrow CH_2OH + H_2O$	$CH_3OH + O \rightarrow CH_2OH + OH$
$CH_3OH + OH \rightarrow CH_3O + H_2O$	$CH_3OH + O \rightarrow CH_3O + OH$
$CH_2OH + O_2 \rightarrow CH_2O + HO_2$	$CH_3O + O_2 \rightarrow CH_2O + HO_2$
$CH_2O + OH \rightarrow HCO + H_2O$	$CH_2O + OH \rightarrow HCOOH + H$
$HCOOH + OH \rightarrow CO_2 + H_2O + H$	$HCO + O_2 \rightarrow CO + HO_2$
$HCO + O \rightarrow CO_2 + H$	$HCO + O \rightarrow CO + OH$
$HCO + OH \rightarrow CO + H_2O$	$HCO + HCO \rightarrow CH_2O + CO$
$HCO + HCO \rightarrow H_2 + CO + CO$	$CO + OH \rightarrow CO_2 + H$
$CO + O + M \rightarrow CO_2 + M$	

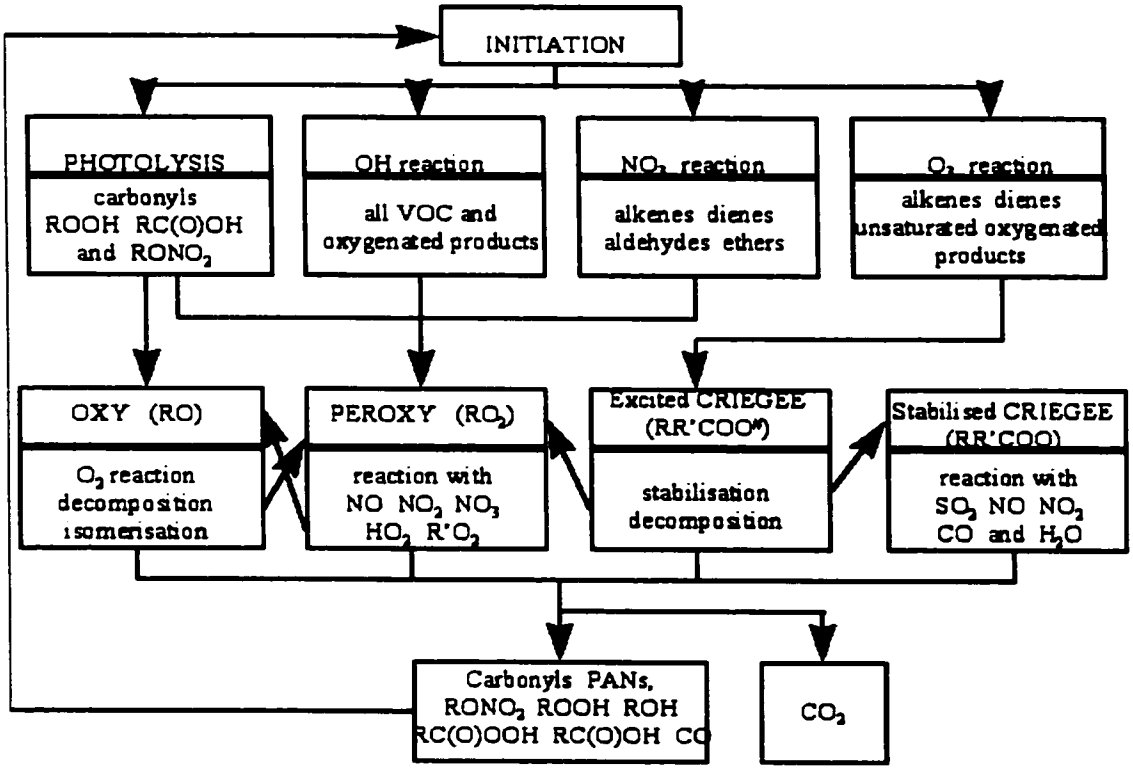

Figure 11. General mechanism of VOC oxidation.

3.4.3. Experimental Matrix

The first version of assembled mechanism of methanol oxidation (in the Thesis only the final, tested mechanism is given) was used for preliminary calculations. They showed that the given set of chemical reactions not always satisfactorily reproduces earlier experimental data [13]. It was suspected that atmospheric reaction rates are not adequate for plasma discharges. In this case it would be necessary to localize at least a part of the mechanism ("reaction channel") to which the destruction is the most sensitive at particular conditions. The discharge physics, in its turn, might also be the case. Both modeling and experimental results must be available to make a distinction. To minimize the uncertainty, some parts of mechanisms must be "switched off" in artificially created conditions such as pure nitrogen, dry air, or humid nitrogen. Table XI defines the objectives for each set of experiments. The pulsed corona discharge would be applied to each of the gas compositions.

TABLE XI. EXPERIMENTAL MATRIX

Gas Composition in the Pulsed Corona Reactor	**To be Found**
Dry Air	NOx concentration, alpha (T)
Dry Air + VOC	Role of "O" reaction channels
N2 + VOC	Role of "N and N2+" reaction channels radicals
N2 + humidity	Role of "OH" radicals
Dry Air + VOC + humidity	Effect of humidity and temperature

The other variables for experiments, in addition to gas composition, were the temperature and corona energy. The latter could be adjusted through changing the Pulse Repetition Rate. In the experiments with humidity it was varied to simulate the Forest Project conditions. Table XII shows relationship between the experimental conditions in air. The experiments would be carried out at five basic temperatures: 40, 80, 130, 180 and 230°C. For the lowest temperature (40°C) the absolute humidity could not exceed the saturation condition (about 2 abs %). In nitrogen a fewer experiments with different humidity are thought to be sufficient (0 and 2% of absolute humidity).

TABLE XII. EXPERIMENTS: HUMIDITY – TEMPERATURE MATRIX FOR AIR

Pulse Repetition Rate, Hz	**Temperature, °C**				
	40	**80**	**130**	**180**	**230**
100	2% abs humidity	0,1,2,5,10 % abs humidity	0,1,2,5,10 % abs humidity	0,1,2,5,10 % abs humidity	0,1,2,5,10 % abs humidity
500	2% abs humidity	0, 1, 2, 5, 10 % abs humidity	0,1,2,5,10 % abs humidity	0,1,2,5,10 % abs humidity	0,1,2,5,10 % abs humidity
1000	2% abs humidity	0,1,2,5,10 % abs humidity	0,1,2,5,10 % abs humidity	0,1,2,5,10 % abs humidity	0,1,2,5,10 % abs humidity

Three basic PRR (100, 500 and 1000 Hz) were chosen to reflect two possible cases of discharge formation. When PRR is low (100 Hz), the new discharge does not "feel" the trace from the previous impulse because there are almost no active particles in the discharge gap. The typical time for the discharge traces to disappear is about 1 ms. Therefore, at 500 Hz and 1000 Hz, the previous discharge would "help" the next discharge to form. Very often this causes a

premature breakdown. The corona becomes a spark, or may even ignite an arc (at very high PRR). All this must be considered and carefully monitored. The PRR of 500 Hz represents an intermediate case to help see a trend in transition from 100 to 1000 Hz.

3.4.4. Figures of Merit

There are too many parameters in the corona discharge that might influence the removal efficiency. Major of them are: power per impulse, voltage, pulse repetition rate, temperature, humidity, residence time, concentration of VOC, composition of the carrier gas. The recent survey [14] on plasma technologies available for abatement of volatile organic compounds showed the results of different authors in terms of several quality factors.

The discharge parameters may be accounted for in many different ways. It is believed that quality factors, or figures of merit, including these parameters, must reflect the following experimental and theoretical results:

1. The Destruction and Removal Efficiency (DRE) exponentially depends on temperature.
2. During the detailed analysis of corona and by comparing the experimental data, we found that methanol is destroyed though the first-order chemical reaction with respect to methanol and radicals.
3. Lower concentrations of VOC require higher energy inputs per unit of volume. The larger the concentration, the less energy is required to destroy every ppm of VOC.

A comparison of commonly used quality factors is given in Table XIII.

TABLE XIII. FIGURES OF MERIT FOR VOC DESTRUCTION

Name	Formula	Dimension	Comment
Destruction and Removal Efficiency (DRE)	$\frac{C_o - C}{C_o}$	-	Does not account for consumed energy
Specific Energy Input (SEI)	Power*(Residence Time)/(Flow Rate)	Watt*hour/m^3	Does not account for concentration
Energy Cost	$\frac{SEI}{DRE\ C_o}$	Watt*hour/m^3/ppm	Does not account for exponential dependence of DRE on power

The parameter called "energy cost" seems to be the best to reflect the energy cost per ppm of VOC. But it does not show the actual percentage of the destroyed VOC. The matter of interest for practical applications is the degree of destruction of 90% and above. In order to find how much energy is needed to destroy 90% of initial quantity of VOC, one should make numerous experiments where he would vary the corona power. Finally, at certain power the DRE of 90% is achieved and energy cost is recorded.

This long and inefficient approach was used in several works to establish DRE-power dependence. The amount of experimental work can be drastically reduced if the energy cost can be predicted from the experimental data for an arbitrary power. For the purposes of forecasting, a dependence of DRE on power and temperature is needed.

The new approach is proposed in this thesis. Preliminary investigation showed that VOCs (in our case it was methanol) are destroyed though the first-order chemical reaction with respect to VOC and radicals. Then the bulk chemical kinetics equation can be written in the form:

$$\frac{dC_{voc}}{dt} = -k_1 C_{voc}[\overline{OH}] - k_2 C_{voc}[\overline{O}] - k_3 C_{voc}[\overline{N}] = -\beta(T, C_{voc})\,\alpha(T)\,C_{voc} W \qquad (51)$$

Here C is the concentration of VOC, k_i are rate constants for radicals, W is the corona power, β is the concentration-dependent coefficient. The solution of this equation can be immediately found:

$$C_{voc}(t) = C_{voc}(0)\exp\left(-\beta(T, C_{voc})\,\alpha(T)\,W\tau\right), \qquad (52)$$

where τ is the residence time.

Destruction and removal efficiency is then obtained:

$$DRE = 1 - \exp\left(-\beta(T, C_{voc})\,\alpha(T)\,W\tau\right), \qquad (53)$$

Using the last equation, it is possible to estimate the energy cost at DRE = 90%. The obtained assessment for the power will be called Projected Energy Cost (PEC), because the value of power for a given DRE (not equal to 90 %) is projected (predicted) for DRE = 90%. The value of PEC will be defined as following:

$$PEC = \frac{SEI}{0.9\,C_o}\,\frac{\ln(1-0.9)}{\ln(1-DRE)}. \qquad (54)$$

Projected Energy Cost has the same dimension as regular Energy Cost (W*hr/ppm/m^3). At DRE = 90% they are equal.

3.5. Experimental Setup

The corona discharge was generated in a wire-into-cylinder coaxial electrode system. The inner, high voltage electrode is a 0.5 mm diameter Inconel® wire. The Inconel® alloy has been selected for its superior heat and oxidation resistance. The outer electrode is a 1.2m long cylindrical stainless steel tube with a 22.2 mm internal diameter. The inner surface is polished to avoid localized enhancements of the electric field due to roughness of the electrode and to provide a uniformly distributed discharge. A tape heater created a uniform temperature field in the reactor. The inner wire is held and centered by means of two Teflon® holders, located at both the ends of the external electrode. These pieces serve for hermetic sealing and for insulation of the discharge region. K-type thermocouples are attached to both inlet and outlet connections of the reactor, with the purpose of providing temperature data. Power is supplied to the plasma source by a thyratron-based power supply, with 100 kΩ internal resistance and no-load voltage values from 0 to 20 kV. Pulses of about 100 ns duration and 10 ns rise time are applied; they are transmitted to the central wire electrode by means of a 50 Ω high–voltage, coaxial cable. The power of the plasma source is varied from 0.4 to 10 W by controlling the high voltage pulse amplitude (typically 11 kV) and pulse repetition rate. Voltage is measured using a high voltage probe (model P6015A 1000X, Tektronix Inc.), current measurements are performed using a standard current monitor (Current monitor #411, Pearson Inc.).

In experiments, temperature, humidity and pulse repetition rates were set according to the matrix of experiments. Temperature values were 40, 80, 130, 180 and 230°C. The humidity was 0, 1, 2, 5 and 10 absolute percents. Standard pulse repetition rates were 100, 500 and 1000 Hz. The gas flow rate through the corona reactor was 2 SLM, resulting in a residence time of about 13 seconds.

An overall schematic of the experimental setup is shown in Figure 12. Typical VOC compositions of tested streams were simulated in the laboratory by blending a combination of gaseous and liquid species to generate industrial-like streams. Inlet gas flow rate was metered by MKS precision mass flow controllers. The air for the experiments is provided by a dry air supply (dew point -70°C), that ensures the removal of residuals of water and organic compounds, which could be present in the air line. Liquid flows of water and VOCs were supplied to the system by two HPLC Pumps (models I and II, Lab Alliance Inc.) with an operating range from 0.01 to 10 ml/min and 2% accuracy. The pumps use step motor driven pistons, ensuring good accuracy and repeatability. In order to evaporate the liquid components and to properly mix the different chemicals, a stainless steel mixing chamber, heated up to 160°C, was placed before the reactors. All stainless steel connecting lines were heated by means of heating tapes to prevent condensation of reactants and products. The developed supply system provides reliable control on the chemical composition of the process streams and allows for varying of VOC concentration in a fairly wide range.

Gas composition was determined by a gas chromatograph (Varian Inc, Model 3600), analyzing input and output samples. For the sampling, a part of the gas stream from the reactors was directed to the GC, collected in a 0.25 ml gas-sampling loop, injected into the capillary column (Supelcowax-10) by means of compressed air operated valves, and analyzed with a Flame Ionization Detector (FID). NO_x evaluation was done by a chemiluminescence analyzer (Thermoenvironmental Instrument 42H). Certified gas mixtures were used for the calibration of the NO_x analyzer and the gas chromatograph. Electrical characteristics were acquired with a digital oscilloscope (HP 546126B, 500 MHz, 2GSa). The digitized waveforms were then transmitted to a computer and analyzed with the HP 34801A-BenchLink Scope software.

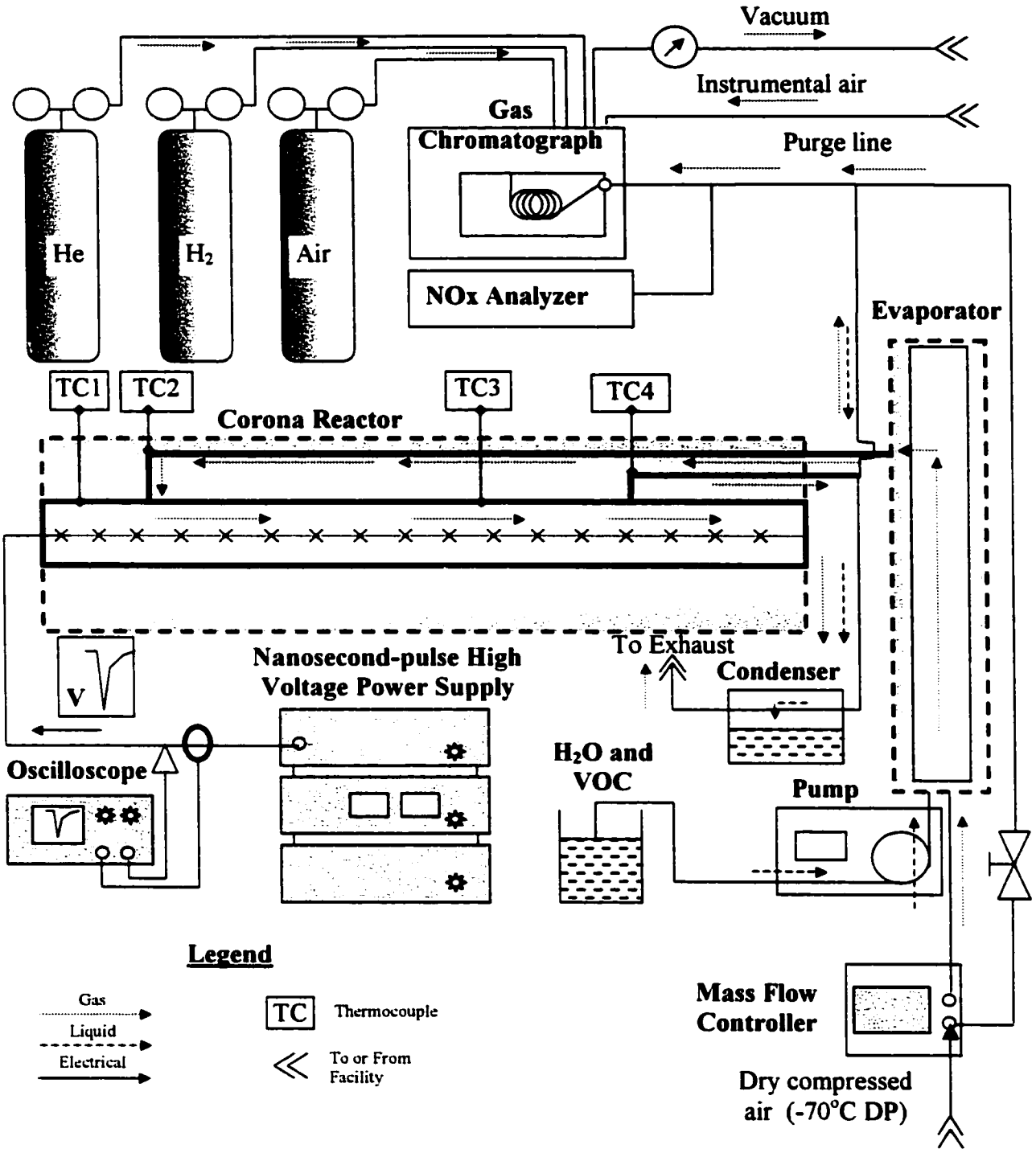

Figure 12. Experimental setup.

3.6. Experimental Results

3.6.1. NOx measurements

The measurements of NO_x in dry air were needed to reconstruct the dependence $\alpha(T)$. Figure 13 shows the experimental values of total $NO+NO_2$ concentration at PRR of 100, 500 and 1000 Hz. The function $\alpha=f(T)$ should be the same for all PRRs if there is a linear dependence of NO_x concentration on corona power . As you can see from the experiment (Figure 14), this conditions holds for the given corona reactor. The maximum pulse voltage was 11 kV.

For simulation, $\alpha(T)$ is taken in the form of a piecewise linear function. Its nodal points are shown in Table XIV. The values of $\alpha(T)$ are also plotted in Figure 15.

TABLE XIV. NODAL POINTS OF $\alpha(T)$.

T, °C	80	130	150	180	210	230
α(T)	0.1	0.12	0.19	0.35	0.61	0.72

In the next chapter we shall compare the experimental temperature dependence of methanol removal efficiency with the results predicted by our theoretical model using experimental $\alpha(T)$. Theory predicts that the increase of α with temperature is due to coupling of energy of electrons and electric field (E/n). Here "n" is the concentration of molecules in the gas phase per unit volume.

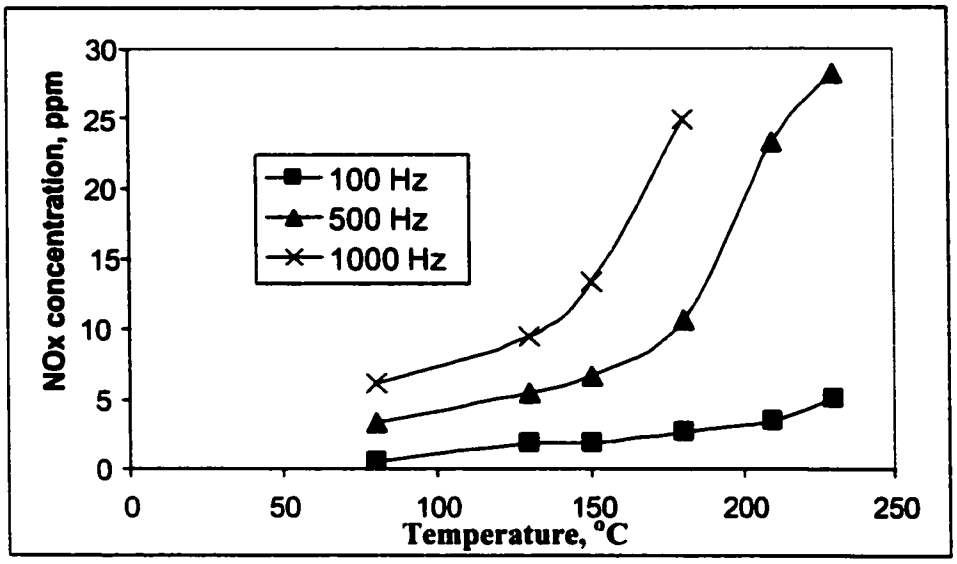

Figure 13. Dependence of NOx concentration on temperature at different PRR.

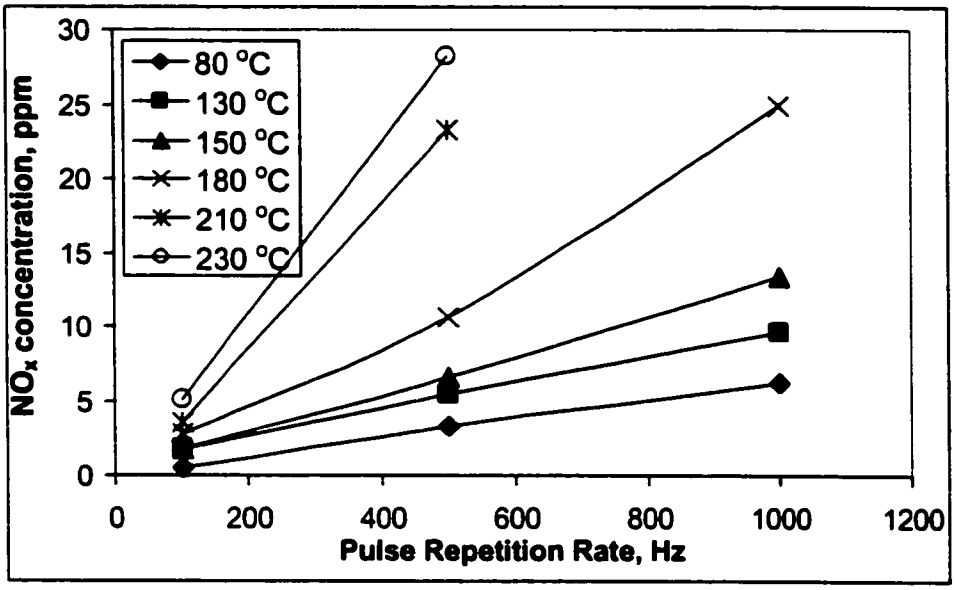

Figure 14. Dependence of NO_x concentration on Pulse Repetition Rate at different temperatures.

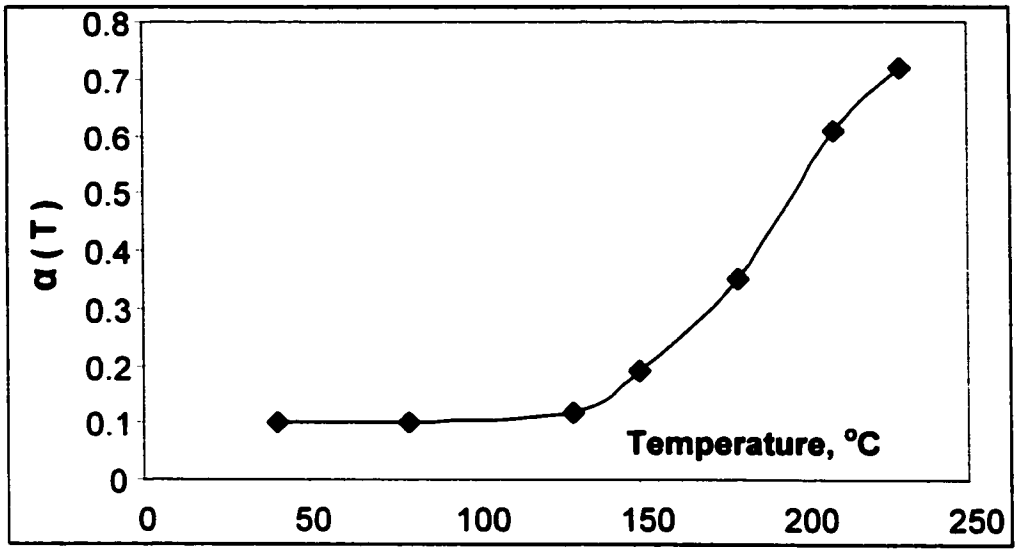

Figure 15. Dependence of α on temperature.

3.6.2. Experiments with methanol

The initial concentration of methanol was 1000 ppm in majority of experiments. For dry air and nitrogen experiments, the concentration of methanol was 2740 ppm. It could not be lower due to limitations of the available experimental equipment. The matrix of experiments was executed, but not all experiments were possible to complete due to premature arcing at higher temperatures, PRR or VOC concentration. In all the experiments the maximum pulse voltage was 11 kV.

A pulsed corona discharge in air produces very little light, which is barely seen with a naked eye even in complete darkness. Luminosity of the discharge increases with PRR, but not with temperature. In contrary, in nitrogen (pure or with water), the discharge is very bright, and more discharge energy is converted to heat. Some temperature increase (up to 40°C) was observed at 1000 Hz. The experimental DRE-Temperature and PEC-temperature dependencies are shown in Figures from 16 to 26.

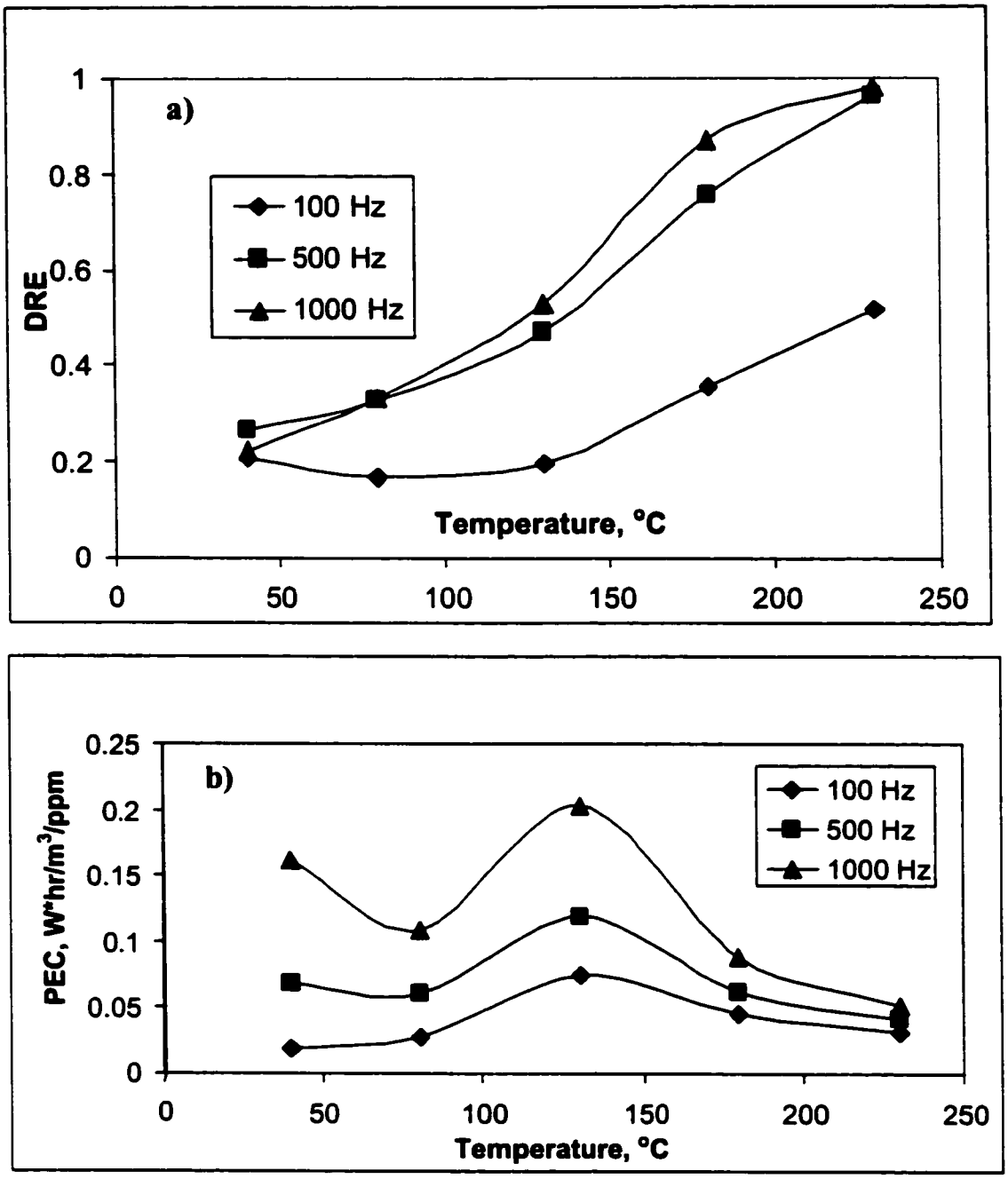

Figure 16. Removal of methanol (2740 ppm) in dry air; a) DRE vs Temperature; b) PEC vs Temperature.

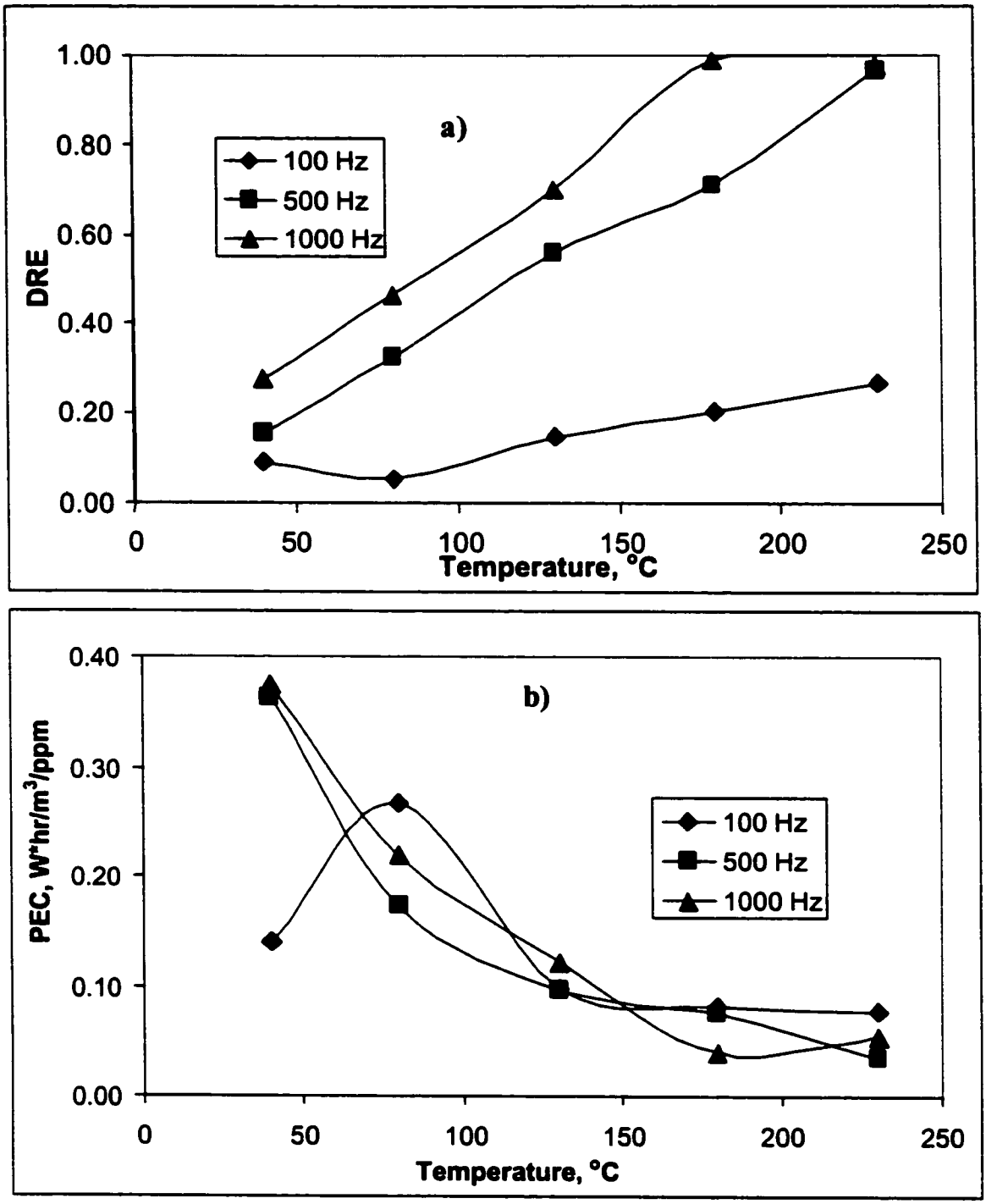

Figure 17. Removal of methanol (1000 ppm) from air with 1% of absolute humidity; a) DRE vs Temperature; b) PEC vs Temperature.

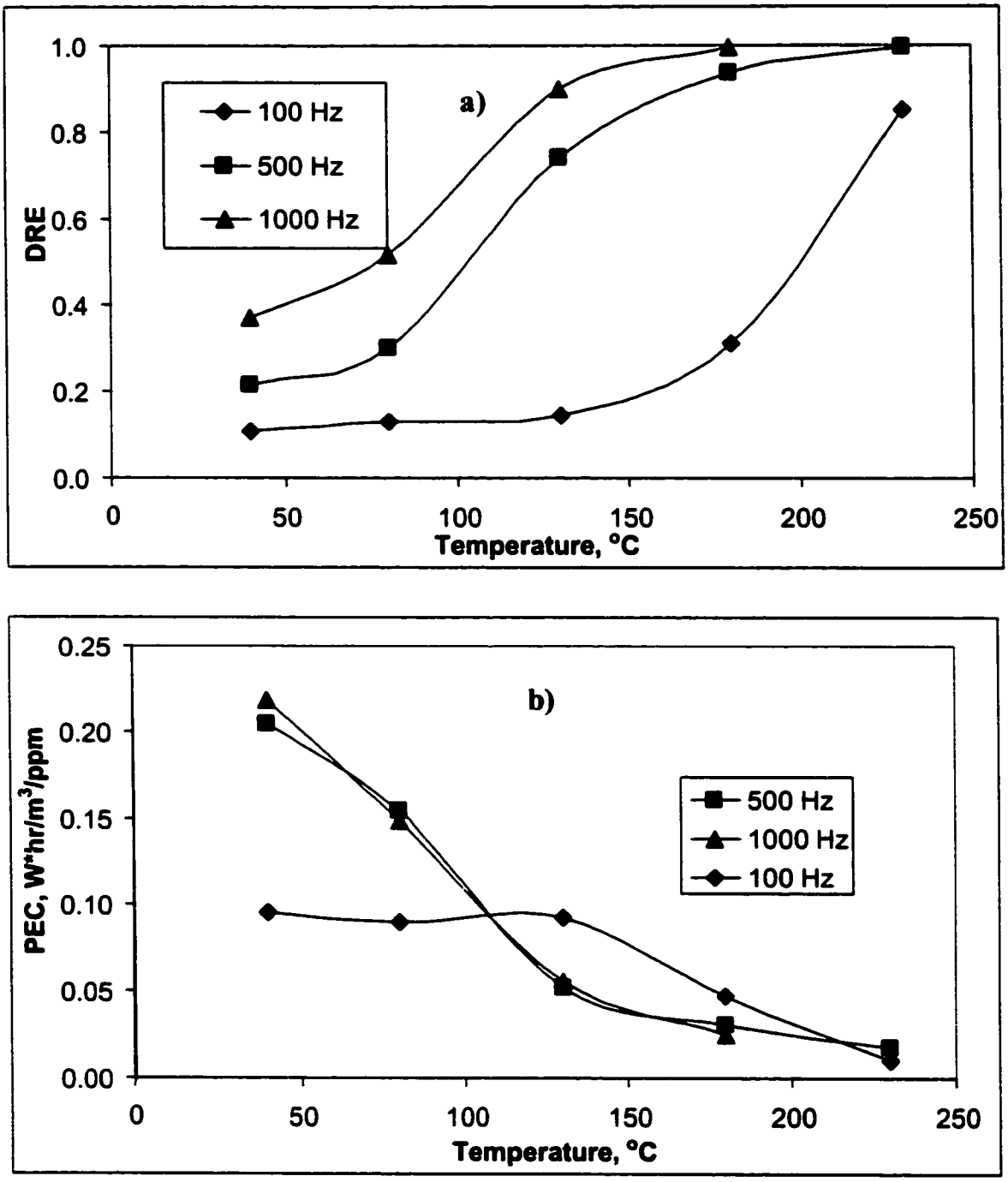

Figure 18. Removal of Methanol (1000 ppm) from air with 2% of absolute humidity; a) DRE vs Temperature; b) PEC vs Temperature.

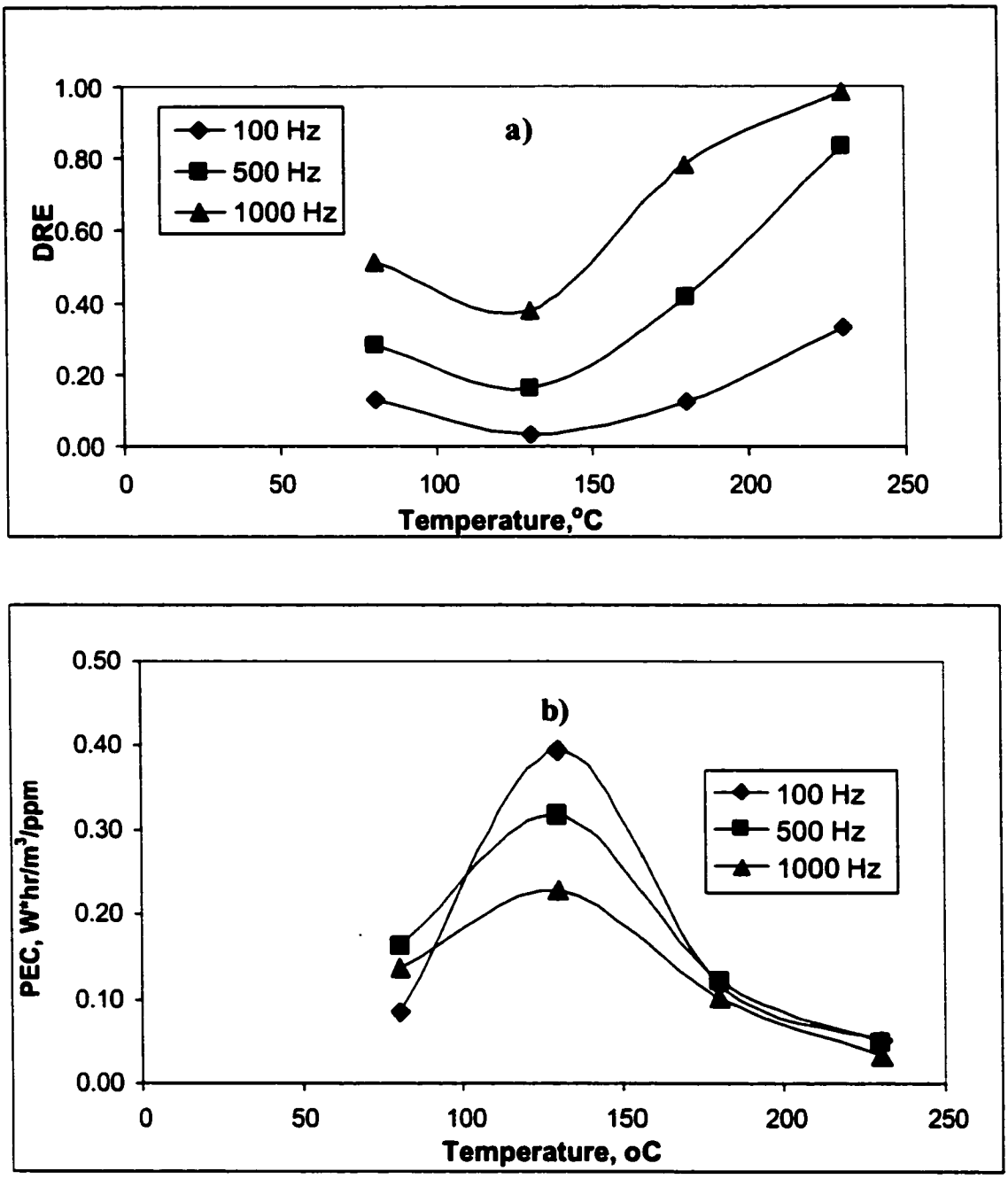

Figure 19. Removal of Methanol (1000 ppm) from air with 5% of absolute humidity; a) DRE vs Temperature; b) PEC vs Temperature.

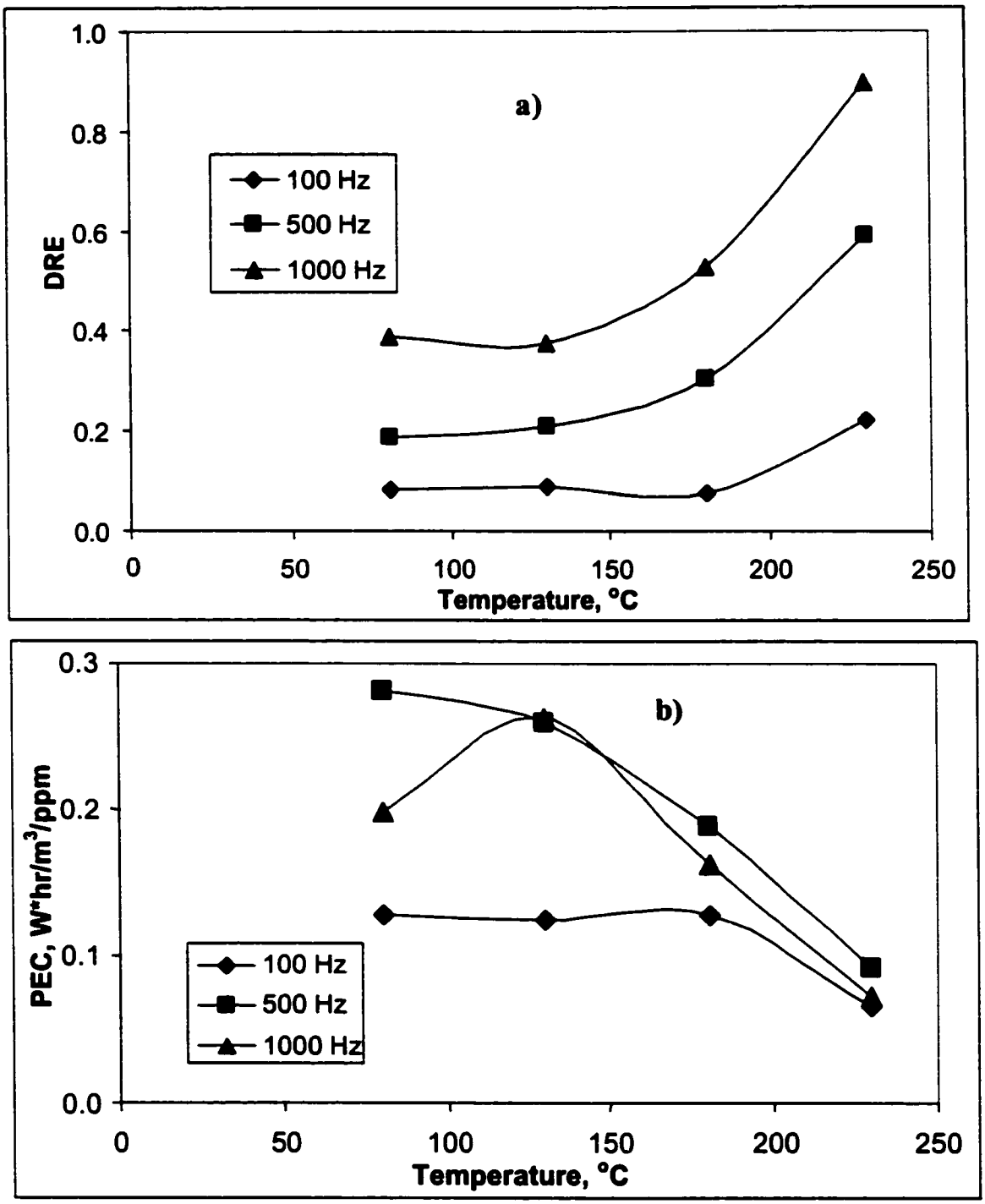

Figure 20. Removal of Methanol (1000 ppm) from air with 10% of absolute humidity; a) DRE vs Temperature; b) PEC vs Temperature.

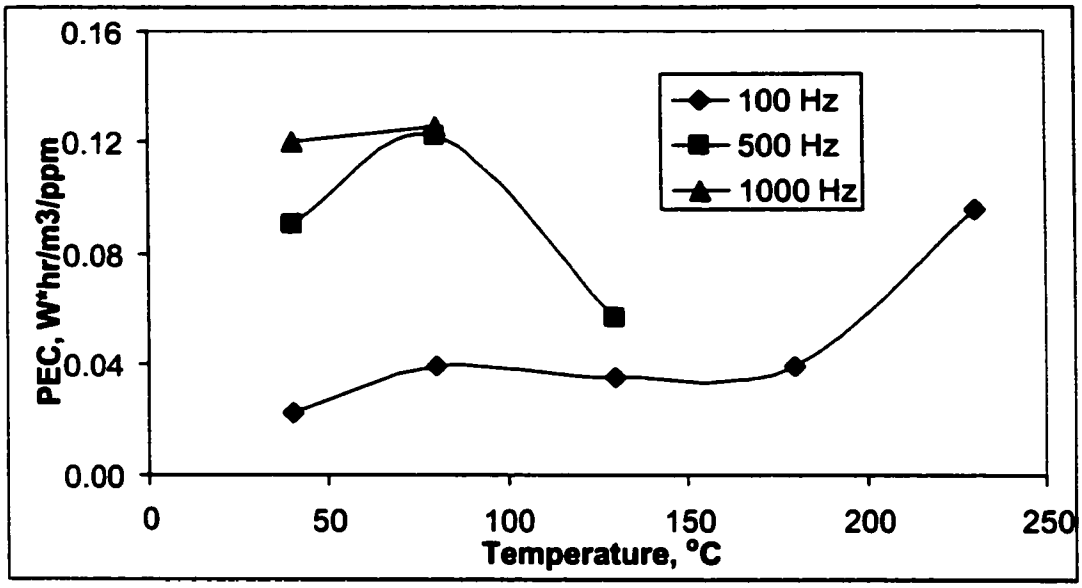

Figure 21. Removal of methanol (2740 ppm) in dry nitrogen.

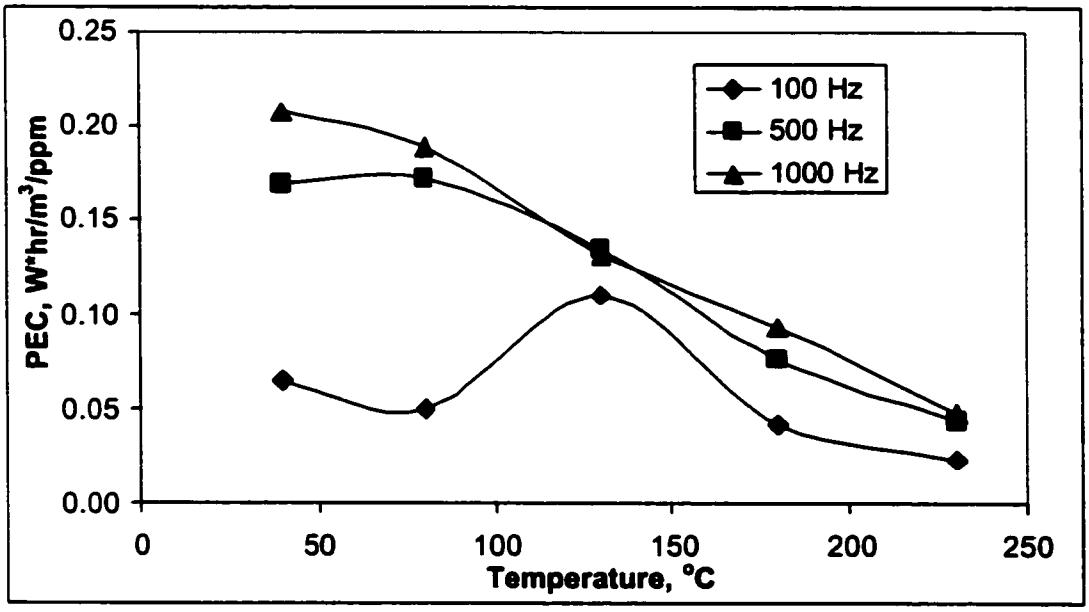

Figure 22. Removal of methanol (1000 ppm) in nitrogen with 2% abs humidity.

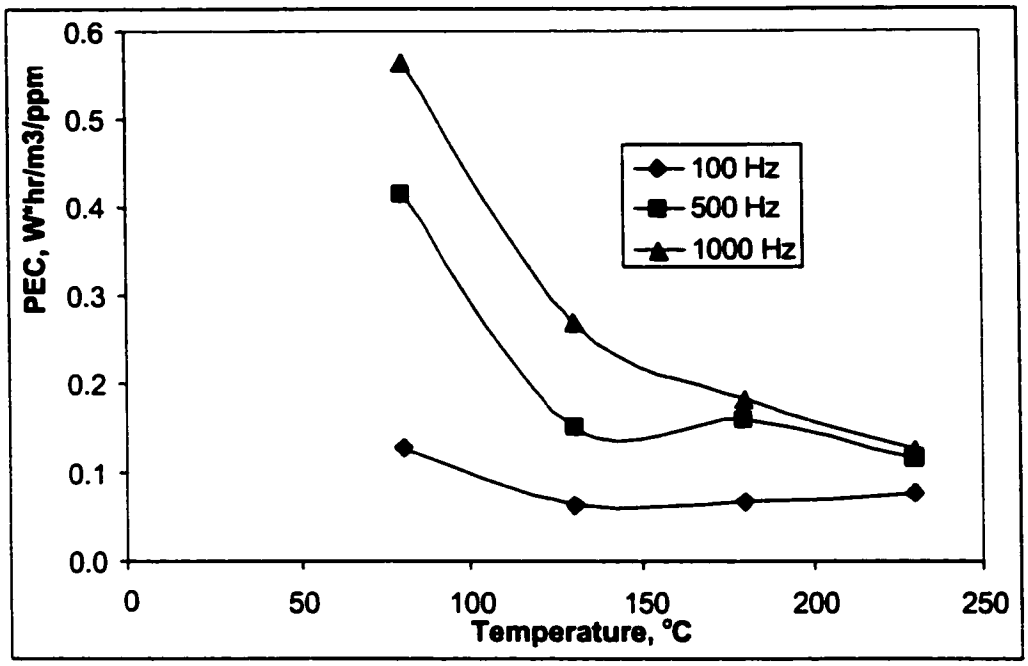

Figure 23. Removal of methanol (1000 ppm) in nitrogen with 10% abs humidity.

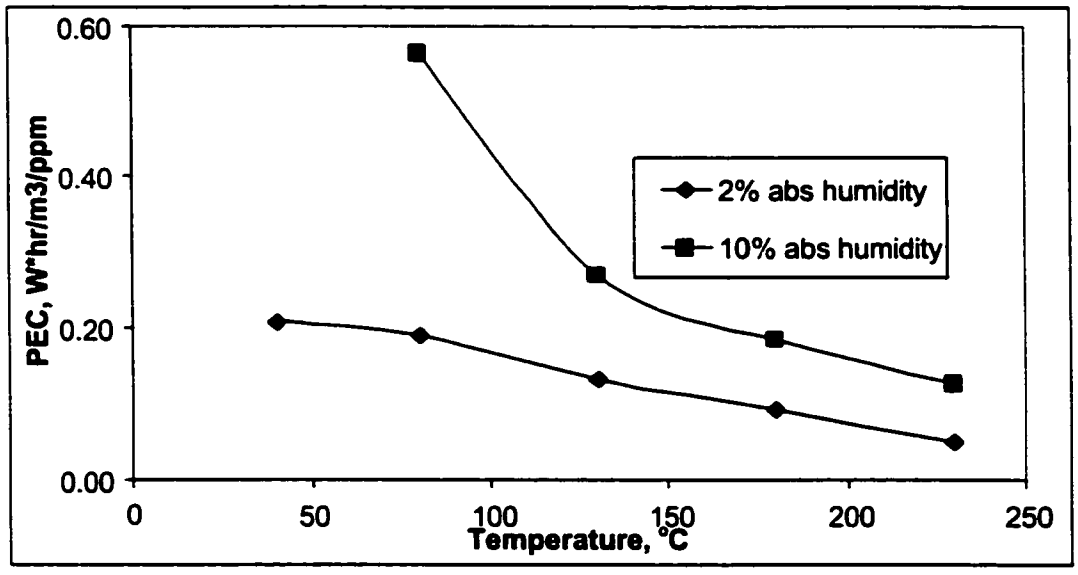

Figure 24. Efffect of humidity on removal of methanol (1000 ppm) in nitrogen (1000 Hz).

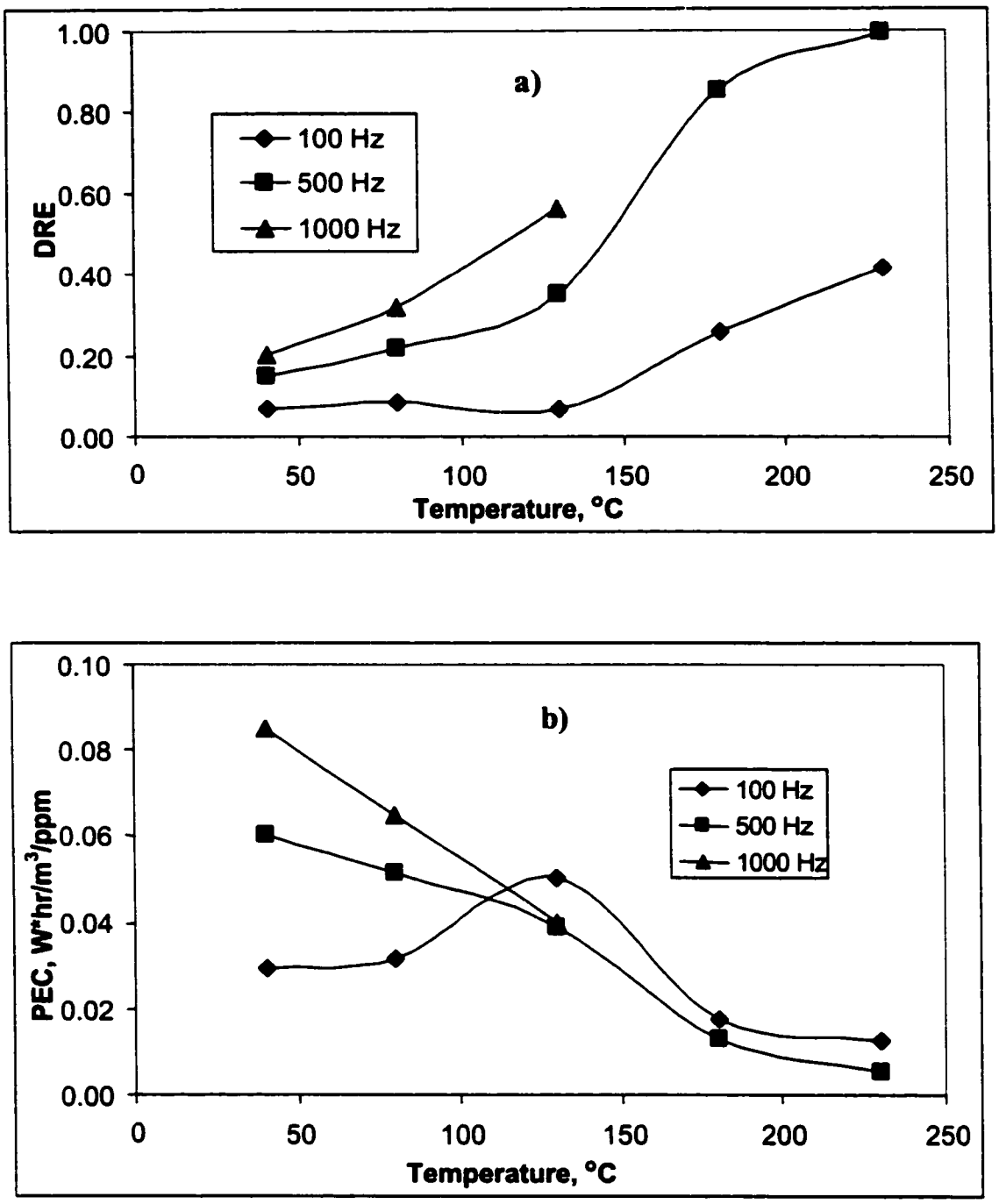

Figure 25. Very high concentration of methanol (5480 ppm) in air: a) DRE vs temperature; b) PEC vs temperature.

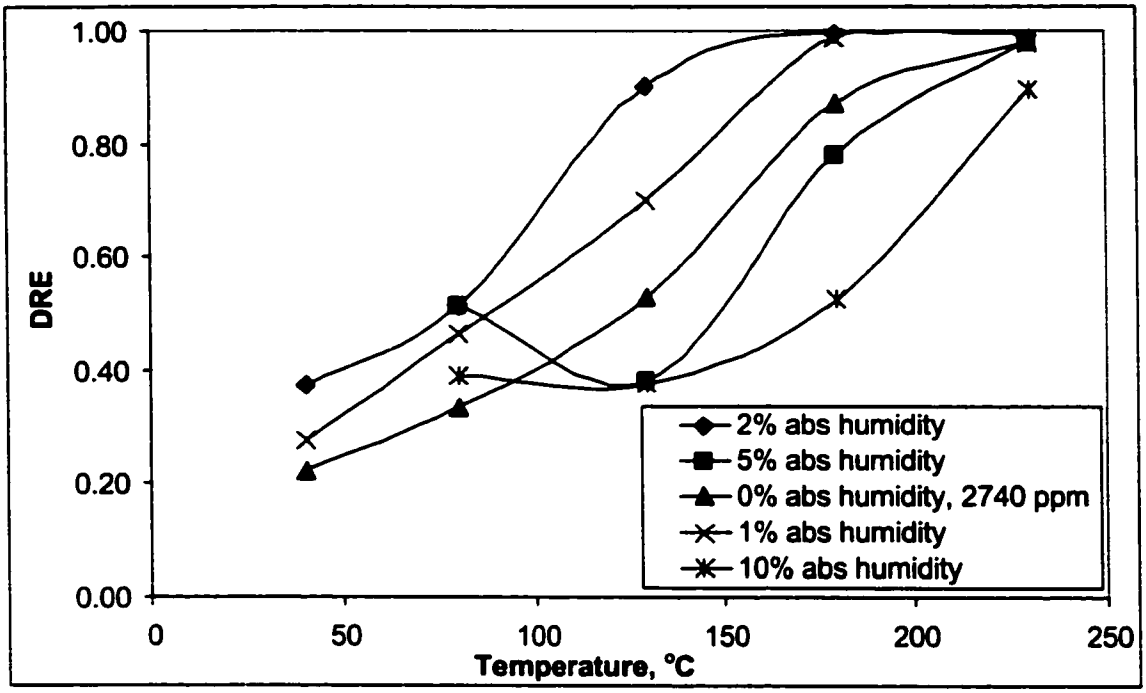

Figure 26. Effect of humidity on the removal of methanol (1000 ppm) in air at 1000 Hz.

The difference of behavior of corona in air and in nitrogen can be explained as following. In air molecules of oxygen are prone to electron attachment. This leads to quenching of avalanches and increase of maximum allowable voltage. In nitrogen there are more excitation and ionization events. The active nitrogen species emit bright light. The streamers are longer, and the breakdown is easier to achieve.

Some peculiarities with gas chromatograph measurements have to be highlighted. It is well known that the response of a FID detector is sensitive to the amount of water in the analyzed gas. There is also a temperature effect. Because the experiments were done at variable humidity and temperature, the calibration must be done at the same conditions. The calibration mixture

contained no water and was at room temperature, so the calibration with the standard (mixture of VOC in the bottle) worked only for dry air and at room temperature.

Fortunately, the concentration of VOC in the stream was controlled by a precision pump and gas flow rate was set by a mass flow controller. Therefore, the standard is given by the experimental setup. The measurements of concentration were done in two stages. At actual experimental conditions (temperature, humidity, VOC concentration) the known concentration of VOC was measured (10 times) at the exit of the reactor. The averaged value was taken as a standard. Then the measurements with corona are taken (from 10 to 15 chromatograms at each point), and relative change of the FID signal is calculated. These procedures gave relative error in determination of DRE not larger than ± 10%.

The measurements of temperature were done by precision K-type thermocouples. The variation of temperature due to control adjustments did not exceed ± 1°C.

3.6.3. Experiments with Acetone

The experiments with acetone were needed to obtain the raw data for the following modeling. The gas composition corresponded to that at paper mill site, with 100RH and temperature about 40°C. Air contained 1000 ppm of methanol and 2% absolute humidity. This value of humidity was known from the previous experiment with methanol to be the optimum for the given corona reactor.

The arcing happens at lower temperature and at lower PRR than in air mixture with 1000 ppm of methanol at the same humidity. The results of experiments are shown in Figure 27. No traces of methanol (expected major byproduct) were found.

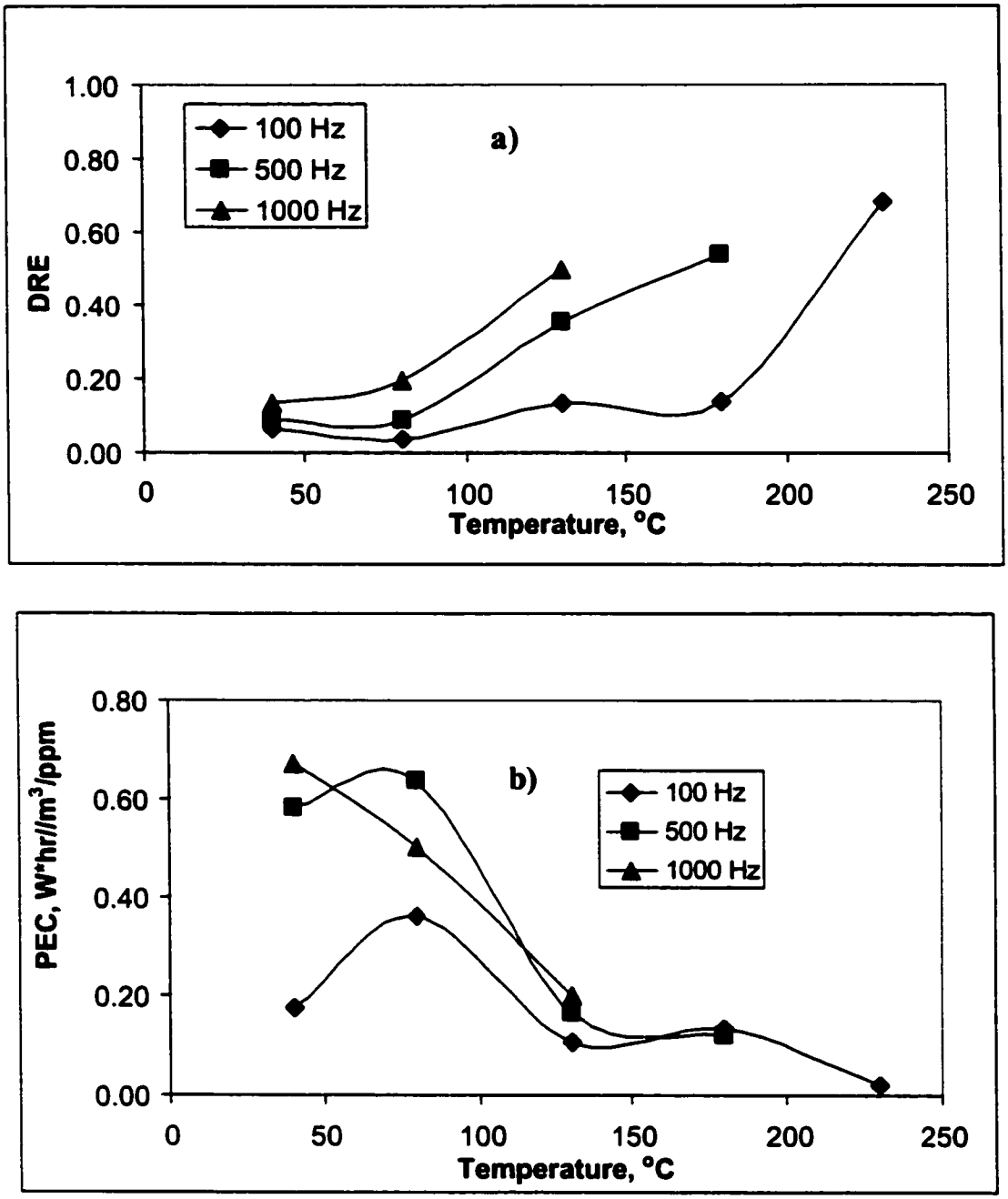

Figure 27. Experiments on removal of acetone (1000 ppm) from air streams, 2% absolute humidity; a) Destruction and removal efficiency versus Temperature; b) Projected Energy Cost versus Temperature.

3.6.4. Experiments with DMS

The experiments were carried out in dry air. Dimethyl sulfide is barely soluble in water, so it was impossible to use our standard technique with evaporation of mixture. The substance was pumped directly into the evaporation chamber. The odor of dimethyl sulfide is unbearable, and even short-term exposure is dangerous for humans. All necessary safety measures were taken. A gas mask was worn while handling of DMS.

The experimental curves are shown in Figure 28. Some methanol (about 100 ppm) was observed in the corona exhaust. Concentration of DMS, as expected, was coupled with concentration of methanol. At high removal rates of DMS, the amount of methanol increased, and vice versa. More of the discharge energy will be spend on methanol destruction. Experiments showed that the removal rate of DMS changes very little with temperature and even decline, when the energy cost increases with temperature. This is exactly opposite to what we observed in experiments with methanol. Therefore, to increase the efficiency of DMS removal, one should somehow clean the treated air from secondary methanol. A corona with a water spray will be feasible for such a purpose.

As in the case with acetone, the arcing starts earlier than with methanol. Because of this reason, no experiments are available at temperatures above 130°C. This "cut-off" temperature is the same for all pulse frequencies (PRR), unlike the case with acetone.

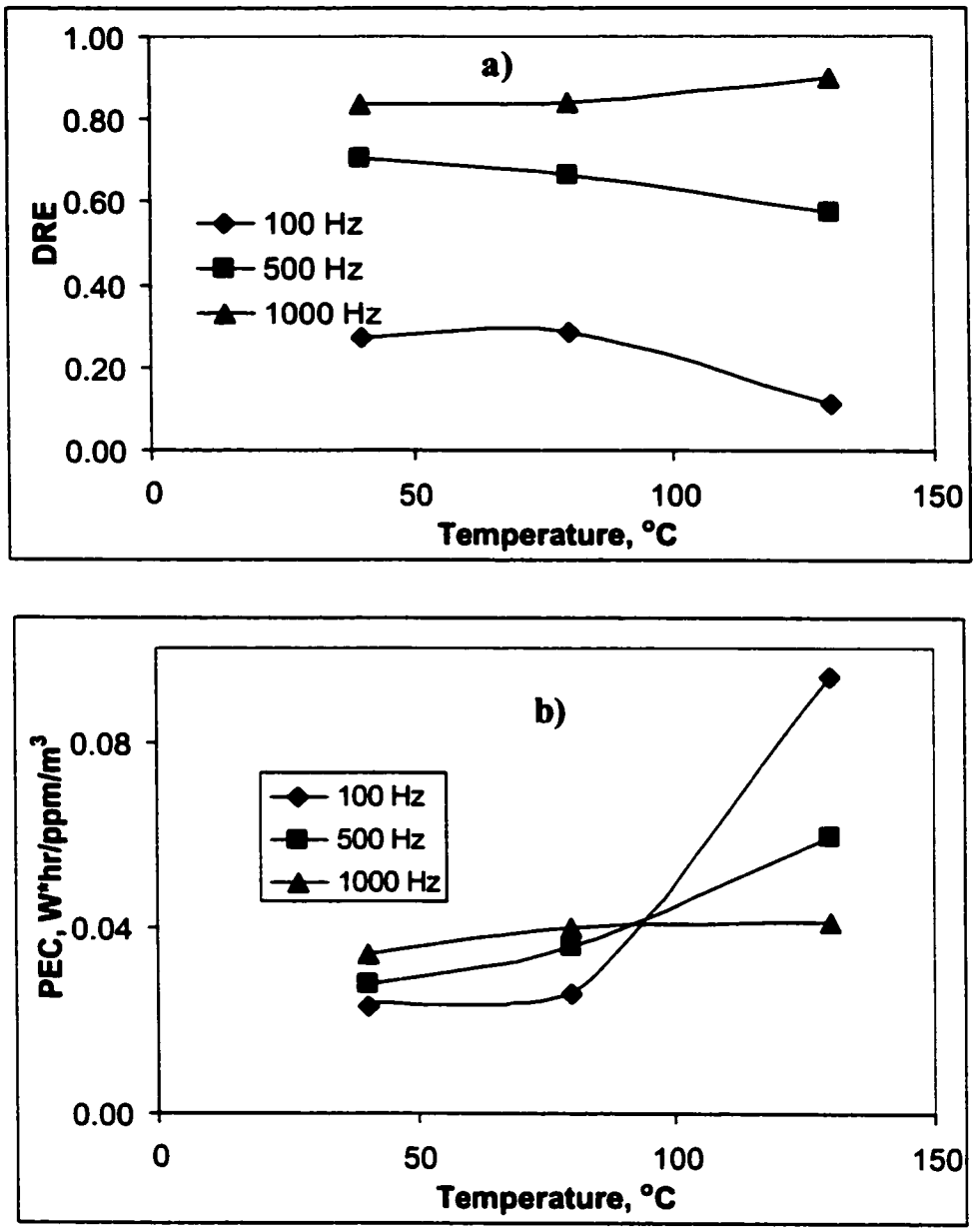

Figure 28. Experiments with Dimethyl Sulfide, 1600 ppm in dry air; a) Destruction and Removal Efficiency versus Temperature; b) Projected Energy Cost versus Temperature. At temperatures above 130 °C the arcing starts. Methanol was a by-product (about 100 ppm) of DMS decomposition. DMS does not dissolve in water.

3.7. Results of Modeling of Pulsed Corona Discharge

The modeling was done using CHEMKIN library of FORTRAN procedures. The detailed reaction mechanism includes 1) NO_x formation; 2) methanol oxidation; 3) DMS oxidation. Here NO_x mechanism is the foundation for the rest of the modeling. The list of all reaction is given in Appendix as a printout of CHEMKIN compiler output file.

Because the concentration of VOC is several orders of magnitude less than the concentration of major constituents of humid air (nitrogen, oxygen and water), the reactions of VOC with electrons are not included in the mechanism.

From the experiments with corona in dry air without VOC, we reconstructed the values of a (the portion of high energy electrons). Alpha serves as a similarity parameter for all reaction mechanisms in the given corona setup, of course, if the experimental conditions do not change.

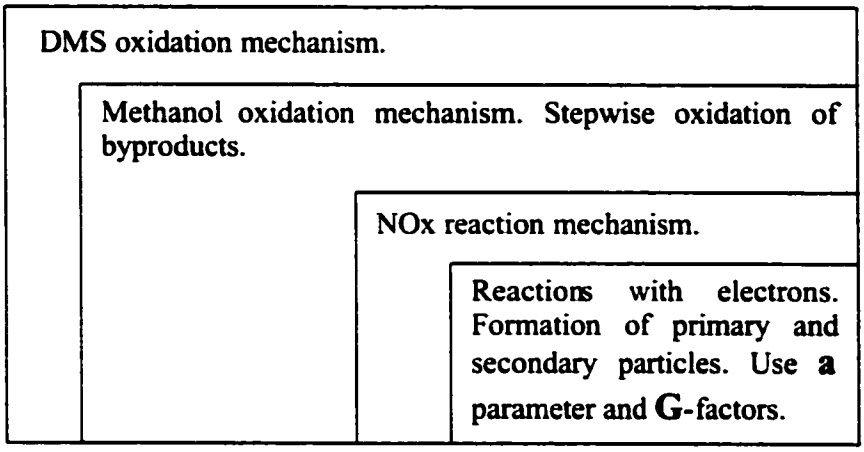

Figure 29. Relationship between NO_x formation, methanol oxidation, and dimethyl sulfide oxidation mechanisms.

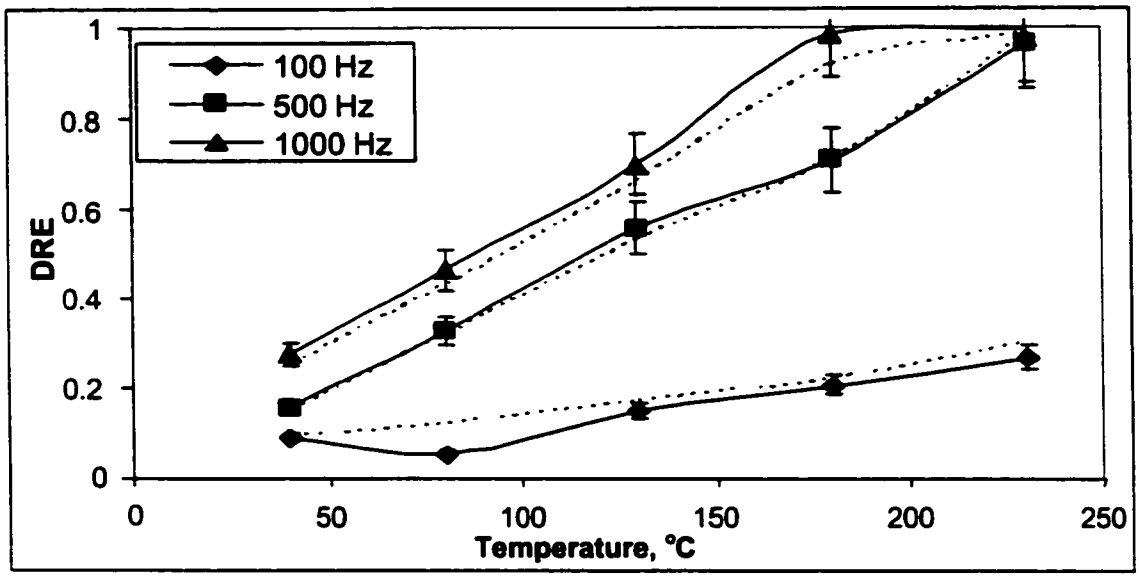

Figure 30. Comparison of experimental (solid lines) and simulation (dashed lines) results for DRE of methanol (1000 ppm) in air with 1% absolute humidity.

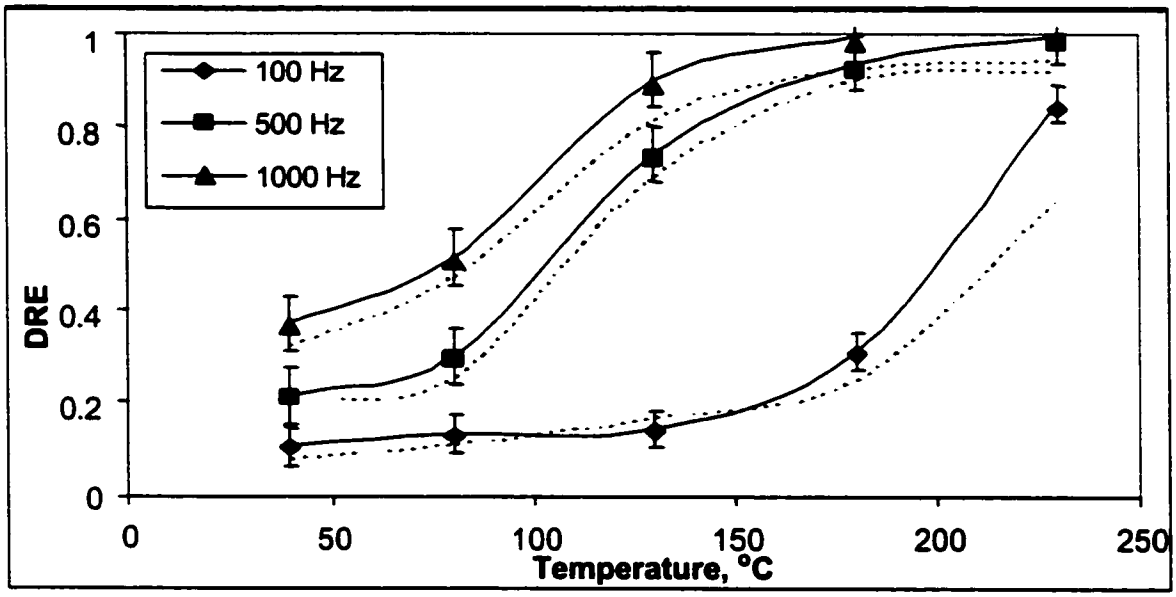

Figure 31. Comparison of experimental (solid lines) and simulation (dashed lines) results for DRE of methanol (1000 ppm) in air with 2% absolute humidity.

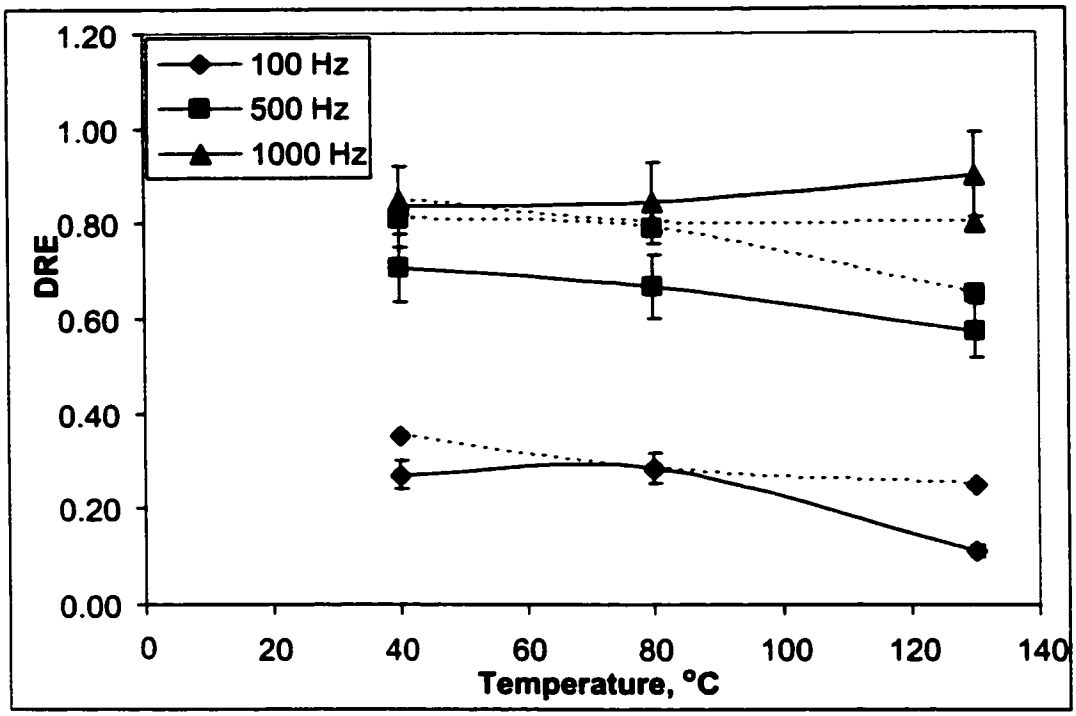

Figure 32. Comparison of experimental (solid lines) and simulation (dashed lines) results for DRE of DMS (1600 ppm) in dry air.

The presented mechanism of methanol oxidation includes additional reactions of radicals with methanol, and the following stepwise destruction of the products up to stable CO_2 and H_2O. At the same time, methanol is a byproduct of DMS oxidation. Therefore, to compose a DMS mechanism, only few reactions must be added to the methanol mechanism. Figure 29 demonstrates the relationship between all three-reaction mechanisms. Figures 30 and 31 show the results of modeling for methanol at 1 and 2 % of absolute humidity, and Figure 32 summarize the results for DMS in dry air. It can be seen that a good agreement of the theory and experiment was achieved.

3.8. Discussion

For the following discussion, it is necessary to generalize the experimental data. The primary goal for the further investigation is to determine the range of optimum operational conditions (target: minimum energy cost per ppm of VOC) for the pulsed corona pilot plant.

In the previous chapters, the Projected Energy Cost (PEC) was proposed as a figure of merit to compare the experimental results obtained at different removal efficiencies. We take a methanol as the simplest substance to show the pattern in experimental results.

The PEC data on methanol, obtained in several runs with different humidity, were arranged as a function of reactor temperature. Figure 33 demonstrates the effect of temperature.

The same data can be plotted as a function of humidity. The effect of humidity is demonstrated in Figure 34.

Let us summarize the major peculiarities in behavior of discharge chemistry as seen in Figures 33 and 34.

1. The effect of humidity is very non-linear. At the value of humidity about 2 absolute percent, there is a minimum of energy cost for the whole set of temperatures.
2. The temperature effect is more complex. The curves represent two different patterns: a) curves with smooth decrease of energy cost with temperature (humidity of 1 and 2%); b) curves with a maximum of energy cost at 130 °C (humidity of 0, 5, and 10 abs %).

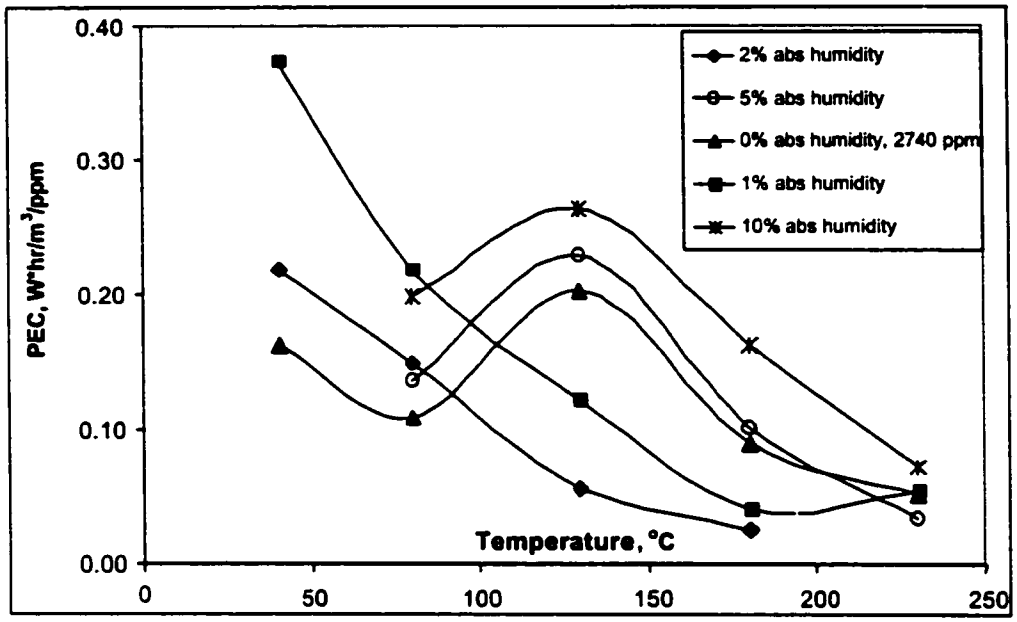

Figure 33. The effect of temperature on energy cost of methanol removal (1000 ppm, 1000 Hz PRR) at different humidities. The maximum of energy cost is observed at 130°C. There is a similarity of curves for no humidity and large humidity cases (0%, 5% and 10%).

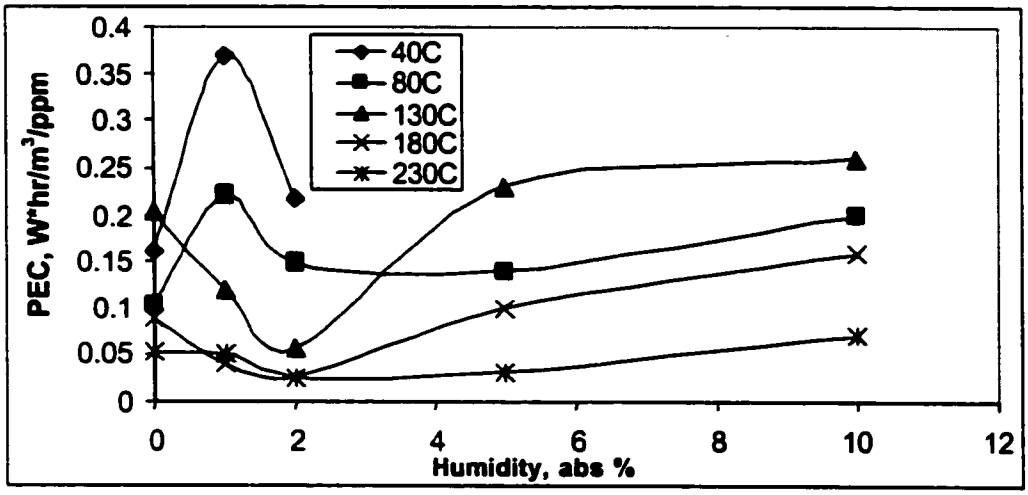

Figure 34. Effect of humidity on removal of methanol (1000 ppm) in air at 1000 Hz.

In the literature we could not find any systematic data on the effect of humidity on removal efficiency of VOC. Majority of experiments were done in dry air (see, for example the work of Penetrante [62]). Methanol kinetics predicts almost linear increase of discharge efficiency with humidity. There should be no minima or maxima.

The temperature effect in corona and barrier discharges were studied in several works. In [14], the magnitude of NO concentration in the coaxial dielectric barrier discharge decreased with temperature, and had minimum at about 130°C. This result is in a very good agreement with our experiments. It also shows that the effect of "130°C" is not due to methanol stage of the mechanism. Our own analysis of humidity and temperature effects through the prism of chemistry in the whole range of these parameters supported this hypothesis. The temperature effect also seems unexplainable by means of kinetics of chemical reactions. It should be concluded that the abovementioned temperature and humidity effects are due to some physical phenomena. Here we attempt to develop physical hypotheses explaining the experimental facts.

Hypohesis 1. Humidity effect is due to competition of two simultaneous processes. The minimum in the PEC-humidity curve is because of the competition of two different processes related to water molecules. From one side, water is needed to produce OH radicals. Chemical modeling shows that with the increase of water molar fraction, the destruction efficiency of VOC should increase. So, this is a positive role of water. From the other side, the water molecules can attach corona electrons. The rate of primary ionization decreases, and so does the rate of free radicals formation. Eventually, there will be fewer radicals to react with VOC, and the rate of VOC removal decreases. This is the negative role of water. The balance of the abovementioned processes can potentially lead to maxima or minima in the energy-humidity curve. More sophisticated modeling is needed to see this effect.

Hypothesis 2. Formation of tiny water droplets in the corona discharge. When viewing the temperature effect, one can see that the processes with high humidity in air (5 and 10 absolute percent) follow the same pattern as the process in dry air. The energy cost reaches maximum at 130 °C in both cases. Again, this experimental fact cannot be described in the framework of the assembled chemical mechanism. But we attempt to explain similarities of the curves at 0, 5 and 10 % of absolute humidity.

What is the common ground for processes in dry air and at high humidity cases? The similarity would exist if there were insufficient amount of water in the gas phase. In the streams with high content of water, plasma can induce condensation of humidity into tiny droplets. Very little amount of water would then remain in the gas phase. The effect of plasma-induced condensation is known and studied theoretically and experimentally [63]. The presented link between low-humidity and high-humidity cases needs experimental confirmation with direct registration of not only the droplets, but also their concentration and size distribution.

The modeling of chemistry in the discharge with the assembled methanol mechanism worked satisfactorily for the gas mixtures with 1 and 2 percent of absolute humidity. It is also feasible to extend the mechanism of methanol to DMS by adding some reactions. Therefore, using the method based on alpha-parameter, one should reliably predict the chemistry of different VOCs in the same discharge.

The other important outcome from the corona research, in addition to understanding the role of temperature and humidity, is the confirmation of applicability of the pulsed corona technology to treatment of flue gases with high content of VOC (up to 5000 ppm). A wider operational range of pulsed corona reactors can be justified. For the particular case of the paper mill operation of the pulsed corona pilot plant, this means that the spikes of VOC concentration

due to the mill process cycle will be treated completely. No additional gas treatment will be needed.

The buildup of methanol at high concentrations of DMS or acetone was a great concern. It was shown that even at 1600 ppm of DMS or at 1000 ppm of acetone, the concentration of methanol stays very low at about 100 ppm. This amount can be easily scrubbed by the amount of water that will be used for spraying in the pilot plant. If a high concentration of methanol (about 1000 ppm) is present in the stream, it is feasible to scrub the methanol in a stand-alone scrubber, and then destroy insoluble compounds in the corona reactor with a spray to wash the secondary methanol.

Water can be also thought not only as a desired agent from the standpoint of process efficiency, but also as a necessary factor to prevent NOx formation. In dry air significant concentration (about 30 ppm) of NOx is formed. While destroying VOC, another undesirable species will be formed. The presence of some water in the gas stream helps convert these species to solvable HNO_3. Therefore, the wet corona seems more feasible than a dry one.

A serious difference between the gliding arc and pulsed corona is in their NOx producing capability. Corona produces one or two orders of magnitude less NOx than the gliding arc. Smaller NOx concentrations are easier to fight with addition of water.

It has to be pointed out that from the chemical point of view our results obtained for a "dry" corona with 2% of absolute humidity in the stream are equivalent to the results in the "wet" corona with a water spray [13]. The spray does not change relative humidity whereas the air is already saturated with water. Because the pulse repetition rate of corona is very high and millions of streamers are formed per second, there is a very little probability of streamer to encounter a droplet. The chemistry with fast electrons and secondary radicals occurs in the gas phase. The role of droplets here is to absorb some VOC in accordance with Henry's law.

3.9. Conclusions and Recommendations for Future Work

The program of experiments aiming to enhance scientific and engineering knowledge required for successful testing and further application of the pulsed corona technology to treat VOC emissions in the forest products industry is completed. According to the tasks of the research objectives, the following conclusions can be made.

Corona reactors can operate at high (>1000 ppm) concentrations of VOC, particularly with large content of either methanol or DMS, or acetone (each taken separately). Large amounts of primary methanol (about 1000 ppm) must be removed in a stand-alone scrubber in the very beginning of the abatement process. The amount of water that will be used for spraying in the corona reactor is sufficient for removing of secondary methanol that was formed during oxidation of DMS and acetone.

A Projected Energy Cost (PEC) was proposed as the figure of merit to compare results on removal of VOC at different gas compositions and regimes of the pulsed corona discharge.

Temperature and humidity have profound effect on DRE of VOC. Destruction and Removal Efficiency increases with temperature, but there is a maximum of PEC at 130°C. Minimum PEC is observed at 2% absolute humidity. It is economically feasible to humidify contaminated air streams for the following pulsed corona processing and keep the temperature either below 80°C or above 200°C. A substantial role of water is recognized to prevent NOx formation.

A plasma-chemical kinetic model is developed to predict removal rates of methanol and DMS in pulsed corona reactors. A fraction of high energy electrons (a) was used as a similarity parameter for primary processes in the discharge chemistry. Together with G-factor data from radiation chemistry, alpha provided necessary linking of the bulk plasma parameters and

concentration of free radicals. A good match of experimental results and calculation was achieved for methanol and DMS.

It was found that the observed dependence of PEC on humidity and temperature could not be described in terms of only chemical kinetics. Two physical hypotheses were proposed to explain these phenomena.

For the future work, the experiments on the industrial-scale or pilot pulsed corona reactors are essential. An experimental program similar to that presented in the thesis should be fulfilled. This will generalize or limit the application of the theory of similarity parameter a in linking bulk plasma parameters and chemistry. The elementary chemical mechanisms for all the substances of interest in the Forest project should be assembled and verified with experimental data.

The proposed hypotheses about the form of dependence of PEC on temperature and humidity must be supported with additional modeling of streamers and experimental results on quantity and size distribution of the droplets which formation is suspected in the pulsed corona plasma with high absolute humidity.

4. CONCLUSIONS

The gliding arc and pulsed corona plasma technologies for abatement of Volatile Organic Compounds in the forest industry were considered theoretically and experimentally.

1. The effect of "overshooting" in transitional regimes of low-current gliding arc was explained in terms of discharge stability.
2. A concept of the mobile pulsed corona pilot plant was described.
3. A program of experiments to investigate the operation of the plant at conditions close to the existing in the paper mill streams was proposed and implemented.
4. A plasma-chemical model of methanol and dimethyl sulfide destruction in the pulsed corona discharge was developed.
5. Projected Energy Cost value was proposed as a figure of merit to characterize the efficiency of the corona reactor.
6. Optimum operational regimes of corona reactor operation were found with respect to temperature and humidity.

CITED LITERATURE

1. Harkness, J.L., Fridman, A.A.: The Technical and Economic Feasibility of Using Low-Temperature Plasmas to Treat Gaseous Emissions from Pulp Mills and Wood Process Plants. Technical Bulletin No.795. National Council for Air and Stream Improvement. September 1999.
2. Lesueur, H., Czernichowski, A., Chapelle, J., Production of Synthetic (CO+H2) Gas from CH4 Oxidation by CO2 in a Gliding-discharge Electroreactor. Journal de Physique 51: C557-C564, 1990.
3. Czernihowski, A., Nassar, H., Ranaivosoloarimanana, A., Fridman, A.A., Simek, M., Musiol, K., Pawelec, E. and Dittrichova, L.: Spectral and Electrical Diagnostics of Gliding Arc. Acta Physica Polonica A 89: 595 -603, 1996.
4. Raizer, Y.P.: Gas discharge physics. Berlin, Springer-Verlag, 1997.
5. Fridman, A., Petrousov, A., Chapelle, J., Cormier, J.-M., Czernichowski, A., Lesueur, H., Stevefelt, J.: Modele Physique de L'Arc Glissant. Journal de Physique III, 4:1449-1465, 1994.
6. Fridman, A., Nester, S., Yardimci, O., Saveliev, A. and Kennedy, L.A.: Gliding Arc Plasma Instability. Proceedings of the 13th International Symposium on Plasma Chemistry. 2: 819-824, 1997.
7. Richard, F., Cormier, J.-M., Pellerin, S., Chapelle, J.: Physical Study of Gliding Arc Discharge. Journal of Applied Physics. 79: 2245-2250, 1996.
8. Pellerin, S., Richard, F., Chapelle, J., Cormier, J.-M. and Musiol, K.: Heat String Model of Bi-Dimensional DC Glidarc. Journal of PhysicsD-Applied Physics, 33(19): 2407-2419,2000.
9. Mutaf -Yardimci, O., Saveliev, A.V., Fridman, A.A. and Kennedy, L.A.: Thermal and Nonthermal Regimes of Gliding Arc Discharge in Air Flow. Journal of Applied Physics. 87: 1632-1641, 2000.
10. Frank–Kamenetski, D.A.: Diffusion and heat transfer in chemical kinetics. Moscow, Nauka, p491, 1987.
11. Rusanov, V.D., Fridman, A.A.: Physics of chemically active plasma. Moscow, Nauka, p416, 1984.
12. Deminskii, M.A., Potapkin, B.V., Cormier, J.-M., Richard, F., Bouchoule, A. and Rusanov, V.D.: On the Effect of the High Propagation Velocity of the Gliding Arc in a Rapid Gas Flow. Phys.-Doklady. 42: 337-339, 1997.
13. Sobacchi, M.G.: Hydrocarbon Processing in Non-equilibrium Gas Discharges. Master of Science Thesis, University of Illinois at Chicago, 2001.
14. Hackam, R. and Akiyama, H.: Air Pollution Control by Electrical Discharges. IEEE Transactions on Dielectrics and Electrical Insulation 7(5):654-683, 2000.

15. Turnipseed, A.A., Barone, S.B., and Ravishankara, A.R.: Reaction of OH with Dimethyl Sulfide. 2. Products and Mechanisms. J. Phys. Chem., 100: 14703 - 14713, 1996.

16. Barnes, I., Bastian, V., and Becker, K.H.: Kinetics and Mechanisms of the Reaction of OH Radicals with Dimethyl Sulfide. Int. J. Chem. Kinet., 20: 415 - 431, 1988.

17. Saltelli, A., and Hjorth, J.: Uncertainty and Sensitivity Analyses of OH - Initiated Dimethyl Sulphide (DMS) Oxidation Kinetics. J. Atmos. Chem., 21: 187 - 221, 1995.

18. http://www.ei.jrc.it/dms/

19. Wallington, T.J., Ellermann, T., and Neilsen, O.J.: Atmospheric Chemistry of Dimethyl Sulfide: UV Spectra and Self - Reaction Kinetics of CH3SCH2 and CH3SCH2O2 Radicals and Kinetics of the Reactions CH3SCH2 + O2 --> CH3SCH2O2 and CH3SCH2O2 + NO --> CH3SCH2O + NO2. J. Phys. Chem., 97: 8442 - 8449, 1993.

20. Spinks, J. W. T. and Woods, R. J.: An introduction to radiation chemistry. John Wiley & Sons, Inc., 1990.

21. Beaujon, E.: Simulation of Dissolution and Removal of VOCs in Corona Discharge. Internship report, University of Illinois at Chicago, Chicago, 2000.

22. Machi, S., Tokunaga, O., Nishimura, K., Hashimoto, Sh., Kawakami, W., and Washino, M.: Radiation Treatment of Combustion Gases. Radiat. Phys. Chem., 9: 371-388, 1977.

23. Willis, C., Boyd, A.W.: Excitation in the Radiation Chemistry of Inorganic Gases. Int. J. Radiat. Phys. Chem., 8: 71-111, 1976.

24. Dixon, R.S.: The Dissociation of Water Vapor by Photolytic, Radiolytic and Electron Iimpact Methods. Radiation Res. Rev., 2: 237-296, 1970.

25. Hoigne, J., and Bader, H.: Rate Constants of Reactions of Ozone with Organic and Inorganic Compounds in Water – II Dissociating Organic Compounds. Water Res., 17: 185-194, 1983.

26. Hoigne, J., Bader, H., Haag, W.R., and Staehelin, J.: Rate Constants of Reactions of Ozone with Organic and Inorganic Compounds in Water – III Inorganic Compounds and Radicals. Water Res., 19, 8: 993-1004, 1985.

27. Amels, P., Elias, H., and Wannowius, K.J.: Kinetics and Mechanism of the Oxidation of Dimethyl Sulfide by Hydroperoxides in Aqueous Medium - Study on the Potential Contribution of Liquid-Phase Oxidation of Dimethyl Sulfide in the Atmosphere. J. Chem. Soc., Faraday Trans., 93(15): 2537-2544, 1997.

28. Senent, M.L., Moule, D.C., Smeyers, Y.G.: Ab-Initio and Spectroscopic Study of Dimethyl Sulfide - An Analysis of The Torsional Spectra of (CH3)(2)S and (CD3)(2)S. J. Phys. Chem., 99: 7970-7976, 1995.

29. Mckee, M.L.: Computational Study of Addition and Abstraction Reactions between OH Radical and Dimethyl Sulfide - A Difficult Case. J. Phys. Chem., 97: 10971-10976, 1993.

30. Mashkin, V.Yu, Kudenkov, V.M: Kinetic Studies of Dimethyl Sulfide Synthesis from Methanol and H2S. React. Kinet. Catal. Lett., 46(2): 263-269, 1992.

31. Ridgeway, R.G., Bandy, A.R., and Thornton, D.C.: Determination of Aqueous Dimethyl Sulfide Using Isotope-Dilution Gas Chromatography / Mass Spectrometry. Marine Chemistry, 33(4): 321-334, 1991.

32. Martinez-Haya, B., Zapater, I., Quintana, P., Menendez, M., Verdasco, E., Santamaria, J., Banares, L., Aoiz, F.J.: Photodissociation of Dimethyl Sulfide at 227.5 nm: Resonance-Enhanced Multiphoton Ionization of the Methyl Fragment. Chemical Physics Letters, 311(3-4): 159-166, 1999.

33. Nielsen, O.J., Sidebottom, H.W., Nelson, L., Treacy, J.J., Ofarrell, D.J.: An Absolute and Relative Rate Study of the Reaction of OH Radicals with Dimethyl Sulfide. International Journal of Chemical Kinetics, 21(12): 1101-1112, 1989.

34. Koshelev, S.N., Paukshtis, E.A., Verkhoturova, N.A., and Mashkina, A.V.: Catalytic Conversion of Dimethyl Sulfide to Methyl Mercaptan. Kinetics and Catalysis, 29(2), Part 1: 326-330, 1988.

35. Hsu, Y.C., Chen, D.S., Lee, Y.P.: Rate Constant for the Reaction of OH Radicals with Dimethyl Sulfide. International Journal of Chemical Kinetics, 19(12): 1073-1082, 1987.

36. Sekusak, S., Piecuch, P., Bartlett, R.J., and Cory, M.G.: A General Reaction Path Dual-Level Direct Dynamics Calculation of the Reaction of Hydroxyl Radical with Dimethyl Sulfide. J. Phys. Chem. A, 104: 8779-8786, 2000.

37. Hynes, A.J., Stoker, R.B., Pounds, A.J., McKay, T., Bradshaw, J.D., Nicovich, J.M., Wine, P.H.: A Mechanistic Study of the Reaction of OH with Dimethyl-d6 Sulfide. Direct Observation of Adduct Formation and the Kinetics of the Adduct Reaction with O2. J. Phys. Chem., 99: 16967-16975, 1995.

38. Hynes, A.J., and Wine, P.H.: The Atmospheric Chemistry of Dimethylsulfoxide (DMSO) Kinetics and Mechanism of the OH + DMSO Reaction. Journal of Atmospheric Chemistry, 24: 23-37, 1996.

39. Barone, S.B., Turnipseed, A.A., and Ravishankara, A.R.: Reaction of OH with Dimethyl Sulfide (DMS). 1. Equilibrium Constant for OH + DMS Reaction and the Kinetics of the OH*DMS + O2 Reaction. J. Phys. Chem., 100: 14694-14702, 1996.

40. Siegrist, T.W.: Chemicals and Allied Products. Journal WPCF, 53: 851-861, 1981.

41. Luck, F., Djafer, M., Karpel Vel Leitner, N., Gombert, B., and Legube, B.: Destruction of Pollutants in Industrial Rinse Waters by Advanced Oxidation Processes. Wat. Sci. Tech., 35(4): 287-292, 1997.

42. Marley, N.A., Gaffney, J.S., and Cunnigham, M.M.: Aqueous Greenhouse Species in Clouds, Fogs, and Aerosols. Environ. Sci. Technol., 27: 2864-2869, 1993.

43. Bellamy, W.D., Hickman, G.T., Mueller, P.A., Ziemba, N.: Treatment of VOC-contaminated Groundwater by Hydrogen Peroxide and Ozone oxidation. Research Journal WPCF, 63: 120-128, 1991.

44. Chang, M.B., Balbach, J.H., Rood, M.J., Kushner, M.J.: Removal of SO2 from Gas Streams Using a Dielectric Barrier Discharge and Combined Plasma Photolysis. J. Appl. Phys., 69(8): 4409-4417, 1991.

45. Storch, D.G., Kushner, M.J.: Destruction Mechanisms for Formaldehyde in Atmospheric Pressure Low-Temperature Plasmas. J. Appl. Phys., 73(1): 51-55, 1993.

46. Hoigne, J., and Bader, H.: Rate Constants of Reactions of Ozone with Organic and Inorganic Compounds in Water – I Non-Dissociating Organic Compounds. Water Res., 17: 173-183, 1983.

47. Balbach, J.H.: Modeling the Removal of Sulfur Dioxide and Nitrogen Oxides from Flue Gases Using Combined Plasma and Optical Processing. Masters Thesis, University of Illinois at Urbana-Champaign, Urbana-Champaign, 1991.

48. Wen, Chih-Peng: Kinetic Studies of Ozonizations of Formic Acid, Formaldehyde, and Methanol in Aqueous Solutions. Masters thesis, Mississippi State University, Mississippi, 1974.

49. Lunin, V.V., Popovich, M.P., and Tkachenko, S.N.: Physical Chemistry of Ozone (in Russian). Publishing House of Moscow State University, Moscow, 1998.

50. Dors, M., Mizeraczyk, J., Czech, T., Rea, M.: Removal of NOx by DC and Pulsed Corona Discharges in a Wet Electrostatic Precipitator Model. Journal of Electrostatics, 45: 25–36, 1998.

51. Sun, B., Sato, M., Clements, J.: Optical Study of Active Species Produced by a Pulsed Streamer Corona Discharge in Water. Journal of Electrostatics, 39: 189-202, 1997.

52. Shimizu, K., Kinoshita, K., Yanagihara, K., Rajanikanth, B., Katsura, S., and Mizuno, A.: Pulsed Plasma Treatment of Polluted Gas Using Wet/Low Temperature Corona Reactors. IEEE, 1432-1439, 1995.

53. Mizuno, A., Shimizu, K., Matsuoka, T., and Furuta, S.: Reactive Absorption of NOx Using Discharge Plasma. IEEE, 1550-1555, 1994.

54. Chakrabarti, A., Mizuno, A., Shimizu, K., Matsuoka, T., and Furuta, S.: Gas Cleaning with Semi-Wet Type Plasma Reactor. IEEE, 1989-1994, 1993.

55. Chakrabarti, A., Mizuno, A., Shimizu, K., Matsuoka, and Furuta, S.: Gas Cleaning with Semi-Wet Type Plasma Reactor, IEEE Transactions on Industry Applications, 31: 500-506, 1995.

56. Dors, M., Mizeraczyk, J.: Influence of Temperature and Humidity on NOx Removal by Corona Discharge. Czech. J. Phys., 48: 1193-1997, 1998.

57. Roberts, J.M.: The Atmospheric Chemistry of Organic Nitrates. Atmospheric Environment, 24A: 243-287, 1990.

58. http://www.chem.leeds.ac.uk/Atmospheric/MCM/main.html

59. Atkinson, R.: Gas-Phase Tropospheric Chemistry of Organic Compounds: a review. Atmospheric Environment, 24A: 1-41, 1990.

60. Creyghton, M.: Pulsed Positive Corona Discharges: Fundamental Study and Application to Flue Gas Treatment. Ph.D. Thesis. University of Eindhoven, Netherlands, 1994.

61. Akishev, Y.S., Napartovich, A.P., and Trushkin, N.E.: Problems of the Pulsed Corona Discharge Use in the Ecology. (in Russian). Information center "Ozone", Moscow, 3, 1995.

62. Penetrante, B.M., and Schultheis, S.E.: Non-Thermal Plasma Technique for Pollution Control, Part A. Overview, Fundamentals and Supportive Technologies. Heidelberg: Springer-Verlag, 1993.

63. Penetrante, B.M., and Schultheis, S.E.: Non-Thermal Plasma Technique for Pollution Control, Part B. Electron Beam and Electrical Discharge Processing. Heidelberg: Springer-Verlag, 1993.

64. Penetrante, B.M., Hsiao, M.C., Bardsley, J.N., Meritt, B., Vogtlin, G.E., Wallman, P.H., Kuhti, A., Burkhart, C.P., Bayless, J.R.: Power Consumption and Byproducts in Electron Beam and Electrical Discharge Processing of Volatile Organic Compounds. In Proceedings of the International Workshop on Plasma Technologies for Pollution Control and Waste Treatment. Beijing: Beijing Institute of Technology. Cambridge: Massachusetts Institute of Technology, Cambridge, 1996.

65. Bugaev, S.P., Kozyrev, A.V., Kuvshinov,V.A., Sochugov, N. S.: Aerosol Formation from Unsaturated Organic Vapors in Pulsed Corona Discharge Plasma. Dokl. Akad. Nauk.:361(5):612-615, 1998.

APPENDIX

```
CHEMKIN INTERPRETER OUTPUT: CHEMKIN-II Version 3.9  Aug. 1994
                                   DOUBLE PRECISION
                            --------------------
                            ELEMENTS      ATOMIC
                            CONSIDERED    WEIGHT
                            --------------------
                             1. O        15.9994
                             2. H        1.00797
                             3. C        12.0112
                             4. AR       39.9480
                             5. S        32.0640
                             6. N        14.0067
                             7. E      0.545000E-03
                            --------------------
                            C
                          P H
                          H A
                          A R
SPECIES                   S G  MOLECULAR  TEMPERATURE  ELEMENT COUNT
CONSIDERED                E E  WEIGHT     LOW    HIGH  O  H  C  AR S  N  E
-------------------------------------------------------------------------------
  1. H                    G 0    1.00797   200    6000  0  1  0  0  0  0  0
  2. OH                   G 0   17.00737   200    6000  1  1  0  0  0  0  0
  3. O                    G 0   15.99940   200    6000  1  0  0  0  0  0  0
  4. O2                   G 0   31.99880   200    6000  2  0  0  0  0  0  0
  5. O3                   G 0   47.99820   300    5000  3  0  0  0  0  0  0
  6. HO2                  G 0   33.00677   200    6000  2  1  0  0  0  0  0
  7. H2O                  G 0   18.01534   200    6000  1  2  0  0  0  0  0
  8. HCOOH                G 0   46.02589   300    4000  2  2  1  0  0  0  0
  9. H2O2                 G 0   34.01474   200    6000  2  2  0  0  0  0  0
 10. CO                   G 0   28.01055   200    6000  1  0  1  0  0  0  0
 11. CO2                  G 0   44.00995   200    6000  2  0  1  0  0  0  0
 12. HCO                  G 0   29.01852   200    6000  1  1  1  0  0  0  0
 13. CH3                  G 0   15.03506   200    6000  0  3  1  0  0  0  0
 14. CH4                  G 0   16.04303   200    6000  0  4  1  0  0  0  0
 15. C2H6                 G 0   30.07012   300    5000  0  6  2  0  0  0  0
 16. O1D                  G 0   15.99940   200    6000  1  0  0  0  0  0  0
 17. CH2O                 G 0   30.02649   200    6000  1  2  1  0  0  0  0
 18. C2H5                 G 0   29.06215   200    6000  0  5  2  0  0  0  0
 19. CH2                  G 0   14.02709   200    6000  0  2  1  0  0  0  0
 20. CH3O                 G 0   31.03446   200    6000  1  3  1  0  0  0  0
 21. CH2OH                G 0   31.03446   200    6000  1  3  1  0  0  0  0
 22. CH                   G 0   13.01912   200    6000  0  1  1  0  0  0  0
 23. C2H2                 G 0   26.03824   200    6000  0  2  2  0  0  0  0
 24. NO                   G 0   30.00610   200    6000  1  0  0  0  0  1  0
 25. C2H4                 G 0   28.05418   300    5000  0  4  2  0  0  0  0
 26. C2H3                 G 0   27.04621   200    6000  0  3  2  0  0  0  0
 27. CH3OH                G 0   32.04243   200    6000  1  4  1  0  0  0  0
 28. CH3HCO               G 0   44.05358   200    6000  1  4  2  0  0  0  0
 29. C2H                  G 0   25.03027   200    6000  0  1  2  0  0  0  0
 30. CH2CO                G 0   42.03764   200    6000  1  2  2  0  0  0  0
 31. HCCO                 G 0   41.02967   200    6000  1  1  2  0  0  0  0
 32. NO2                  G 0   46.00550   200    6000  2  0  0  0  0  1  0
 33. CH3O2H               G 0   48.04183   200    6000  2  4  1  0  0  0  0
 34. H2                   G 0    2.01594   200    6000  0  2  0  0  0  0  0
 35. CH3CO                G 0   43.04561   200    6000  1  3  2  0  0  0  0
```

APPENDIX (continued)

36. CH3CO3	G	0	75.04441	300	5000	3	3	2	0	0	0	0
37. CH3CO3H	G	0	76.05238	300	5000	3	4	2	0	0	0	0
38. CH2HCO	G	0	43.04561	300	5000	1	3	2	0	0	0	0
39. C2O	G	0	40.02170	200	6000	1	0	2	0	0	0	0
40. HNO	G	0	31.01407	200	3500	1	1	0	0	0	1	0
41. CH3O2	G	0	47.03386	300	5000	2	3	1	0	0	0	0
42. C2H5O2H	G	0	62.06892	200	6000	2	6	2	0	0	0	0
43. C2H5O2	G	0	61.06095	300	5000	2	5	2	0	0	0	0
44. C2H5OH	G	0	46.06952	200	6000	1	6	2	0	0	0	0
45. C2H5O	G	0	45.06155	300	5000	1	5	2	0	0	0	0
46. CH3SCH3	G	0	62.13412	300	6000	0	6	2	0	1	0	0
47. CH3S(OH)CH3	G	0	79.14149	300	5000	1	7	2	0	1	0	0
48. HNO2	G	0	47.01347	300	4000	2	1	0	0	0	1	0
49. CH3S	G	0	47.09906	300	5000	0	3	1	0	1	0	0
50. SO2	G	0	64.06280	300	5000	2	0	0	0	1	0	0
51. SO3	G	0	80.06220	300	5000	3	0	0	0	1	0	0
52. CH3SO	G	0	63.09846	300	5000	1	3	1	0	1	0	0
53. CH3SOCH3	G	0	78.13352	300	5000	1	6	2	0	1	0	0
54. CH3SO2	G	0	79.09786	300	5000	2	3	1	0	1	0	0
55. CH3SO3	G	0	95.09726	300	5000	3	3	1	0	1	0	0
56. NO3	G	0	62.00490	200	6000	3	0	0	0	0	1	0
57. CH3SO3H	G	0	96.10523	300	5000	3	4	1	0	1	0	0
58. CH3SOO	G	0	79.09786	300	5000	2	3	1	0	1	0	0
59. CH3SO2CH3	G	0	94.13292	300	5000	2	6	2	0	1	0	0
60. H2SO4	G	0	98.07754	300	5000	4	2	0	0	1	0	0
61. CH3SO4	G	0	111.09666	300	5000	4	3	1	0	1	0	0
62. H2SO3	G	0	82.07814	300	5000	3	2	0	0	1	0	0
63. CH3SCH2	G	0	61.12615	300	5000	0	5	2	0	1	0	0
64. N2D	G	0	14.00670	200	6000	0	0	0	0	0	1	0
65. CH3SOH	G	0	64.10643	300	5000	1	4	1	0	1	0	0
66. CH3SCH2OO	G	0	93.12495	300	5000	2	5	2	0	1	0	0
67. CH3SCH2O	G	0	77.12555	300	5000	1	5	2	0	1	0	0
68. C2	G	0	24.02230	200	6000	0	0	2	0	0	0	0
69. SCH2	G	0	14.02709	300	4000	0	2	1	0	0	0	0
70. PC2H5O	G	0	45.06155	300	5000	1	5	2	0	0	0	0
71. N2	G	0	28.01340	300	5000	0	0	0	0	0	2	0
72. N	G	0	14.00670	200	6000	0	0	0	0	0	1	0
73. N2O	G	0	44.01280	300	5000	1	0	0	0	0	2	0
74. HNO3	G	0	63.01287	200	6000	3	1	0	0	0	1	0
75. N2O5	G	0	108.01040	200	6000	5	0	0	0	0	2	0
76. N2P	G	0	28.01340	200	6000	0	0	0	0	0	2	0
77. H2OP	G	0	18.01534	200	6000	1	2	0	0	0	0	0
78. H3OP	G	0	19.02331	200	6000	1	3	0	0	0	0	0
79. NH	G	0	15.01467	200	6000	0	1	0	0	0	1	0

APPENDIX (continued)

REACTIONS CONSIDERED	(k = A T**b exp(-E/RT)) A	b	E
Comments: Reactions in Humid Air			
1. O1D+H2O=>OH+OH	7.61E+12	0.5	0.0
2. O1D+O2=>O+O2	1.32E+12	0.5	0.0
3. O1D+N2=>O+N2	1.08E+12	0.0	-212.9
4. O1D+H2O=>O+H2O	4.10E+11	0.5	0.0
5. O+OH=>H+O2	1.38E+13	0.0	-212.9
6. O+O2+O2=>O3+O2	1.30E+14	0.0	0.0
7. O+O2+N2=>O3+N2	2.00E+19	-2.0	0.0
8. O+H2O+O2=>O3+H2O	5.40E+17	-1.5	0.0
9. O1D+O2+M=>O3+M	3.00E+14	0.0	0.0
10. O1D+O3=>O2+O2	1.21E+13	0.5	0.0
11. O1D+O3=>O2+O+O	1.21E+13	0.5	0.0
12. O1D+NO2=>NO+O2	9.69E+12	0.5	0.0
13. O+O+M=>O2+M	2.50E+15	0.0	0.0
14. O3+M=>O+O2+M	9.90E+14	0.0	22686.0
15. O+O3=>O2+O2	1.14E+13	0.0	4577.0
16. H+O2+M=>HO2+M	2.40E+15	0.0	-577.1
17. HO2+O=>OH+O2	1.62E+13	0.0	-445.8
18. HO2+HO2+M=>H2O2+O2+M	6.84E+14	0.0	-1950.2
19. OH+HO2=>H2O+O2	1.44E+16	-1.0	0.0
20. OH+OH+M=>H2O2+M	1.80E+17	0.0	0.0
21. H+OH+M=>H2O+M	1.55E+17	0.0	0.0
22. OH+H2O2=>H2O+HO2	1.74E+12	0.0	318.4
23. O+H2O2=>OH+HO2	1.00E+09	0.0	0.0
24. O1D+H2O2=>HO2+OH	1.38E+13	0.5	0.0
25. OH+O3=>HO2+O2	3.70E+10	0.0	0.0
26. HO2+O3=>OH+O2+O2	1.10E+09	0.0	0.0
27. H+HO2=>OH+OH	3.70E+13	0.0	0.0
28. H+HO2=>H2+O2	2.00E+12	0.0	0.0
29. H+HO2=>H2O+O	5.70E+11	0.0	0.0
30. H+H2O2=>H2O+OH	3.00E+10	0.0	0.0
31. H+O3=>OH+O2	1.70E+13	0.0	0.0
32. N2D+O2=>NO+O	2.35E+11	0.5	0.0
33. N2D+NO=>N2+O	2.18E+12	0.5	0.0
34. N2D+NO2=>N2O+O	5.10E+10	0.5	0.0
35. N2D+NO2=>2NO	5.10E+10	0.5	0.0
36. N2D+N2O=>NO+N2	9.84E+10	0.5	0.0
37. N2D+N2=>N+N2	8.30E+08	0.5	0.0
38. N+NO2=>N2O+O	8.16E+10	0.5	0.0
39. O1D+N2O=>N2+O2	3.46E+12	0.5	0.0
40. O1D+N2O=>NO+NO	3.46E+12	0.5	0.0
41. N+NO2=>NO+NO	2.04E+10	0.5	0.0
42. N+N+M=>N2+M	7.29E+18	-1.5	0.0
43. N+O3=>NO+O2	1.73E+07	0.5	0.0
44. NO+N=>N2+O	1.07E+12	0.5	0.0
45. NO+HO2=>NO2+OH	2.22E+12	0.0	-477.6
46. NO+OH+M=>HNO2+M	2.35E+23	-2.4	0.0
47. OH+HNO2=>NO2+H2O	1.08E+13	0.0	776.1
48. OH+HNO=>H2O+NO	2.42E+12	0.5	0.0
49. OH+NO2+N2=>HNO3+N2	1.20E+25	-2.9	0.0
50. OH+NO2+O2=>HNO3+O2	1.42E+25	-2.9	0.0
51. OH+HNO3=>NO3+H2O	9.00E+09	0.0	-1293.5
52. OH+NO2+H2O=>HNO3+H2O	1.20E+25	-2.9	0.0
53. OH+N2O=>HNO+NO	1.32E+06	0.5	0.0
54. OH+N=>NO+H	2.28E+13	0.0	-169.2
55. NO+NO3=>NO2+NO2	9.60E+12	0.0	-298.5
56. N2+O=>N+NO	5.44E+13	0.1	75518.3
57. O+NO+N2=>NO2+N2	3.30E+20	-1.6	0.0
58. O+NO+O2=>NO2+O2	8.90E+20	-1.8	0.0
59. NO+NO+O2=>NO2+NO2	1.19E+09	0.0	-1054.7
60. NO+O3=>NO2+O2	1.08E+12	0.0	2726.3
61. NO2+O2=>NO+O3	1.68E+12	0.0	50546.0
62. NO2+O3=>NO3+O2	7.20E+10	0.0	4800.0

APPENDIX (continued)

63.	O+NO2+M=>NO3+M	2.90E+21	-2.0	0.0
64.	O+NO2=>NO+O2	3.90E+12	0.0	-238.8
65.	O+NO3=>O2+NO2	3.46E+11	0.5	0.0
66.	NO2+NO3=>NO+NO2+O2	2.70E+10	0.0	-2507.4
67.	NO3+NO2+M=>N2O5+M	2.56E+26	-3.4	0.0
68.	N2O5=>NO2+NO3	7.30E+01	0.0	0.0
69.	N2O5+H2O=>HNO3+HNO3	1.73E+02	0.5	0.0
70.	N2P+H2O=>H2OP+N2	1.20E+15	0.0	0.0
71.	H2OP+H2O=>H3OP+OH	1.10E+15	0.0	0.0

Comments: Methanol Oxidation Mechanism

72.	CH3OH+N2P=>CH3+N2+OH	7.10E+14	0.0	0.0
73.	CH3OH+N=>CH3+HNO	3.30E+14	0.0	9000.0
74.	CH3OH+O1D=>CH2OH+OH	3.00E+14	0.0	0.0
75.	CH3OH+CH3=>C2H6+OH	2.00E+12	0.0	15000.0
76.	OH+OH=>H2O+O	2.10E+08	1.4	-1660.0
77.	OH+H=>O+H2	5.50E+12	0.0	0.0
78.	OH+H2=>H2O+H	4.20E+09	0.0	0.0

Comments: Dimethyl Sulfide Oxidation Mechanism

79.	CH3SCH3+OH=>CH3S(OH)CH3	3.00E+12	0.0	0.0
80.	CH3SCH3+O=>CH3+CH3SO	7.80E+12	0.0	-320.0
81.	CH3SCH3+OH=>CH3S+CH3OH	6.62E+12	0.0	0.0
82.	CH3S+O2=>CH3+SO2	3.00E+06	0.0	0.0
83.	CH3S+O2=>CH3SOO	1.00E-19	0.0	0.0
84.	CH3SOO=>CH3S+O2	1.00E+02	0.0	0.0
85.	CH3SOO=>CH3+SO2	2.00E+07	0.0	0.0
86.	CH3SO+O3=>CH3+SO2+O2	1.80E+11	0.0	0.0
87.	CH3S(OH)CH3+O2=>CH3SO+CH3O2H	1.20E+12	0.0	0.0
88.	CH3S+O3=>CH3SO+O2	1.20E+12	0.0	0.0
89.	CH3SOO+O3=>CH3SO+O2+O2	4.00E+11	0.0	0.0
90.	CH3SOCH3+OH=>CH3SO+CH3OH	1.00E+10	0.0	0.0
91.	CH3SO+O3=>CH3SO2+O2	1.80E+11	0.0	0.0
92.	CH3SOO=>CH3SO2	1.00E-02	0.0	0.0
93.	CH3SO2CH3+OH=>CH3SO2+CH3OH	3.00E+11	0.0	0.0
94.	CH3SO2=>CH3+SO2	1.00E+03	0.0	0.0
95.	CH3SO2+O3=>CH3SO3+O2	1.00E+10	0.0	0.0
96.	CH3S(OH)CH3+O2=>CH3SOCH3+HO2	1.20E+12	0.0	0.0
97.	CH3SOCH3+OH=>CH3SO2CH3+H	2.00E+13	0.0	0.0
98.	CH3SO3=>CH3+SO3	5.00E+12	0.0	0.0
99.	CH3SO2+O2=>CH3SO4	4.60E+06	0.0	0.0
100.	CH3SO4=>CH3SO2+O2	1.00E+03	0.0	0.0
101.	OH+CH3SCH3=>CH3SCH2+H2O	3.00E+12	0.0	0.0
102.	OH+CH3SCH3=>CH3+CH3SOH	3.00E+09	0.0	0.0
103.	CH3S(OH)CH3=>OH+CH3SCH3	1.07E+07	0.0	0.0
104.	CH3SCH2+O2+M=>CH3SCH2OO+M	6.00E+11	0.0	0.0
105.	CH3SCH2OO+CH3SCH2OO=>CH3SCH2O+CH3SCH2O+O2	5.00E+12	0.0	0.0
106.	CH3O2+CH3SCH2OO=>CH3O+CH3SCH2O+O2	5.00E+12	0.0	0.0
107.	CH3SOH+O2=>CH3SO3H	1.00E+09	0.0	0.0
108.	CH3SCH2O=>CH3S+CH2O	3.30E+04	0.0	0.0

APPENDIX (continued)

Comments: Reactions with Radicals

109.	CH3OH+OH=>CH2OH+H2O			3.60E+06	2.0	-338.3
110.	CH2OH+O2=>CH2O+HO2			1.50E+15	-1.0	0.0
111.	HCO+OH=>CO+H2O			1.00E+14	0.0	0.0
112.	CH2O+OH=>HCO+H2O			7.20E+09	1.0	-571.1
113.	CH2O+OH=>HCOOH+H			1.20E+11	0.0	0.0
114.	HCOOH+OH=>H2O+CO2+H			2.90E+11	0.0	0.0
115.	HCO+M=>H+CO+M			5.10E+21	-2.1	85307.0
116.	HCO+O2=>CO+HO2			5.10E+13	0.0	7055.0
117.	CO+OH=CO2+H			9.90E+10	0.0	0.0
118.	CO+O+M=CO2+M			6.16E+14	0.0	3000.0
	H2	Enhanced by	2.500E+00			
	H2O	Enhanced by	6.200E+00			
	CO	Enhanced by	1.875E+00			
	CO2	Enhanced by	3.750E+00			
	CH4	Enhanced by	3.200E+00			
	CH3OH	Enhanced by	7.500E+00			
119.	HCO+O=CO2+H			3.00E+13	0.0	0.0
120.	HCO+H=CO+H2			9.00E+13	0.0	0.0
121.	HCO+CH3=CO+CH4			1.20E+14	0.0	0.0
122.	HCO+HO2=CO2+OH+H			3.00E+13	0.0	0.0
123.	HCO+HCO=CH2O+CO			2.00E+13	0.0	0.0
124.	HCO+HCO=H2+CO+CO			2.20E+13	0.0	0.0
125.	HCO+O=CO+OH			3.00E+13	0.0	0.0
126.	CH3O+HO2=CH2O+H2O2			3.00E+11	0.0	0.0
127.	CH3O+OH=CH2O+H2O			1.80E+13	0.0	0.0
128.	CH3O+O=CH2O+OH			1.80E+12	0.0	0.0
129.	CH3O+H=CH2O+H2			1.80E+13	0.0	0.0
130.	CH3O+O2=CH2O+HO2			2.20E+10	0.0	1750.0
131.	CH3O+CH2O=CH3OH+HCO			1.00E+11	0.0	2980.0
132.	CH3O+HCO=CH3OH+CO			9.00E+13	0.0	0.0
133.	CH3O+H=CH2OH+H			3.40E+06	1.6	0.0
134.	CH2O+HO2=HCO+H2O2			4.11E+04	2.5	10210.0
135.	CH2O+O=HCO+OH			1.80E+13	0.0	12807.0
136.	CH2O+H=HCO+H2			1.26E+08	1.6	2166.0
137.	CH3OH+HO2=CH2OH+H2O2			9.64E+10	0.0	12580.0
138.	CH3OH+OH=CH3O+H2O			1.00E+13	0.0	1700.0
139.	CH3OH+O=CH2OH+OH			1.63E+13	0.0	5030.0
140.	CH3OH+H=CH2OH+H2			1.64E+07	2.0	4520.0
141.	CH3OH+H=CH3+H2O			2.00E+14	0.0	5300.0
142.	CH3OH+O=CH3O+OH			1.00E+13	0.0	4680.0
143.	CH3OH+CH3O=CH2OH+CH3OH			3.00E+11	0.0	4070.0
144.	CH3OH(+M)=CH2OH+H(+M)			1.38E+16	0.0	95950.0
	Low pressure limit:	0.53500E+17	0.00000E+00	0.70800E+05		
	TROE centering:	0.82000E+00	0.20000E+03	0.14380E+04		
145.	CH3OH+H=H2+CH3O			4.00E+13	0.0	6095.0
146.	CH3OH+O2=CH2OH+HO2			2.05E+13	0.0	44900.0
147.	CH2OH+M=CH2O+H+M			1.14E+43	-8.0	43000.0
	H2O	Enhanced by	1.600E+01			
	CH4	Enhanced by	3.000E+00			
	CO2	Enhanced by	3.750E+00			
	CO	Enhanced by	1.875E+00			
	H2	Enhanced by	2.500E+00			
	CH3OH	Enhanced by	6.000E+00			
148.	CH2OH+H=CH2O+H2			1.00E+13	0.0	0.0
149.	CH2OH+O=CH2O+OH			9.00E+13	0.0	0.0
150.	CH2OH+OH=CH2O+H2O			1.00E+13	0.0	0.0
151.	CH2OH+HO2=CH2O+H2O2			1.21E+13	0.0	0.0
152.	CH2OH+CH2OH=CH3OH+CH2O			4.82E+12	0.0	0.0
153.	CH2OH+CH2OH=CH2O+CH2O+H2			1.00E+15	-0.7	0.0
154.	CH2OH+HCO=CH3OH+CO			1.21E+14	0.0	0.0
155.	CH2OH+CH2O=CH3OH+HCO			5.49E+03	2.8	5900.0
156.	CH2OH+CH3O=CH3OH+CH2O			2.40E+13	0.0	0.0
157.	CH3O+CH3O=CH3OH+CH2O			2.32E+13	0.0	0.0

NOTE: A units mole-cm-sec-K, E units cal/mole

VITA

NAME: Nikolay Yurevich Kalashnikov

PLACE OF BIRTH: Moscow (Russian Federation)

DATE: May 20th,1971

EDUCATION: Ph.D. in Mechanical Engineering, University of Illinois at Chicago, Chicago, Illinois, USA, 2002

M.S. Nuclear Engineering (Minor in Materials Science), University of Florida, Gainesville , Florida, USA, 1995

Diploma with Honors, Mechanical Engineering (Rocket Engines), Moscow State Technical University named after N.E. Bauman, Moscow, Russian Federation, 1994

EXPERIENCE: Research Assistant, High Temperature Laboratory and Materials Characterization Laboratory, Mechanical Engineering Department, University of Illinois at Chicago, USA, 9/1999 - present

Research and Development Project Manager, Scientist, Research Institute LUCH, High Temperature Technology and Design Division, Podolsk, Moscow Region, Russia, 5/1996 – 9/1999

Assistant Manager, Babcock & Wilcox Nuclear Environmental Services, Inc., Lynchburg, VA, USA, 1/1996-5/1996

PUBLICATIONS:

Kuznetsova, I.V., Kalashnikov, N.Y., Gutsol, A.F., Fridman A.A., Kennedy, L.A.: The effect of "overshooting" in the transitional regimes of the low-current gliding arc discharge (Accepted for publication in Journal of Applied Physics).

Kuznetsova, I.V., Kalashnikov, N.Y., Gutsol, A.F., Fridman A.A., Kennedy, L.A.: Theoretical consideration of gliding arc discharge, Proceedings of the 15th International Symposium on Plasma Chemistry, Orleans, France, 9-13 July 2001, Vol. IV, p. 1509.

Gogotsi, Y., Libera, J.A., Kalashnikov, N., Yoshimura, M.: Graphite polyhedral crystals, Science, 290 (5490): 317-320, 2000.

Kalashnikov, N.Y., Mitrofanov, V.I., Vishnevski, V.Y., Zagryazkin, V.N.: Testing of candidate materials for space solar heat storage in hydrogen and ammonia at temperatures above 2000K, Proceedings of the 4th International Conference "Nuclear Power in Space", Podolsk, Moscow Region, Russian Federation, March 1999.